CRANFIELD UNIVERSITY

Z.L. HTIKE

Control for Motion Sickness Minimisation in Autonomous Vehicles

Advanced Vehicle Engineering Centre

SCHOOL OF AEROSPACE,TRANSPORT AND MANUFACTURING

PhD THESIS

CRANFIELD UNIVERSITY

ADVANCED VEHICLE ENGINEERING CENTRE
SCHOOL OF AEROSPACE,TRANSPORT AND MANUFACTURING

PhD THESIS

ACADEMIC YEAR 2020- 2021

Zaw Lin HTIKE

CONTROL FOR MOTION SICKNESS MINIMISATION IN AUTONOMOUS VEHICLES

SUPERVISOR: DR S. Longo & DR E. Velenis

June 2021

This page is intentionally left blank.

Abstract

Automated vehicles are expected to push towards the evolution of transportation systems and exploit the use of vehicular technologies. This thesis investigates the fundamentals of motion planning for minimising motion sickness in transportation systems of higher automation levels. The optimum velocity profile is sought for a predefined road path from a specific starting point to a final one within specific and given boundaries and constraints in order to minimise the motion sickness and the journey time. Motion sickness is minimised by taking the optimum trajectory and velocity profile for any given road path generated by the motion planner. The trajectory tracking controllers based on PID control method were able to track the reference trajectory with good performances. The trade-off between motion sickness and journey time was solved using the application of multi-objective optimisation by altering the weighting factors to find a compromise solution. The Pareto front representing the correlation between the two components is obtained and this front also allows user to select their preference driving style. From the three case studies, driving styles have a bigger impact on reducing motion sickness and journey time rather than vehicle speed and the road width. However, the effect of road width is negligible when travelling on longer road for the reduction of motion sickness and journey time. This finding is crucial considering the need for automated vehicles to drive on a fixed road path in respect to road safety and also to allow the employment of connected and automated vehicles in the future. Finally, an approach combining two optimisation algorithms, the optimal control problem and the $k - \varepsilon$ method, is applied successfully to seek the best trajectory profile that ensures the optimum compromise between motion comfort and driving behaviour, energy efficiency, vehicle stability, occupant's confidence to ride and journey time.

This page is intentionally left blank.

Contents

Acknowledgments

My sincerest thanks go to my supervisor, Dr Stefano Longo, for giving me the opportunity to work on this challenging project and for giving so freely of his time, constant advice, guidance and support with immense knowledge of the subject area, throughout the span of the project. Also, Dr Efstathios Velenis for his advice and expertise on many aspects of vehicle dynamics and control.

I am indebted to Dr Georgios Papaioannou, thank you for everything you have done for me and my family. You have had a greater impact on my life than you know. You are a friend for life.

I would also like to thank Dr Efstathios Siampis, Dr Edward Smith, Chenhui Lin, Lewis Liu and Zhaozhong Zhang for the discussions on the theory of optimal control and vehicle modelling.

I am sincerely grateful to all my family for their love, unwavering support and encouragement all these years that I have been studying, as nothing of what I have succeeded until now, would have been achieved without their support.

My wife, Yihan, for her unconditional support, without her, the final lap of the PhD would have felt more like scaling a cliff face. To our newborn daughter, Lily, you brought so much joy into our life.

The research is supported by the UK Engineering and Physical Sciences Research Council (EPSRC) under Grant EP/N509450/1.

This page is intentionally left blank.

Publications

The following papers are the result of research conducted during my doctoral studies:

1. Htike Z, Papaioannou G, Velenis E, Longo S. *Motion Planning of Self-driving Vehicles for Motion Sickness Minimisation.* In 2020 European Control Conference (ECC), 2020 May 12 (pp. 1719-1724). IEEE. [25]

2. Htike Z, Papaioannou G, Siampis E, Velenis E, Longo S. *Minimisation of Motion Sickness in Autonomous Vehicles.* In 2020 IEEE Intelligent Vehicles Symposium (IV) (pp. 1135-1140). IEEE. [27]

3. Htike Z, Papaioannou G, Siampis E, Velenis E, Longo S. *Motion Sickness Minimisation in Autonomous Vehicles Using Optimal Control.* In International Conference on Robotics in Alpe-Adria Danube Region 2020 Jun 19 (pp. 275-282). Springer, Cham. [26]

4. Htike Z, Papaioannou G, Siampis E, Velenis E, Longo S. *Fundamentals of motion planning for mitigating motion sickness in automated vehicles.* IEEE Transactions on IEEE Transactions on Vehicular Technology. under review, 2021.

5. Papaioannou G, Htike Z, Lin C, Siampis E, Velenis E, Longo S. *Multi-criteria evaluation for sorting alternatives from motion planning in automated vehicles for minimizing motion sickness.* IEEE Transactions on Intelligent Transportation Systems. under review, 2021.

This page is intentionally left blank.

List of Figures

List of Tables

This page is intentionally left blank.

Nomenclature

a	acceleration, inertial acceleration
a_x	longitudinal acceleration
a_y	lateral acceleration
a_{max}	maximum absolute acceleration
$\dot{\psi}$	yaw rate
I_z	the yaw moment of inertia about the vertical axis
l_f	distances of the front axles to the centre of gravity (CM)
l_r	distances of rear axles to the centre of gravity (CM)
C_f	the front tyre cornering stiffnesses
C_r	the rear tyre cornering stiffnesses
v_x	the longitudinal vehicle velocity
v_y	the lateral vehicle velocity
δ	the steering angle
m	mass
L	wheel base
h	height of CM
μ_{max}	tyre-road friction coefficient
η_f	front tyre cornering coefficient
η_r	rear tyre cornering coefficient
α	is the tyre slip angle, vehicle relative heading to the road
F_{zj}	is the axle normal load
F_{yj}	is the axle lateral force on front and rear
g	is the gravitational acceleration constant
s	the longitudinal position on the road strip
s_n	the lateral position on the road strip
κ	road curvature
θ	The road heading angle
J	the cost function
R_w	road width
t	time
t_0	initial time
t_f	final time

T	total time period
T_{demand}	fixed journey time
u	speed
K_p	proportional gain
K_i	integral gain
K_d	derivative gain
W_f	frequency weighting factor
K_m	an empirically derived constant (=1/50)
w_m	weighting factor for motion sickness
w_t	weighting factor for journey time
ω	angular velocity, head angular velocity
ω_s	sensed angular velocity
τ_a	adaptation time constant of SCC
τ_d	dominant decay time constant of SCC (6.5 to 10 s)
f	gravito-inertial acceleration
v_s	sensed vertical
τ	time constant (low pass) range from2 to 10 s (5s in Bos and Bles)
τ_I	large time constant to simulate the habituation (12 mins in Bos , Wada)

Abbreviations

AVs	autonomous vehicles, automated vehicles
BS	british Standards
GIA	gravito-inertial acceleration
IR	illness rating
ISO	international organization for standardization
MOO	multiobjective optimization
MS	motion sickness
MSDV	motion sickness dose value
OCP	optimal control problem
OTO	the otolith organs
PID	proportional-integral-derivative controller
SCC	the semicircular canals
SVC	subjective vertical conflict

This page is intentionally left blank.

CHAPTER 1

Introduction

1.1 Motivation

The race to develop fully automated vehicles (AVs) has become a focus point in automotive engineering research. The recent advancement in sensory systems and computational power has accelerated the development of AVs. It is expected to push towards the evolution of mobility environment in the near future and will have a significant social, economic and environmental impact on the way we live, commute and work. This is due to its ability to reduce traffic accidents, decrease pollution and emissions, improve parking space, reduce traffic congestion, boost productivity, making transportation more affordable and ensuring equal access [1]. At the same time many challenges arise surrounding the issue of safety, ride comfort, human perception as well as the political consideration are the ongoing problems required to be addressed. However, motion sickness (MS) the primary focus for the passenger comfort may severely jeopardise the successful introduction of AVs, as well as their acceptance by the public [2, 3] .

Research into motion sickness on automated vehicles has just started to get attention. On contrary to the past when the cause, the function, the symptoms, and the estimation of motion sickness were the main issues, nowadays the answer to the question of how to minimise it has arisen. The literatures within the context of motion sickness in automated vehicles are available, but very limited. Griffin [4], Diels and Bos [5], Wada [28, 29, 34],

and Elbanhawi [17] investigated the causes of motion sickness in autonomous driving and the potential design for the mitigation. On the other hand, Schoettle and Sivak [3] provide the study into the activities the passengers are likely to engage in AVs that could result in an increase in the motion sickness occurrences. Finally, there has been some attempts by Wada [30–32], Diels and Bos [6, 19], Salters [12, 13] with various methods to alleviate this motion sickness problem.

In autonomous vehicles, the root cause that leads to most significant motion sickness is the driving dynamics during turns on curvy road, stop-and-go traffic that can cause repeated low frequency lateral and longitudinal accelerations at higher magnitude [14]. The vehicles driving speed, road route, and driving style (i.e. driver) are all the main factors [15] and that affect the driving dynamics which ultimately leads to motion sickness. It is also worth mentioned that low frequency oscillation found in road vehicle are the longitudinal, lateral and yaw acceleration. On the other hand, the heave, roll and pitch motion are found to be more intense at higher frequencies than 0.5 Hz [9], [10] and [4].

Other factors also include passenger's onboard visual activities, engaging in non-driving task, and the air quality in the car [15], that arise from the the human factors and ergonomics perspective. Considering these factors, susceptibility of motion sickness is expected to increase significantly in automated vehicles [3], since the loss of controllability (handing over the vehicle controls to automation) will free up the occupant's time, and then finally the complete transformation of the entire interior into a more leisurely and economically design could take place [16], [17], [18] , [30] and [10]. For example, the steering wheel, pedal and gear level will be removed, while seating arrangement will also change by adding a table or a working station. As a result of the above, the passengers will be able to engage more and more in either leisurely or economically productive (non-driving) tasks (i.e. reading, watching movies, working and playing games), which will make them unable to anticipate the direction of travel increasing their susceptibility to motion sickness, its severity and its frequency [19] and [20]. This makes motion sickness *"the elephant in the room"* in high-level AVs [5], as more than 2 in every 9 autonomous vehicle passengers are expected to experience motion sickness based on surveys [16].

In reality, a human driver is thought to drive in a manner that prevents motion sickness

occurrence, because the driver, who does not want to get carsick, functions as a type of motion sickness detector or predictor [30]. The above argument depicts the main difference between passengers riding on an automated vehicle and a taxi. With the automated vehicles not having this driver's function, the consideration of the minimisation of motion sickness in their implementation and design frameworks, is crucial in order to fully replace the driver and develop the ability to sense as the occupant's motion detector. It is therefore imperative to consider basic perceptual mechanisms in the design process since automated vehicles cannot simply be thought of as living rooms, offices, or entertainment venues on wheels [6].

Some potential design for countermeasure to motion sickness problem in AVs can be summarised as follows:

1. Implementing a perfect human driver like algorithm and vehicle control to minimise the magnitude of low frequency motion in driving dynamics. (i.e. smooth driving, optimal motion profile)

2. Designing vehicle ergonomic and vehicle cabin such that larger windows, seating arrangement, seat suspension, seat design are designed accordingly for passenger comfort.

3. Monitoring devices such as camera and other sensors to inform passenger the possibility of motion sickness occurrences.

In particular, recent researches have focused on providing solutions to mitigate motion sickness with ideas from the field of human factors and ergonomics, interior design and automotive engineering. In addition, regarding ergonomics, research has focused into seat design [37] and their arrangement [13], active head-tilting [29] and [32], cabin lighting, vection (illusion of self-motion) and passenger biometric data collection [12]. In terms of vehicle dynamics, few researchers have focused on comfort from the view of braking control [38], suspension design [39], and adaptive cruise control [40], but limited work has been done in motion planning for vehicle control in terms of motion sickness minimisation. Recent studies have emphasized the smooth driving style (i.e. time derivative of acceleration) has been prioritized as one of the main factor in path planning and motion planning problem toward developing self driving vehicles [40] and [72]. However, the motion sickness that causes nausea and other physical discomfort to passengers is relatively

ignored. Wada [30] proposed a countermeasure to minimise motion sickness by designing velocity profile of self-driving vehicles on a fixed road with different straight and curve regions. There are examples of motion planning for tilted train [21], [22] and high-speed rail [23], [24]. However, there is limited work [25–27] done that investigates the motion planning algorithms in reducing motion sickness in automated road vehicles.

In this work, the attention will be turned on developing a perfect human driver algorithm in respect to minimising motion sickness and journey time. More specifically, for a predefined road path from a specific starting point to a final one, the optimum trajectory is sought within specific and given boundary and constraints in order to minimise the motion sickness and the journey time. Therefore, motion planning technique is applied for autonomous driving and it is solved based on optimal control problem approach. Arguably, it is likely that for minimum sickness the vehicle would move in a slow manner, at constant velocity or come to a stop. Similarly, for minimum journey time, the vehicle would move very fast or at constant acceleration. Therefore, a trade off between the two components is investigated through multi-objective optimisation (MOO) by altering the weighting factors. The correlation between sickness and journey time is represented as a Pareto front. Despite the importance of mitigating motions sickness and minimising journey time, the optimum velocity profile with which the vehicle will finally drive should be selected after taking into consideration other multiple objectives such as energy efficiency, vehicle stability driving behaviour. This can be described as multi-criteria decision making problem and it is solved based on a sorting algorithm seeking the optimum solution among the pareto alternatives.

1.2 Aims and Objectives

The fundamental aim of this project is to develop a perfect human driver algorithm such that it will minimise motion sickness occurrence in autonomous vehicles. In addition, this project also aims to pave the way for implementing the idea that passengers would be able to select a driving profile according to their preference in term of comfort, journey time, energy efficiency and route. These will be achieved through following objectives:

1. Develop understanding of motion sickness modelling through a series of case studies and investigate the sensitivity of each motion sickness models.

2. Develop a robust optimal control strategy for motion sickness minimisation. Investigate the fundamental of motion planning when seeking to minimise motion sickness and compare the results with minimum-time manoeuvring problem.

3. Determine the trade-off between motion sickness with journey time by investigating the weighting factor for multi-objectives optimisation between the two components. Perform case studies to investigate the effect of driving dynamics in motion sickness minimisation.

4. Define various metrics for additional objectives and develop a multi-criteria decision making algorithm to identify the absolute optimum among multiple objectives in addition to the optimal control solutions.

1.3 Thesis structure

In Chapter 2 a review into motion sickness is presented. This chapter discusses the theory behind motion sickness and the factors that causes motion sickness. In addition, both empirical and sensory conflict models are presented for motion sickness modelling including cases studies to compare the pro and cons of each approach, while in chapter 3, demonstrates the application of motion planning in motion sickness minimisation and the tracking controllers design. Chapter 4 extends the problem into multi-objective optimisation to investigate the trade off between the conflicting correlation between motion sickness and journey time. Chapter 5 investigates the multi-criteria decision algorithm making to provide the absolute optimum solution by introducing additional objectives .Finally, the key conclusions, contributions to knowledge, areas of future work and the various ways in which the findings of this research have been disseminated are presented in Chapter 6.

This page is intentionally left blank.

CHAPTER 2

Motion Sickness: A Literature Review

The purpose of this chapter is to review and analyse existing modelling methods for motion sickness, which is a vast topic on its own; by no means is this chapter intended to cover motion sickness entirely, and references to the literature will be given when appropriate. The discussion will be restricted to the theory of MS that are strictly necessary or relevant to automated vehicles. This chapter summaries together numerous articles to give an overall review of motion sickness and for those interest in the detail explanation of motion sickness, one should consult following literatures:

- "Human vibration" by Griffin [8] and "Human response to vibration" by Mansfield [20].
- Sensory conflict model in Reason [49–52], Bos & Bles [44]. and Wada [28–36].
- Human factors and ergonomic in [5, 6, 12, 13, 18, 19].
- British standard and International standard [41, 42].
- Experimental work in motion sickness in Griffin and Turner [10, 11], Lawther [45–47] and Golding [53, 54].

2.1 What is motion sickness ?

Motion sickness is a condition marked by symptoms of yawning, irregular breathing, cold sweating, nausea dizziness and vomiting [3]. The environments in which we experience these circumstances can be found in various transportation (e.g., passenger car, boats, rail and planes) and in common entertainment and leisure activities (e.g., virtual reality, video games, and 3D movie theatres). Susceptibility to motion sickness varies widely, but it appears all normal persons can be made sick by a suitable stimulus. The diverse range of stimulation that causes the condition is indicative of a complex phenomenon with no single cause and no simply defined mechanisms. A conceptual model of some of the many relevant factors possibly causing the occurrence of motion sickness by Griffin [8] has been summarised and reproduced in Figure 2.1. To make sense of the theories behind motion sickness, the author would firstly direct the attention of the reader to the next section for throughout explanation of the sensory conflict theory involve in the cause of motion sickness together will examples which are mostly relevant to automated vehicle. So that the involvement of the remaining factors such as the condition of motion environment, the role of low frequency motions, individual susceptibility and behaviour given in Figure 2.1 could be easily understood (related).

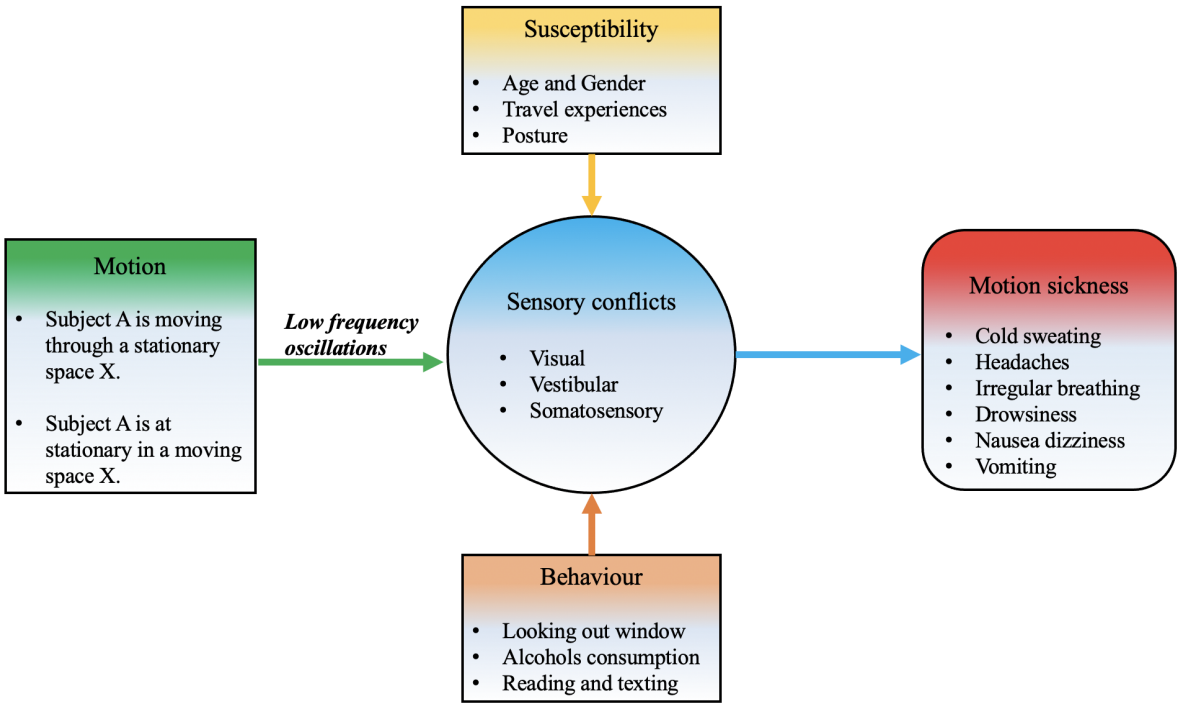

Figure 2.1: Conceptual model of factors possibly involved in the causation of motion sickness [8]

2.2 Sensory conflict theory

There have been several theories on explaining the cause of motion sickness. The most successful explanation of motion sickness and widely accepted is the theory of the sensory conflict. It stated that motion sickness resulted from a sensory conflict between inputs from the visual, vestibular and somatosensory systems of human body [3], [16] and [10]. Also, the long-standing explanation of why this sensory conflict causes sickness is that the brain falsely identifies a toxin in the body, with nausea and vomiting a protective response to get rid of it.

"Some passengers experience carsick while reading a book on a moving car"

For instance, a passenger travelling in a car might be reading a book while the driver steers the vehicle around a corner. In this case, the passenger might not be anticipated on the turn or concentrating on the route, the visual system will not see the moving visual sense but only the words on the page, which move with the car and therefore appear to be stationary and tell her brain that she is sitting still. However, the vestibular system which sense the rotational movement and centrifugal forces would tell her brain that she is in fact turning around the corner. At the same time, the somatic system will feel the changes in pressure across the body.

Before diving into the sensory conflict theory, it is worth mention some of the anatomy of the human vestibular system as it will provide the reader to gain a better understanding of its role in provoking motion sickness. It will be reflected in the discussion in the later section.

2.2.1 Human vestibular system

The vestibular system is a sensor system responsible for providing our brain with the information about motion, head position and spatial orientation. It also is involved with motor functions that allow us to keep our balance, stabilise our head and body during movement, and maintain posture. The main components of vestibular system are located within the inner ear in a system of compartments called vestibular labyrinth, which continuous with the cochlea shown in Figure 2.2. The organ consists of two different sensory systems: the semi-circular canals sensitive to angular acceleration and the otoliths

sensitive to tilt and specific force.

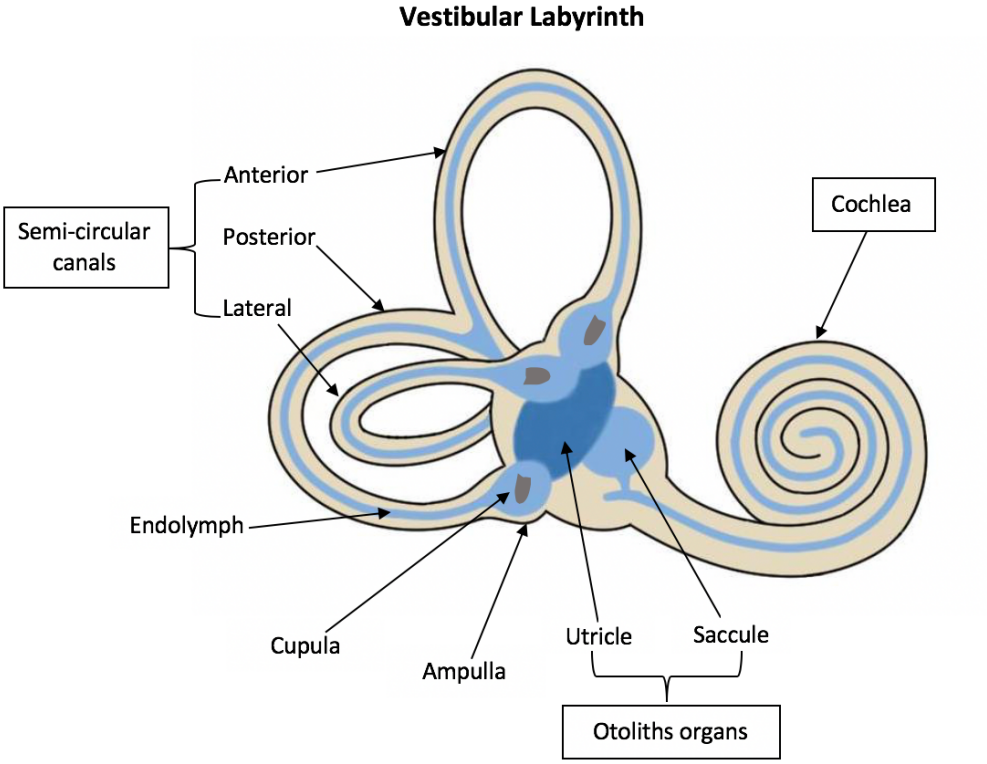

Figure 2.2: The vestibular system in the inner ear

The system of the semi-circular canals (SCC) consists of three circular canals; anterior, posterior and lateral are in approximately three orthogonal planes in which head can rotate. Each of the canals can detect one of the following head movements: nodding up and down, shaking side to side, or tilting left to right. The otoliths (OTO) consist of two sac-like swellings, the utricle and saccule. The utricle, which detects movement of the horizontal plane, and the saccule, which detects movement in the vertical plane. In other words, OTO organs can detect forward and backward movements and the gravitational forces. Together it is called gravito-inertial force (GIF) shown in Figure 2.3. At stationary, GIF would be acting as only gravity (g) however when exposed to an inertial force (i), GIF would be the resultant from the sum of gravity and inertial force.

The semi-circular canals and the otoliths are interconnected and filled with a fluid, the endolymph. Both the end of each of the fluid-filled semi-circular ducts are continuous with the utricle. Each duct bears an enlargement called the ampulla. Inside the ampulla containing hair-cells called ampullary crest or crista which is then covered with a gelatinous capsule called the cupula. At the top of each hair cell is a collection of small hairs

called stereocilia.

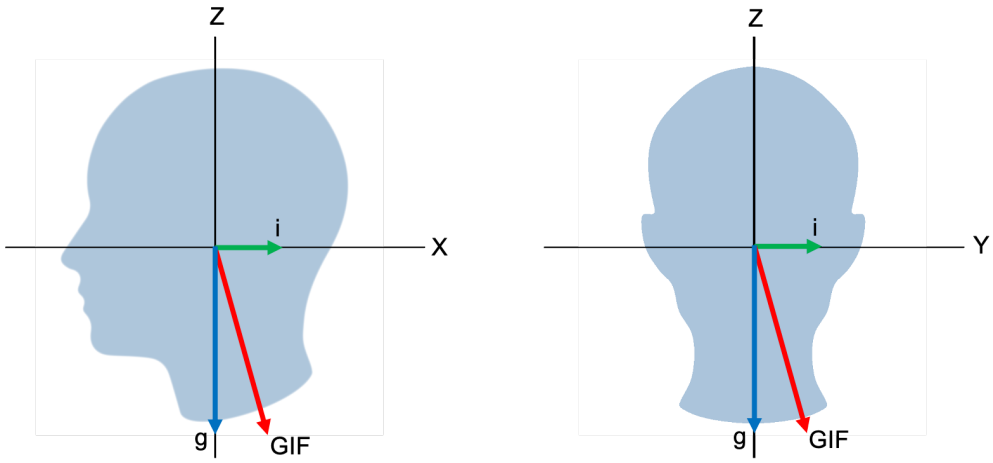

Figure 2.3: Illustration of resultant GIF for longitudinal (left) and lateral (right) motion

When the head is rotated or undergoes an angular acceleration, it causes the movement of endolymph through the canal that corresponds to the plane of the movement. The endolymph flows into the ampulla causes a pressure differential over the cupula. The resulting distortion of the cupula elicits a receptor potential in the crista causes movement of the stereocilia, which leads to the release of neurotransmitters to send information about the plane of movement to the brain. When subjected to a translation acceleration, the hair cells within the utricle and saccule detect movement when crystals of calcium carbonate called otoconia shift in response to it, leading to movement in the layers below the otoconia and displacement of hair cells will excite the sensory cells and thus alter the firing rate of the afferent neurons. The mathematical representation of both OTO and SCC are described in equation 2.1 and 2.2 as transfer functions $H_{OTO}(s)$ and $H_{SCC}(s)$ responsible for filtering the input accelerations from the external motion.

$$H_{OTO}(s) = K_a(s)\left[\frac{(1+\tau_1 s)}{(1+\tau_2 s)(1+\tau_3 s)}\right] \tag{2.1}$$

$$H_{SCC}(s) = K_\omega(s)\left[\frac{\tau_a \times \tau_d s^2}{(1+\tau_a s)(1+\tau_d s)}\right] \tag{2.2}$$

Where K_a and K_ω are the translation and rotational gains. τ_1, τ_2 and τ_3 are the time constant for otolithic organs. τ_a is the adaptation time constant and τ_d is the dominant decay time constant of the canals.

2.2.2 Sensory arrangement theory

It is understood that motion sickness occur due to a conflict between inputs from two or more sensory systems of human body. In fact this is not sufficient theory because much of the sensory information has little absolute meaning, as human learn the meaning of most stimuli and adapts to changes in sensory experiences produced by stimuli. Since the sensory information have little meaning, it follows that a conflict between signals received from different senses of motion is more easily considered to be a conflict with what is expected that with what is correct. The ideal of sensory rearrangement theory on motion sickness was then proposed and developed by Reason and Brand [52] and it is widely accepted today. Reason outlined that all situation that provoke motion sickness are characterised by a condition of sensory rearrangement in which the motion signals transmitted by the eyes, the vestibular system and the non-vestibular proprioceptors are at variance either with one another or with what is expected from previous experience. Reason also identified two classes of sensory rearrangement mismatches that elicit motion sickness: an intersensory conflict dealing with visual-vestibular mismatch and intrasensory conflict for a canal-otolith mismatch.

Visual-vestibluar mismatch examples

1. Watching a 3D cinema or using a virtual reality headset, where there exist a visual movement signal but the vestibular system does not detect body movement.

2. When the visual view of the passenger travelling on moving car is limited while travelling on a moving car. The visual signal could either be stationary or very differences compare to the actual motion sense by the vestibular system.

    - *Passenger seat facing backward could result in the visual system detecting motion opposite to the direction of the actual vehicle motion.*
    - *Passenger seating at the rear of the car and the windows on the car are not large enough for passengers to be able to have the view of the outside to detect correct visual movement.*

Canal-otolith mismatch examples

1. When the vehicle is making harsh braking, acceleration and also traversing bends. A titling resultant of gravity and horizontal translational acceleration occurs, also known as gravito-inertial force (GIF) at greater magnitude in the frequency range below 0.5 Hz, which the head tends to tilt with respect to the gravity in the opposite direction or misaligned with GIF due to the Newton 3rd Law. An example of showing what passenger being push by centrifugal force hence the head tilt towards opposite direction with GIF and a driver who actively lean toward GIF is shown in Figure 2.4.

2. The low frequency translational oscillations below 0.5 Hz also occurs when travelling on country road, driven by an inexperience driver or type of the vehicle. Hence, the occurrence of this of low frequency oscillation and its intensity are dependent on the type of vehicle, the road and the driving dynamics. Which, these three variables are the root causes of motion sickness in automated vehicles this work would be investigate further.

Both cases above would result in conflict as the otolithic organs would lead to misinterpretation of low-frequency translational forces as a change in body orientation whereas the canals sense no signals. In addition, this interpretation of the translational motion experienced will also be inconsistent with cues obtained from the visual system

Increases in the sensory conflict would also produce proportional increases in motion sickness [10]. Sensory conflict theory therefore predicts that the greater the amount of low-frequency translational motion experienced during road travel, the greater the occurrence of motion sickness. However, sensory conflict theory provides only a qualitative explanation of why sickness occurs. No quantitative predictions of when people will become ill or how prevalent illness will be are possible from the theory.

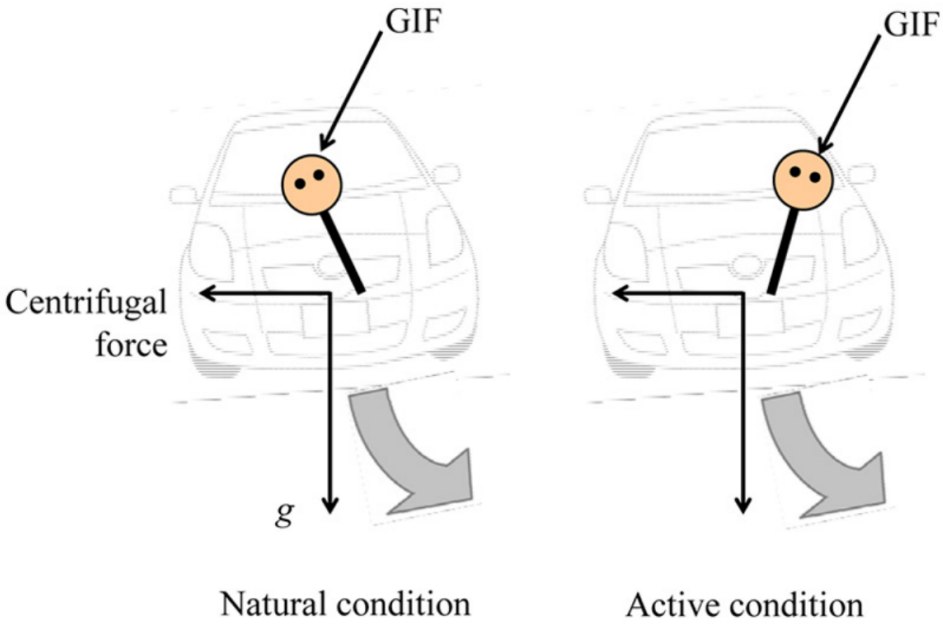

Figure 2.4: An example of showing what passenger being push by centrifugal force hence the head tilt towards opposite direction with GIF and a driver who actively lean toward GIF [33]

2.3 Effect of the frequency of oscillation

The ability of human sensory system to resolve the motion of the body experienced is provided by the frequency of oscillation mainly because the different senses do not all respond to the imposed acceleration. All the experimental studies in aircraft, road vehicles, sea vessel and titling train have shown that they are consistent with the frequency range suggested for motion sickness in the British standards [41] and ISO [42].A summary of the effects of frequency of oscillation on motion sickness for all type of air, sea and land transport are illustrated in Figure 2.5. It is consistent with the standards that at lower frequency range particularly between 0.1 to 0.5 Hz is the most provocative for motion sickness occurrence, whereases higher frequency result in injury and could causes serious harm to human health. The direction, magnitude and duration of the oscillation are important for determining motion sickness. For example, vertical and roll motion are found to cause sea sickness, while longitudinal and lateral motion are the main cause of car sickness. The greater magnitude and longer duration of oscillation indicate the higher severity of motion sickness occurs.

Griffin [10] has proven that the frequency-weighted room mean square acceleration has

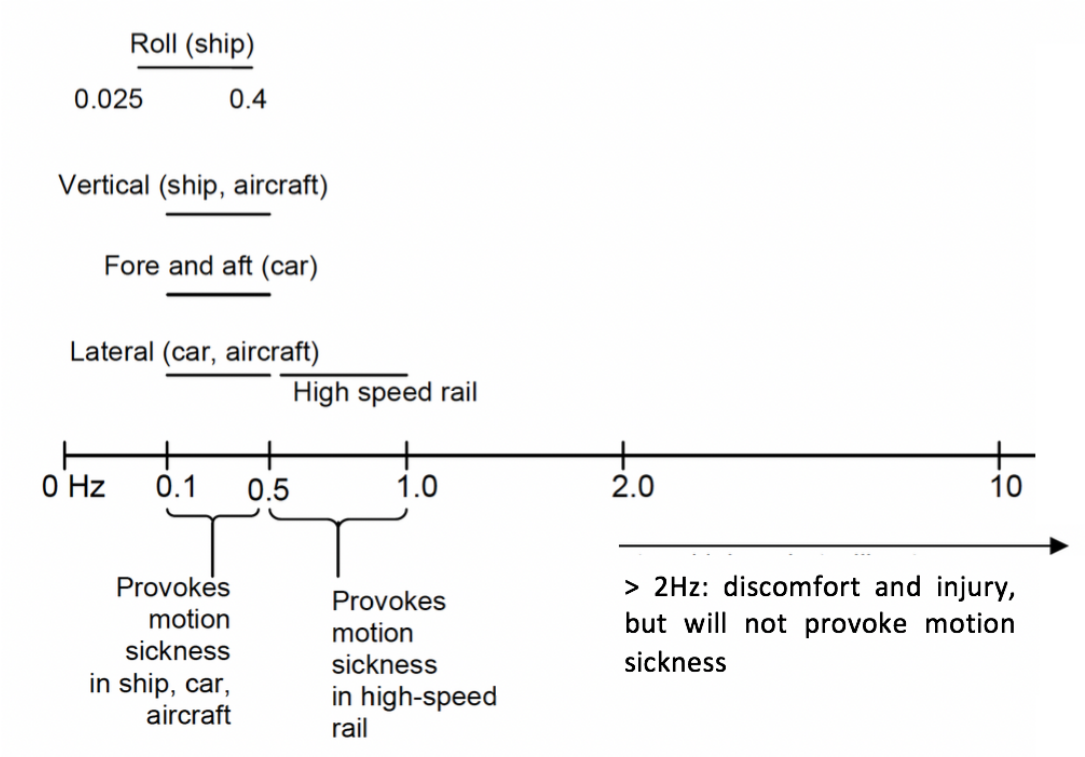

Figure 2.5: Effects of frequency on motion sickness [9]

the direct interpretation of the incidence of motion sickness. This is shown in Figure 2.6 where, the frequency weighted power spectral densities in longitudinal [x] and lateral [y] accelerations are in the frequency range between 0.1 to 0.5 Hz, based on 24 different road journeys carried out by single vehicle. The vertical [z] motion in automated vehicle are found to be at higher frequency range which does not contribute to motion sickness. Although the yaw motion are at low frequency range, their magnitude tend to be low and become less dominance motion. The approximate values for the indication of the likely reactions to various magnitudes of the frequency-weighted r.m.s acceleration taken from the standards [41] is given as:

$< 0.315\ ms^{-2}$	comfortable
0.315 - 0.63 ms^{-2}	a little uncomfortable
0.5 - 1.0 ms^{-2}	fairly uncomfortable
0.8 - 1.6 ms^{-2}	uncomfortable
1.25 - 2.5 ms^{-2}	very uncomfortable
$> 2.0\ ms^{-2}$	extremely uncomfortable

The values given above would also vary depending on individual expectations with regards to the duration of travel and their behaviour and engagement in activities during the trip.

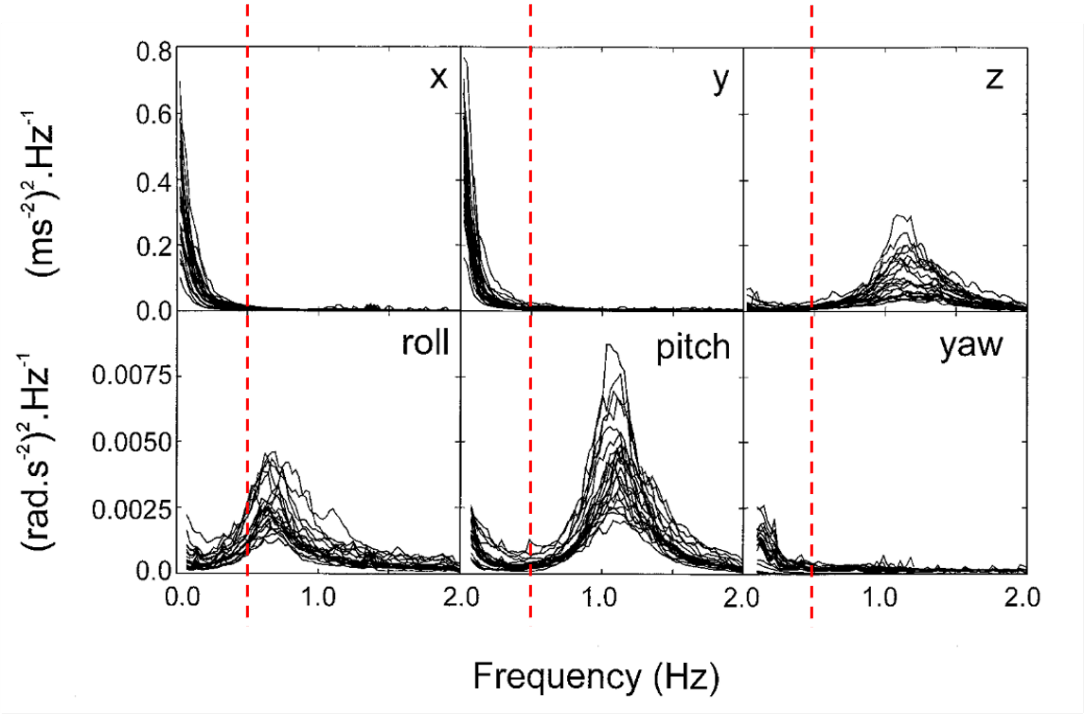

Figure 2.6: Experimental data showing frequency weighted acceleration power spectral densities of 6 axes motions for the journey 24 journeys from single vehicle by Griffin. Red dash-line shows the frequency at 0.5 HZ [10]

2.4 Individual susceptibility and behaviour

This section would discuss the involvement of individual susceptibility and passenger behaviour on motion sickness concerning mainly on automated vehicle.

- ***Age and travel experience***: children in the age range around 9 to 12 years old are highly susceptible to motion sickness. On the other hand, the susceptibility to motion sickness decreases in older passenger. In addition, people who travel more often in the same age group are less likely to be motion sick due to their travel experience (i.e. habituation).

- ***Gender***: Females are found to be more susceptible than males when engaging in non-divining task that limit the visual view of the outside. However, this tends to be overcome with age and travel experience.

- ***Posture***: Siting upright position is more susceptible than on a recline seat at the same time. When the outside view is limited, head movements should be avoided

as it increases sickness occurrence. Although head movement should only be made to aligned with GIF or lean toward it, especially during harsh braking, accelerating and cornering turn. (i.e. driver vs passenger scenario).

- ***Alcohol***: Moderate consumption of alcohol could be beneficial as it act similar to anti-sickness drug. However, excessive drinking of alcohol should be avoided, as it would result in sensory conflict due to fault indication of rotation arise from the cupula being deflected by gravity in SCC while OTO detect no motion [8].

2.5 Motion sickness modelling

There are two most widely used methods for quantifying motion sickness, the empirical method [41], and the subjective vertical conflict (SVC) theory [44] and [28]. Both methods provide, to a certain extent, a good approximation of motion sickness evaluation.

2.5.1 BS/ISO

The British Standard (BS 6841-1987) [41] and International Standard (ISO 2631) [42] documents provide guideline for measurement and evaluation of human exposure to whole-body mechanical vibration and repeated shock. From these standards, an empirical method can be found for evaluating the motion sickness mainly for vertical motion because sea sickness had been the focus in the early research works [45], [46] and [47]. The method proposes the estimation of motion sickness dose value, $MSDV$, such that higher values correspond to a greater incidence of motion sickness. The $MSDV$ is given by the square root of the integral of the square of the z-axis acceleration after it has been frequency weighted:

$$MSDV_z = \left(\int_0^T (a_{z,w}(t))^2 dt \right)^{\frac{1}{2}} \tag{2.3}$$

where $MSDV_z$ is the motion sickness dose value for vertical motion (in $\mathrm{ms}^{-1.5}$), T is the total period (in seconds) during which motion could occur. $a_{z,w}(t)$ is the frequency-weight acceleration in vertical direction and it is obtained by applying the relevant frequency weighting filters directly to the time domain acceleration measurements from the vehicle. In the case of low frequency whole body application, W_f is used as the frequency weighting filter.

Frequency weighting

Frequency weighting is required for evaluating motion sickness dose value in human vibration. The vestibular systems would sense different frequency compare to other part of human body when expose to a motion. Therefore, it is required to apply to a filter in order to approximate the correct frequency of the motion that human sensory systems detect. Equations 2.4 gives the overall frequency weighting W_f and it is a product of band-limiting (i.e. combination of high and low pass filters), acceleration-velocity transition and upward-step filters and their transfer functions are given from equations 2.5 to 2.8.

$$H(s) = H_h(s) \times H_l(s) \times H_t(s) \times H_s(s) \tag{2.4}$$

where $H_h(s)$ is the high pass filter, $H_l(s)$ is the low pass filter, $H_t(s)$ is the transition filter and $H_s(s)$ is the upward-step filter.

$$H_h(s) = \frac{1}{1 + \frac{\omega_1}{Q_1 s} + \left(\frac{\omega_1}{s}\right)^2} \tag{2.5}$$

$$H_l(s) = \frac{1}{1 + \frac{s}{Q_2 \omega_2} + \left(\frac{s}{\omega_2}\right)^2} \tag{2.6}$$

$$H_t(s) = \frac{\left(1 + \frac{s}{\omega_3}\right) K}{1 + \frac{s}{Q_4 \omega_4} + \left(\frac{s}{\omega_4}\right)^2} \tag{2.7}$$

$$H_s(s) = \frac{1 + \frac{s}{Q_5 \omega_5} + \left(\frac{s}{\omega_5}\right)^2}{1 + \frac{s}{Q_6 \omega_6} + \left(\frac{s}{\omega_6}\right)^2} \left(\frac{\omega_5}{\omega_6}\right)^2 \tag{2.8}$$

Where $i = (1, 2, .., 6)$, the angular frequencies $\omega_i = 2\pi f_i$, f_i are the frequencies and the resonant quality factors Q_i are the parameters of the filters for determining the overall vibration acceleration frequency weightings. The value of each parameter is tabulated in

Table 2.1 for both ISO 2631 for vertical motion and Griffin 2004 [48] for lateral motion. The weighting curves are also shown in Figure 2.7.

Table 2.1: Parameters for the frequency weighting

W_f	ISO 2631	Griffin 2004
f_1 (Hz)	0.08	0.02
Q_1	$1/\sqrt{2}$	$1/\sqrt{2}$
$f_2(Hz)$	0.63	0.63
Q_2	$1/\sqrt{2}$	$1/\sqrt{2}$
f_3 (Hz)	∞	∞
$f_4(Hz)$	0.25	0.25
Q_4	0.86	0.86
$f_5(Hz)$	0.0625	∞
Q_5	0.8	1
$f_6(Hz)$	0.1	∞
Q_6	0.8	1
K	1	0.55

Motion sickness due to longitudinal and lateral motion

The suitability of this model to predict motion sickness for road vehicle had been examined by Turner and Griffin [10] and [11]. After investigating the relationships between vehicle motion and passenger sickness within all axes, they concluded that the model is also suitable for approximating motion sickness in x-axis and y-axis. Therefore, the total motion sickness dose value resulted from lateral and longitudinal motion could be given by equation (2.9) :

$$MSDV_{xy} = \left(\int_0^T k_x^2 a_{x,w}^2(t)dt \right)^{\frac{1}{2}} + \left(\int_0^T k_y^2 a_{y,w}^2(t)dt \right)^{\frac{1}{2}} \tag{2.9}$$

where $MSDV_{xy}$ is the combined motion sickness dose value from lateral and longitudinal motion; k_x and k_y are the multiplying factors for x-axis and y-axis respectively and both are equal to 1 for motion sickness study; $a_{x,w}(t)$ and $a_{y,w}(t)$ are the frequency-weighted accelerations in the longitudinal and lateral direction. In this work, rather than applying W_f based on z-direction which is available in the standards [42] and [41], and is commonly used, we adopted the W_f by Barnaby and Griffin [48], (Figure. 2.7) which is validated and used for weighting lateral acceleration. However, there is no available weighting fil-

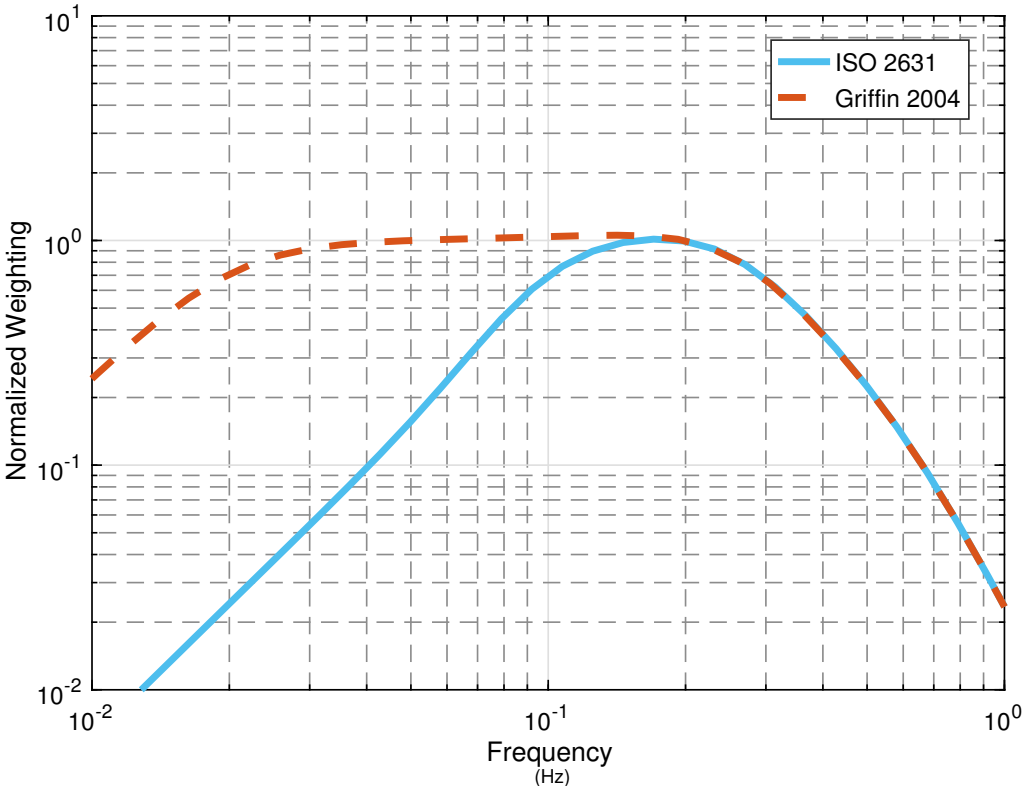

Figure 2.7: Frequency weighting W_f [48]

ter for the longitudinal acceleration can be found. Therefore, in this work, the authors assumed that W_f could be used for the longitudinal acceleration as well. The assumption is taken based on the fact that there is no clear guideline on which W_f should be used to apply on longitudinal acceleration. However, it is based according to the literature and the standards. More specifically, in some of the previous works on evaluating frequency-weighted accelerations in road vehicles [4] and [10] W_f that filter based on z-direction has been applied to longitudinal, lateral and vertical acceleration. Finally, for evaluating high-frequency whole-body vibration analysis, the standards suggest that the same W_d frequency weighting filter should be used for both x-axis and y-axis. Considering the above, W_f proposed by [48] is selected for the frequency weighting filter of both the longitudinal and later accelerations.

According to the literature [10] and the standard [41], a simple linear approximation

between $MSDV_{xy}$ and mean passenger illness rating is given as:

$$IR = K_m \times MSDV_{xy} \tag{2.10}$$

where IR is predicted illness rating and K_m is an empirically derived constant (=1/50) based on data from studies of motion sickness in road [10] and sea [45], [46]. The illness rating scale can be divided into four levels; 0 indicates feeling fine, 1 indicates slightly unwell, 2 indicates quite ill, and 3 indicates absolutely dreadful. For example, if the person's illness rating is 0.9 which could indicate that the person is feeling slightly unwell. In this work, illness rating will be used to represent motion sickness.

2.5.2 Subjective vertical conflict model

The subjective vertical conflict model has started to gain attention and used in many research works into motion sickness. It is the only existing model that takes into account of sensory cues from the sensory organs. The development of SVC model first arises from Oman theory of sensory arrangement. Oman [50, 51] first proposed a model for the sensory rearrangement theory described by Reason [52] on motion sickness in a mathematical form and the conflict theory portion of the model was developed by application of Observer theory from control engineering (Luenberger Observer). In Oman's model, motion sickness is related to the vector difference between a vector representing all the available afferent sensory information and a vector representing the expected sensory information from internal model (observer model). The severity of motion sickness will increase with the increase in the difference vector. Oman's conflict theory has been based on the fact that the visual world is assumed to be stable despite movements of the head and eyes (i.e efference copy). Oman proposed that the site of visual perception receives a copy of the efferent signals sent to the eyes and contains a model of how the sensory pathways operate.

Bels and Bos [44] addressed the problem in Reason and redefined the sensory rearrangement theory on motion sickness such that all situations which provoke motion sickness are characterised by a condition in which the sensed vertical (sensed gravity) as determined on the basis of integrated information from the eyes, the vestibular system and the nonvestibular proprioceptors is at variance with the subjective vertical (expected gravity) as predicted on the basis of previous experience. The sensed and subjective vertical represent vectors indicating the magnitude and direction of the estimates of gravity. Bels

and Bos then developed a subjective vertical conflict motion sickness model or (SVC) model in 1-DOF linear motion, which is an extension of Oman model by adding modules for the calculation of sensed and subjective vertical and the conflict between these two. Kamiji [35] extend Bels's 1-DOF model into 6 DOF in three-dimensional space to predict motion sickness incidence for various motion stimuli including translation and rotation of the head shown in Figure A.1 in the Appendix A. It has been verified that the SVC model could predict distribution characteristics of Griffin's 'mild nausea' [48] very well.

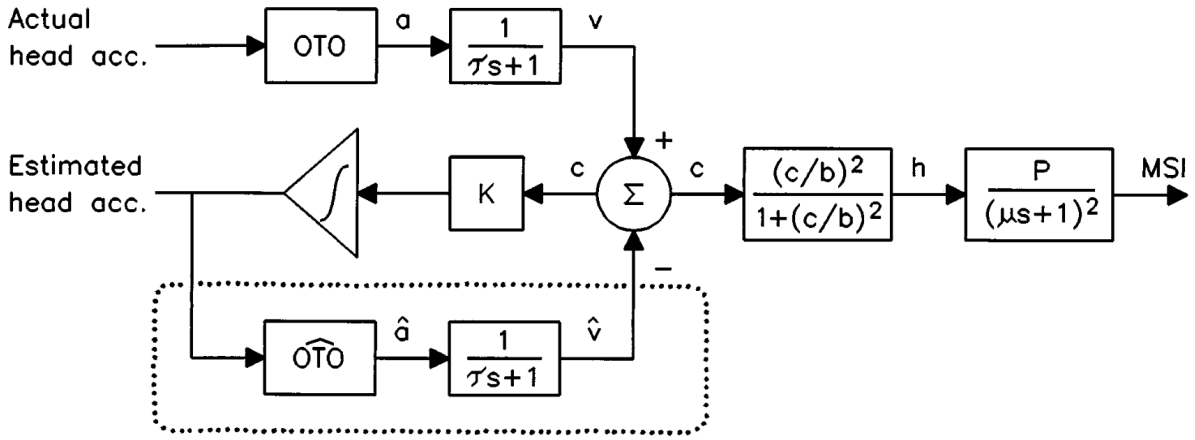

Figure 2.8: 1 DOF-SVC model [44]

Subjective vertical conflict model gives indication of motion sickness as a form of index known as motion sickness incidence (MSI) which is in percentage form. As it has been mentioned that the dominant motions are the longitudinal and lateral acceleration. The combination of two 1 DOF-SVC models that deal with translation acceleration in x-axis and y-axis only, would be sufficient enough to give good approximation for predicting motion sickness. Therefore, this section will mainly focus on detailing one degree of freedom model, however some relevant information about six degree of freedom model would also be provided for better understanding the differences in Appendix A. Similar to MSDV, the subjective vertical conflicts model was first development in order to approximate seasickness [44]. No doubt, the simplified 1 DOF model would contain many assumptions such as the SCC is inactive such that no rotational motions are presented, the subject can only move along translational axis by external enforcement. Furthermore, the model is restricted to single motion (i.e. longitudinal or lateral).

As mentioned in section 2.2.1, OTO organs behave as linear accelerometers which measure gravito-inertial force (GIF) (i.e the sum of gravitational force (g) and inertial force (a) due to linear acceleration), this is given as:

$$f = a + g \tag{2.11}$$

In addition, the gravity is also assumed to be constant, so $f = a$ and for simplicity, the transfer function for OTO organs have been assumed as unit matrix from its dynamic response characteristics. In other words, the afferent signals from the OTO are directly proportional to the specific GIF. Hence, sensed acceleration a_{se} is the same as the actual input acceleration a. According to Einstein's equivalence principle, gravitational force is indistinguishable from inertial force due to linear acceleration. This can be solved by applying a low pass filter. Therefore, sensed vertical v_{se} in laplace form is given as:

$$v_{se} = \frac{1}{\tau s + 1} a_{se} \tag{2.12}$$

where a_{se} represents the acceleration sensed by the otoliths. τ is the time constant, typically it is in the range from 2 to 10 seconds under 1g gravity condition. The expected vertical or subjective vertical, v_e on the other hand is estimated by applying optimal estimation theory as internal model with relevant gain K_c through and integrator shown in Figure 2.8.

$$v_e = \frac{1}{(\tau s + 1)} \frac{1}{s} K_c \Delta v \tag{2.13}$$

The conflict Δv is then given in equation 2.14 as:

$$\Delta v = v_{se} - v_e \tag{2.14}$$

By substituting equations 2.12 and 2.13 into equation 2.14, Δv can be expressed as :

$$\Delta v = \frac{\tau s^2 + 1}{(\tau s + 1)(\tau s^2 + s + K_c)} a_{se} \tag{2.15}$$

Since the conflict can become large both negative and positive, whereas MSI is only ranges from 0% to 100% sickness. The conflicts Δv is filtering through Hill function in equation 2.16 to confirm that people cannot get sicker than sick, and a maximum of sickness is

reached asymptotically. Therefore,

$$h = \frac{(\Delta v/b)^2}{1 + (\Delta v/b)^2} \tag{2.16}$$

Where, b is the indifferent point, and its value can be chosen such that the model fits the experimental data best in a quantitative sense. Finally, the cumulation of the quantity h over time is further filtered through second-order lag with a large time constant τ_l (to simulate the habituation). The MSI is defined as the percentage of a passenger or group of passenger vomiting due to motion sickness is given in Equation 2.17 as :

$$MSI = \frac{P}{(\mu s + 1)^2} \tag{2.17}$$

where μ is the large time constant, and P= 85 % is given such the maximum MSI would not exceed to simulate the realistic condition. However, currently, there is no clear information such that in what range of percentage of MSI would indicate whether a person is feeling fine, unwell, or ill. Thus, more studies and research would require such as carry out experiment and survey study to obtain relevant data and information.

For the application of this model concerning both longitudinal and lateral motion. The 1 DOF-SVC model is extended to accommodate both acceleration such that Δv_i for each component can be expressed as :

$$\Delta v_i = \frac{\tau s^2 + 1}{(\tau s + 1)(\tau s^2 + s + K_c)} a_{se_i} \qquad (i = x, y) \tag{2.18}$$

By taking modulus of the conflict the scalar conflict $c(t)$ such as;

$$c(t) = \mid \Delta v_i \mid \tag{2.19}$$

Similarly, MSI can be calculated using Equation 2.16 and 2.17 for both accelerations.

2.6 Simulation results

This section performs a simple analysis to illustrate the proposed motion sickness modelling. In this respect, it is assumed that a passenger sitting upright on a chair is exposed to only longitudinal acceleration. A sinusoidal wave acceleration is selected for this case study. In the first half hour, a stronger motion is first applied then the weaker motion is applied at the remaining half hour. This will be tested with three acceleration scenarios in Table 2.2:

Table 2.2: The sinusoidal acceleration for the first half hour

Case	Amplitude (ms^{-2})	Frequency (Hz)
ax_1	5	0.25
ax_2	2	0.4
ax_3	2	0.25

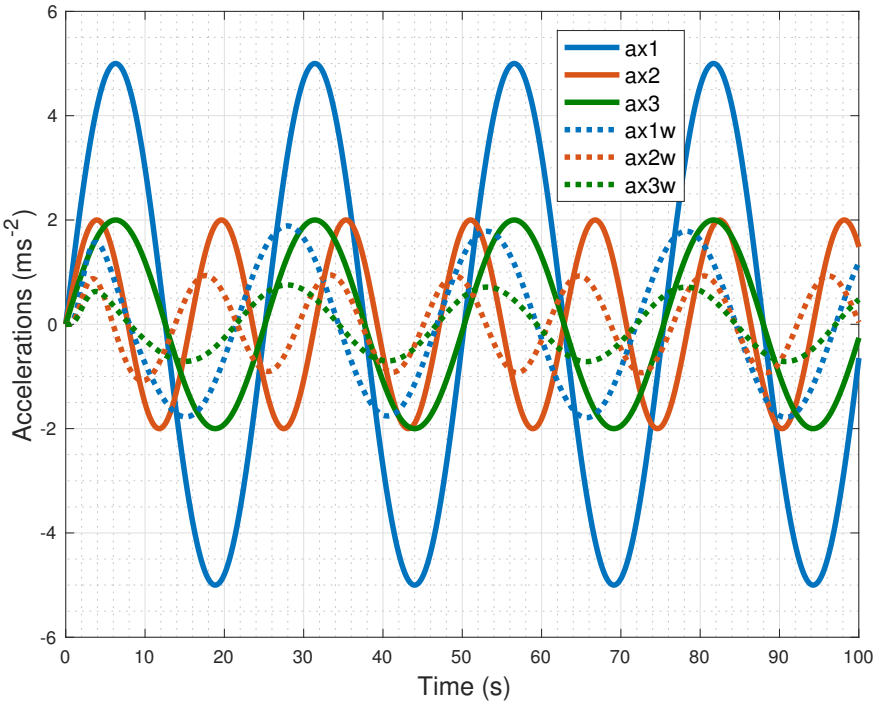

Figure 2.9: The actual accelerations vs. frequency weighted accelerations for the three sinusoidal cases showing first 100s for empirical approach, where dotted lines are frequency weighted signals and solid lines are the original signals.

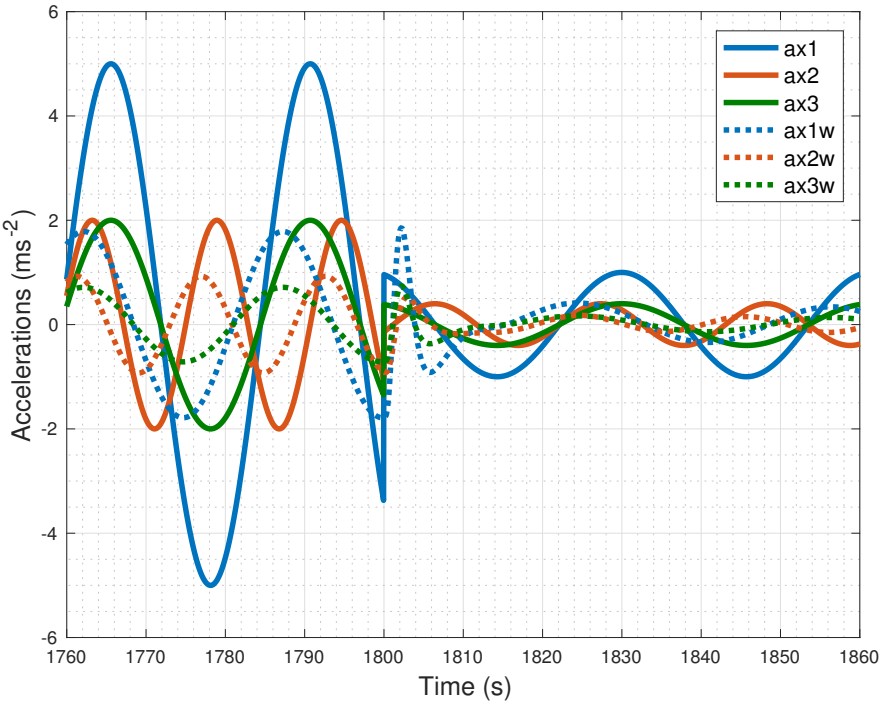

Figure 2.10: The actual accelerations vs. frequency weighed accelerations for the three sinusoidal cases showing the transition to a weaker motion after half an hour for empirical approach, where dotted lines are frequency weighted signals and solid lines are the original signals.

The amplitude for the remaining half hour in all cases are reduced by a fifth and the frequency is kept around 0.2 Hz to simulate a more comfortable motion. All cases are applied to both motion sickness models, and the results are compared and discussed in this section. Firstly, the frequency weighted accelerations for empirical approach are given in Figure 2.9 and 2.10. These are ax_{1w}, ax_{2w} and ax_{3w} based on the original acceleration ax_1, ax_2 and ax_3. It is clear that the frequency weighted accelerations are relatively smaller after filtered through the W_f weighting filter.

On the other hand, the accelerations filtered by the low pass filter in subjective vertical conflict model are given in Figure 2.11. Similarly, they are given as ax_{1f}, ax_{2f} and ax_{3f} and again relatively lower than the actual accelerations. In addition, the comparison of the filtered acceleration from both approaches are shown in Figure 2.12. Although SVC appear to be much larger compares with empirical approach. However, changing the time constant τ in the low pass filter could reduce or increase the magnitude of the accelerations. This work will not discuss the parameter study of the variables in the SVC model as they have been investigate in [44].

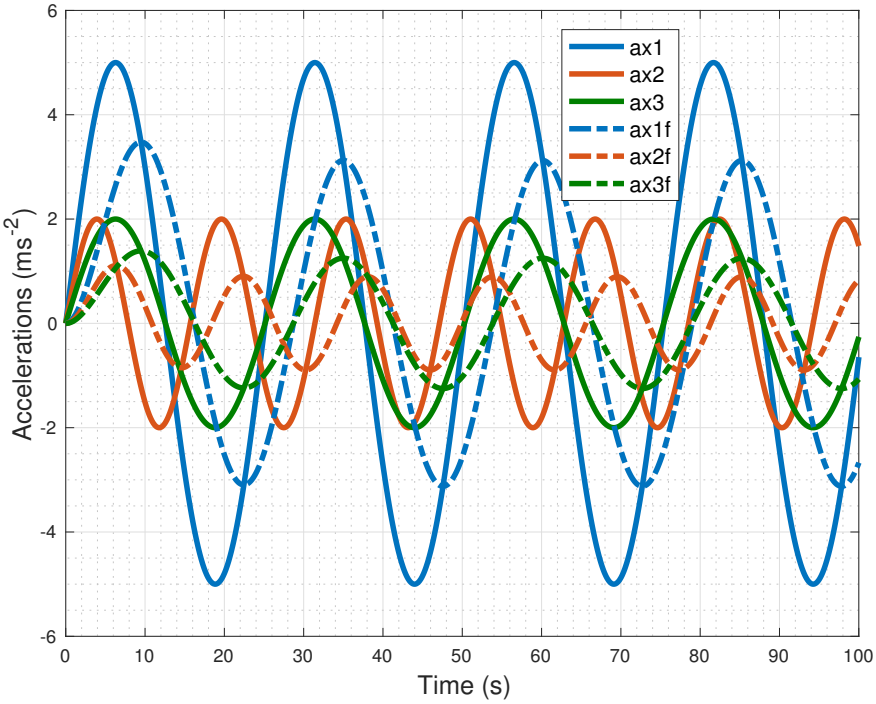

Figure 2.11: The actual accelerations vs. filtered accelerations for the three sinusoidal cases showing first 100s for SVC approach, where dashed lines are filtered signals and solid lines are the original signals.

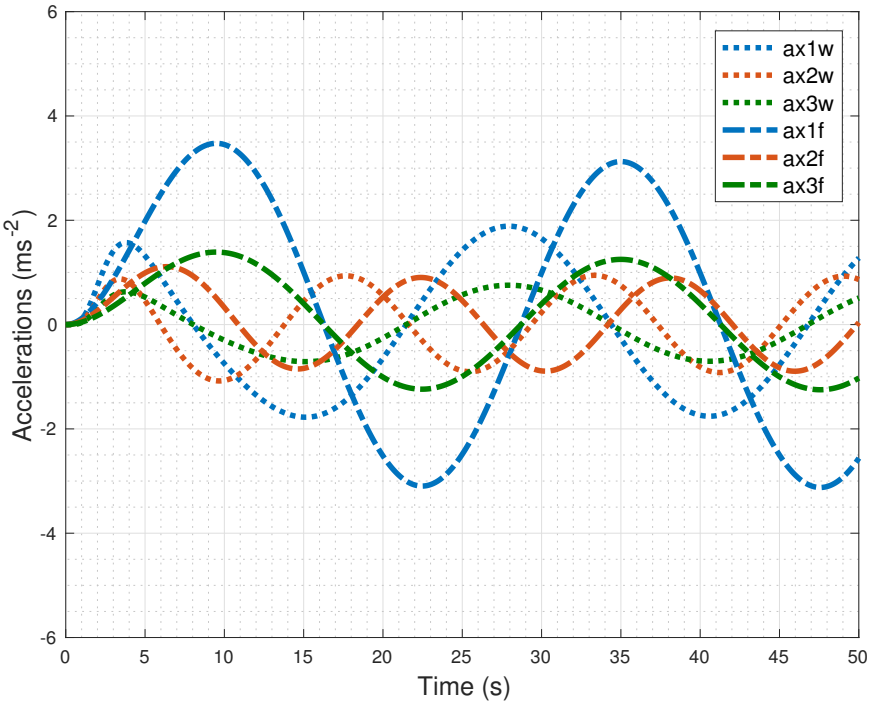

Figure 2.12: Frequency weighted accelerations vs. filtered accelerations for the three sinusoidal cases showing first 50s, where dotted lines are frequency weighted signals and dashed lines are the filtered signals.

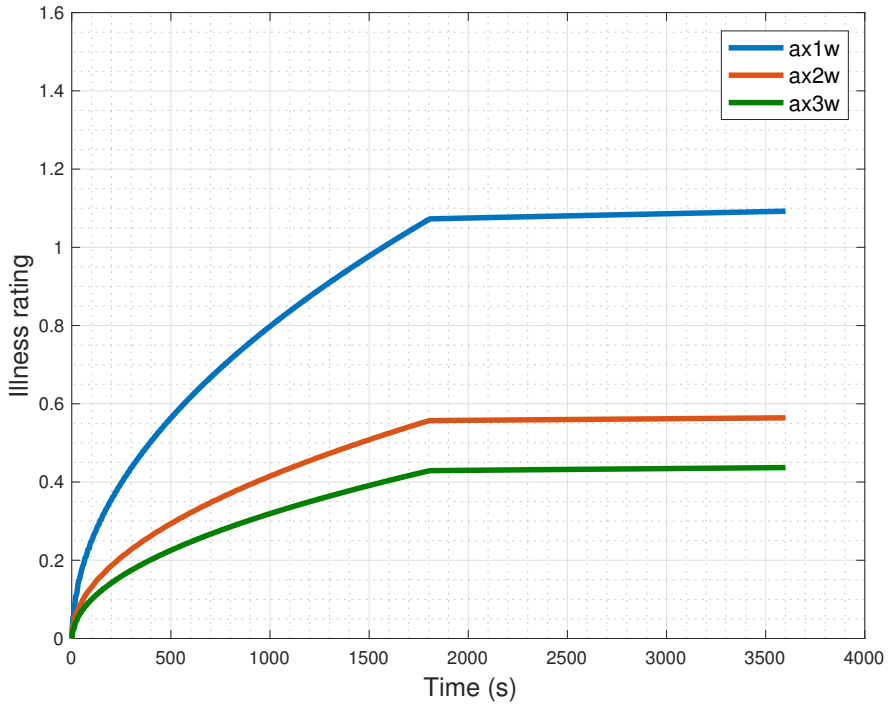

Figure 2.13: Cumulative illness rating for three cases of accelerations showing case 1 with highest illness rating and case 3 with the least illness rating

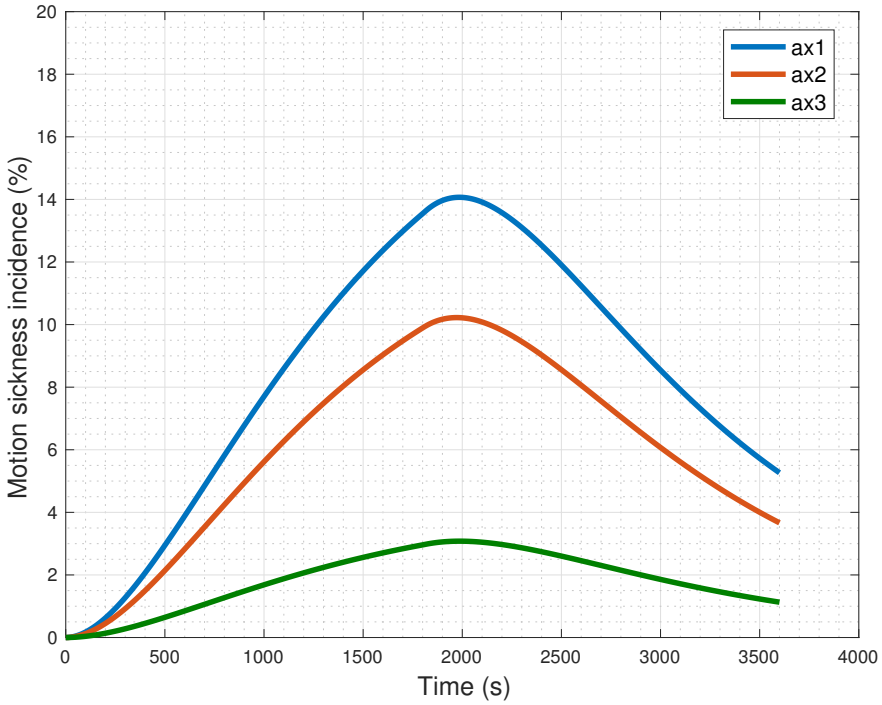

Figure 2.14: Motion sickness curve for three cases of accelerations showing case 1 with highest motion sickness incidence and case 3 with lowest sickness incidence

The accumulated illness rating curve for each case can be seen in Figure 2.13. Similarly, motion sickness curves according to SVC model are given in Figure 2.14. As expected, case 1 results in higher motion sickness than other cases as it has the highest magnitude of accelerations. The case 2 also result in higher sickness than case 1 due to harsh oscillation (longer duration of oscillation). It can be noticed that after half hour the illness rating curves keep increasing whereas motion sickness curves decrease gradually. The is the weakness of the empirical approach as it does not consider habituation as opposed to SVC as for longer journey time. However, for a journey time of up to 2 hours, the suitability of the model is validated and investigated by Turner and Griffin [10].

2.7 Conclusion

This chapter provides an overall review of the theory behind motion sickness and motion sickness modelling. The theory of sensory conflict has been discussed in great detail. Motion sickness is caused by low frequency motion typically below 0.5 Hz as this motion causes conflict in the sensory system. In the automated vehicles, the driving dynamics has been found to be the root cause due to driving behaviour, vehicle driving speed and

road route. In addition, ergonomics and seating arrangements are also found to be the key factors in causing motion sickness. The severity of motion sickness is determined by the direction, magnitude, and duration of the oscillation of the motion. From the comparison of the two methods for motion sickness modelling, it can be concluded that both approach applying weighting or filtered to the actual acceleration before they are evaluated in different manner. Therefore, in some sense they are similar, though only SVC model could provide habituation. The next chapters of the work are to investigate on how to implement the models in the motion planning problem for motion sickness minimisation.

CHAPTER 3

Optimal trajectory generation for motion sickness minimisation

3.1 Introduction

This chapter first discusses a review into motion planning system in automated vehicles and introduces the optimal control method for solving motion planning problem. This chapter will develop motion planning algorithm for automated vehicles in respect to reducing motion sickness with a fixed journey time. Therefore, two case studies had been proposed to investigate the application of motion planning for mitigating the motion sickness problem. Firstly, the minimum-time manoeuvring problem is investigated such that its optimal solutions is used as the baseline for the study of motion sickness minimisation. Both empirical and SVC models for motion sickness modelling are implemented individually as the objective functions in the optimal control formulation. In addition, the optimal solutions from motion planner will be tracked by the feedback controller for validation.

3.2 Motion planning: the optimal control problem

Motion planning is an important part of the decision-making system of an autonomous vehicle taking place after the route planning, the behavioural decision making, and before

the vehicle control in the hierarchy of decision-making process [57]. Motion planning system is responsible computing an optimal trajectory of a selected driving behaviour (such as lane-changing or overtaking manoeuvre), from a starting position to a final destination. This trajectory must account for safety, passenger comfort and dynamically feasible for the vehicle. Finally, this optimum trajectory will be used as a reference trajectory which is tracked by the low-level feedback controller. Sometimes, the motion planners are used to generate not only a collision-free trajectory or a minimum-journey-time trajectory, but also to minimise a given objective function. In addition to journey time, the objective function may also minimise harsh motions or motions that cause passenger discomfort. In a typical setup, the output of the motion planner is then passed to the local feedback control layer. In this way, the feedback controllers generate an input signal to regulate the vehicle to follow this given motion plan.

There are great amount of motion planning techniques in automated driving [58], however they will fall into one of the three categories depending on how they are implemented. These categories are the variational methods, graph search methods, and incremental tree-based methods. There are a range of excellent literatures which discuss these methods in greater details [57]. However, this section will touch on the variational methods which is most relevant in this work. The variational methods are the numerical optimisation often refer to as solving the optimal control problems or trajectory optimisation [59–62]. Although, trajectory optimisation is often used in motion planning. The work here use the more generic terminology "optimal control problem". This is discussed in next section.

3.3 The Optimal control problem

In general, the optimal control problem (OCP) [66] is solved by finding continuous control inputs that, considering constraints on controls and states, forces the states of a nonlinear system to minimise an objective function defined over a certain interval and for the final state. The solution is iteratively improved by modifying the controls until the objective function becomes stationary (i.e. when the derivatives of the controls are zero). A general framework for OCP problem is given:

Find the optimal trajectory $[\mathbf{x}^*(t), \mathbf{u}^*(t)]$ that optimise s the cost function

$$J = \phi[\mathbf{x}(t_0, t_f)] + \int_{t_0}^{t_f} L[\mathbf{x}(t), \mathbf{u}(t)] \tag{3.1}$$

where 0 and f subscripts denote initial and final values, ϕ denotes the Mayer term and L denotes the Lagrange integral term. This is subject to system dynamics or the dynamic constraints (i.e. the vehicle equations of motion):

$$\dot{\mathbf{x}} = f[\ \mathbf{x}(t),\ \ \mathbf{u}(t)], \tag{3.2}$$

the equality and inequality path constraints:

$$\mathbf{g}[(\mathbf{x}(t), \mathbf{u}(t)] = 0, \qquad\qquad \mathbf{h}[(\mathbf{x}(t), \mathbf{u}(t)] \leq 0 \tag{3.3}$$

and initial and final boundary conditions:

$$\mathbf{x}(t_0) = \mathbf{x}_0, \qquad\qquad \mathbf{x}(t_f) = \mathbf{x}_f \tag{3.4}$$

The three numerical methods for solving the optimal control problems are the dynamic programming, indirect methods and direct methods. A detail comparison of these methods and the description of each method have been covered in [57,61]. However, following previous work [64, 65], this section will restrict to direct methods since direct optimisation by nonlinear programming (NLP) has broader convergence domain and lower requirements for the accuracy of initial value evaluation. More importantly it is the best method for solving optimal control with path constraints. Direct optimisation takes the "first discretise, then optimise" approach. This approach transcribes the continuous OCP into a finite-dimensional nonlinear programming problem, which is then solved with a NLP solver such as SNOPT [67] or IPOPT [68]. The comparison of these solvers had been described in detail in [69, 70]. A commercially available software GPOPS-II [63] is found to give a result that is able to approach the constraints more closely by virtue of the barrier method employed by IPOPT solver. Hence, GPOPS-II is used in this work, and it is executed in MATLAB suite.

3.4 Methods and materials

This section aims to describes the mathematical formulation for motion planning to simulate the perfect human driver performing (i) a minimum time, and (ii) minimum motion sickness manoeuvring. These will be presented as two case studies in Section 3.6 for detail discussion. The problem is to find the appropriate vehicle control inputs, that can drive the vehicle along a predefined path from the initial position (s_0) to the final position (s_f), such that minimum journey time or minimum motion sickness is sought. This could be solved as an OCP method, by setting specific cost function which represent the objectives and a set of differential equality and algebraic inequality constraints.

3.4.1 Vehicle and Track models

Point mass model

For motion planning, the simplest vehicle model and most commonly used is the point mass model [71, 72]. The vehicle is considered as a vehicle of mass m travelling through a prescribe path, given the acceleration limits and boundary conditions. This model consider no slip when travelling through the path so that the velocity is assumed to be acting in the longitudinal direction. Tire modelling is not considered in this model and yaw dynamics is also neglected. The Equations of motion describing the point mass model are given below (3.34) :

$$\ddot{x} = a_x, \qquad \ddot{y} = a_y \tag{3.5}$$

where a_x, a_y are the longitudinal and lateral accelerations, while a_{max} is the maximum absolute acceleration that the vehicle is constrained to reach.

$$\sqrt{{a_x}^2 + {a_y}^2} \leqslant a_{max} \tag{3.6}$$

Single-Track Vehicle Model

A three degree of freedom (3 DOF) single track dynamic model shown in Figure 3.1 with linear tyres model is used to validate the optimal solutions (i.e. tracking the optimal trajectory from the motion planner). The Equations of motion describing single track dynamic model are given in Equation 3.7- 3.9. The vehicle parameters used are given in Table 3.1.

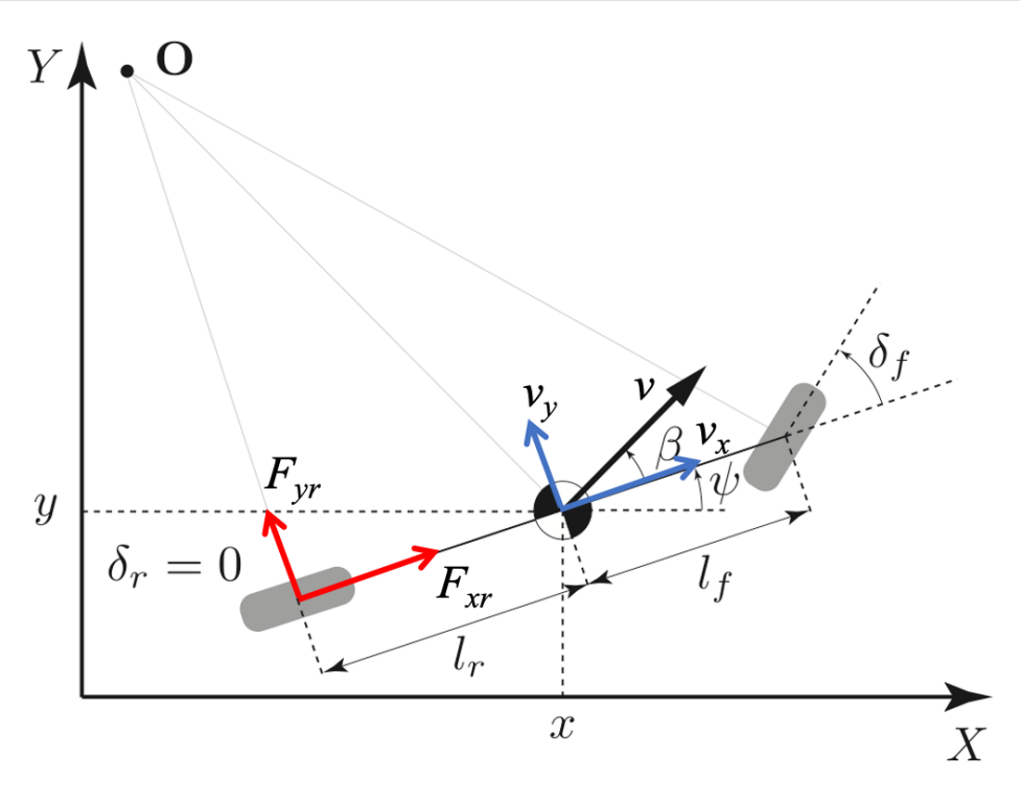

Figure 3.1: 3DOF single-track vehicle model

$$m\dot{v}_x = m(a_x + v_y\dot{\psi}) \tag{3.7}$$

$$m\dot{v}_y = -\frac{(C_f + C_r)}{v_x}v_y + \left(-mv_x + \frac{(-l_fC_f + l_rC_r)}{v_x}\right)\dot{\psi} + C_f\delta \tag{3.8}$$

$$I_z\ddot{\psi} = -\frac{(l_fC_f - l_rC_r)}{v_x}v_y - \frac{(l_f^2C_f + l_r^2C_r)}{\dot{\psi}} + l_fC_f\delta \tag{3.9}$$

where a_x is the longitudinal acceleration, considered as an input to the system, m is the vehicle mass; $\dot{\psi}$ is the yaw rate; I_z is the yaw moment of inertia about the vertical axis; l_f and l_r are the distances of the front and rear axles to the centre of gravity (CM) ; C_f and C_r and the front and rear tyre cornering stiffnesses; v_x and v_y are the longitudinal and lateral vehicle velocities respectively. The steering δ will be the front wheels steering δ_f as rear wheels steering δ_r is assumed to be zero. The control inputs in this case would be the longitudinal acceleration and steering.

Table 3.1: Vehicle parameters for Single-track vehicle model

Symbol	Name	Unit	Value
m	mass	kg	1137
I_z	yaw moment of inertia	kgm^2	1174
L	wheel base	m	2.5
h	height of CM	m	0.317
l_f	distance of CM to front axle	m	1.18
l_r	distance of CM to rear axle	m	1.313
μ_{max}	tyre-road friction coefficient	-	1
η_f	front tyre cornering coefficient	rad^{-1}	24
η_r	rear tyre cornering coefficient	rad^{-1}	30

Linear Tyre Model and Limit Friction circle

A linear tyre model with cornering stiffness dependent on normal load is used, considering a quasi-steady-state approximation to normal load:

$$F_{yj} = -C_j \alpha_j, \qquad j \in [f, r] \tag{3.10}$$

$$where: \quad C_j = \eta_j F_{zj} \tag{3.11}$$

$$\alpha_f = \frac{v_y + l_f \dot{\psi}}{v_x} - \delta \tag{3.12}$$

$$\alpha_r = \frac{v_y - l_r \dot{\psi}}{v_x} \tag{3.13}$$

$$and: \quad F_{zf} = \frac{mgl_r}{L} - \frac{h}{L} m a_x \tag{3.14}$$

$$F_{zr} = \frac{mgl_f}{L} + \frac{h}{L} m a_x \tag{3.15}$$

η_j is the tyre cornering coefficient, α_j is the tyre slip angle, F_{zj} is the axle normal load and F_{yj} is the axle lateral force on front and rear. g is the gravitational acceleration constant, L is the wheelbase, h is the height of the CM.

Longitudinal and lateral forces are coupled and saturated at the limit by friction circle constraints and front and rear:

$$\left(\frac{F_{xj}}{F_j}\right)^2 + \left(\frac{F_{xj}}{F_j}\right)^2 \leq \mu_{max}^2 \tag{3.16}$$

$$F_j = \mu_{max} F_{zj} \tag{3.17}$$

where μ_{max} is the tyre-road coefficient.

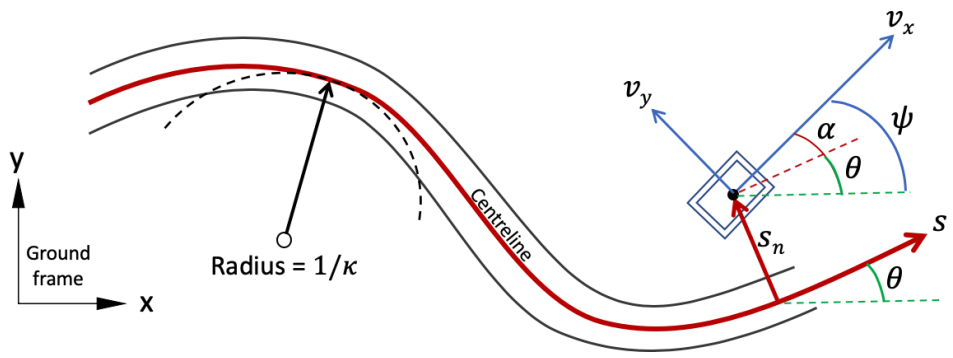

Figure 3.2: Curvilinear coordinates for road tracking.

3.4.2 Road Tracking model

The roads are considered similar to strips and could be described by specifying x, y coordinates of the road centreline and lateral width [73]. The curvilinear coordinates approach have been used in many research works to provide a compact way of describing the vehicle's progress and constraining it to remain within the road boundaries [64]. It is the most effective way to describe road centreline using only the line curvature (κ) as a function of length (s), [65] as presented in Figure 3.2. The road heading angle θ as well as x, y coordinates may be calculated as follows:

$$\frac{d\theta}{ds} = \kappa(s), \qquad \frac{dx}{ds} = cos\theta, \qquad \frac{dy}{ds} = sin\theta \tag{3.18}$$

The main advantage of curvilinear coordinates approach is their usage in tracking the orientation of the vehicle based on forward (v_x) and lateral velocity(v_y):

$$\dot{s} = \frac{v_x cos\alpha - v_y sin\alpha}{1 - s_n\kappa} \tag{3.19}$$

$$\dot{s}_n = v_x sin\alpha + v_y cos\alpha \tag{3.20}$$

$$\dot{\alpha} = \dot{\psi} - \dot{s}\kappa \tag{3.21}$$

where $\dot{\psi}$ is the yaw rate; s and s_n are the longitudinal and lateral position on the road strip; α is the vehicle relative heading to the road.

3.5 Mathematical Formulation

In summary, the Equations of motion of the point mass vehicle dynamics can be summarised as general state-space form:

$$\dot{\mathbf{x}} = f[\ \mathbf{x}(t),\ \mathbf{u}(t)] \tag{3.22}$$

where $\mathbf{u}$ is the control vector, $\mathbf{x}$ is the state variable vector, and t is the elapsed time. The state and control vectors for the vehicle model configurations are:

$$\mathbf{x}(t) = [v_x(t), v_y(t), s(t), s_n(t), \alpha(t), x(t), y(t), \theta(t)]^\top \tag{3.23}$$

$$\mathbf{u}(t) = [a_x(t), a_y(t)]^\top \tag{3.24}$$

3.5.1 Cost functions

There are three cost functions in this work. They are the objective for seeking minimum time J_T , and two objectives are for seeking minimum motion sickness: J_{IR} from empirical approach and J_{SV} based on Bos's SVC conflict model. For seeking minimum time manoeuvre, the objective function is expressed as:

$$J_T(t) = \int_{t_0}^{t_f} dt \tag{3.25}$$

For seeking minimum motion sickness, each approach which is described in Chapter 2 as the methods for motion sickness evaluation will be used for comparison. Hence, the objective function for illness rating based on empirical approach is given as :

$$J_{IR}(t) = K \times \left[\left(\int_{t_0}^{t_f} k_x^2 a_{x,w}^2(t) dt \right)^{\frac{1}{2}} + \left(\int_{t_0}^{t_f} k_y^2 a_{y,w}^2(t) dt \right)^{\frac{1}{2}} \right] \tag{3.26}$$

On the other hand, the objective function for motion sickness based on 1 DOF-SVC model is given as:

$$J_{SV}(t) = \left(\int_{t_0}^{t_f} V_c^2(t) a_x^2(t) dt \right)^{\frac{1}{2}} + \left(\int_{t_0}^{t_f} V_c^2(t) a_y^2(t) dt \right)^{\frac{1}{2}} \tag{3.27}$$

where V_c is the filter dynamics in time domain, a_x and a_y are the longitudinal and lateral acceleration. This is obtained by differentiating the conflict Δv in Chapter 2 and taking the r.m.s value to compute the sickness over the time period.

3.5.2 Change of independent variable

The distance travelled and the time are related closely however both are independent variables, therefore using time or distance travelled in the optimal control problems formulation would have no effect on the solution. Therefore using the 'distance travelled' as the independent variable has the advantage of maintaining an explicit connection with the track position, as well as reducing the number of problem variables. Following the approach used in many research works [64, 65, 75], it is convenient to change the independent variable from time (t) to distance (s) in the Equations of motion (3.22). This transformation is based on the following derivation rule:

$$\dot{x} = \frac{dx}{dt} = \frac{dx}{ds}\frac{ds}{dt} = x'\dot{s} = x'\gamma \tag{3.28}$$

The variable change transforms the differential Equation (3.19) into an algebraic one, that should be eliminated from the Equations of motion in Equation (3.22). Similarly, the variable s no longer belongs to the state vector. The variable t is re-introduced as a state to allow analysis as a function of time to be performed by writing Equation (3.19) as (3.36):

$$\frac{dt}{ds} = t' = \frac{1}{\gamma} = \frac{1 - s_n\kappa}{v_x cos\alpha - v_y sin\alpha} \tag{3.29}$$

Therefore, in s distance domain, the state variables $\mathbf{x}$ and control inputs $\mathbf{u}$ can be summarised as:

$$\mathbf{x}(s) = [v_x(s), v_y(s), s_n(s), \alpha(s), x(s), y(s), \theta(s), t(s)]^\top \tag{3.30}$$

$$\mathbf{u}(s) = [a_x(s), a_y(s)]^\top \tag{3.31}$$

The time domain Equation (3.22) is then transformed into the distance domain as given in Equation (3.32):

$$\gamma\mathbf{x}'(s) = f[(\mathbf{x}(s), \mathbf{u}(s)] \tag{3.32}$$

The OCP now seeks to find the control vector sequence to minimise the cost function:

$$J = \phi[\mathbf{x}(s_0, s_f)] + \int_{s_0}^{s_f} L[\mathbf{x}(s), \mathbf{u}(s)] \tag{3.33}$$

subject to system dynamics in Equation 3.32 , initial and final conditions:

$$\mathbf{x}(s_0) = \mathbf{x}_0, \qquad \mathbf{x}(s_f) = \mathbf{x}_f \tag{3.34}$$

and equality and inequality constraints:

$$\mathbf{g}[(\mathbf{x}(s), \mathbf{u}(s)] = 0, \qquad \mathbf{h}[(\mathbf{x}(s), \mathbf{u}(s)] \leq 0 \tag{3.35}$$

Tthe cost function can be represented only by the Lagrange integral and mapping the dynamics equations from the independent variable of time to distance along the road centreline such that the equation 3.25 becomes :

$$J_T(t) = \int_{t_0}^{t_f} dt \qquad \longmapsto \qquad J_T(s) = \int_{s_0}^{s_f} \frac{1}{\dot{s}} ds \tag{3.36}$$

Similarly equations 3.26 and 3.27 in distance domain are given as:

$$J_{IR}(s) = K \times \left[\left(\int_{s_0}^{s_f} \frac{k_x^2 a_{x,w}^2(s)}{\dot{s}} ds \right)^{\frac{1}{2}} + \left(\int_{s_0}^{s_f} \frac{k_y^2 a_{y,w}^2(s)}{\dot{s}} ds \right)^{\frac{1}{2}} \right] \tag{3.37}$$

$$J_{SV}(s) = \left(\int_{s_0}^{s_f} \frac{V_c^2(s) a_x^2(s)}{\dot{s}} ds \right)^{\frac{1}{2}} + \left(\int_{s_0}^{s_f} \frac{V_c^2(s) a_y^2(s)}{\dot{s}} ds \right)^{\frac{1}{2}} \tag{3.38}$$

3.5.3 Constraints and Boundary conditions

In addition, the five inequality constraints in Equations (3.39, 3.40, 3.41, 3.42 and 3.43) will be considered, such that the vehicle will be able to accelerate within the bounds Equation (3.39) set by the friction circle with a_{max} equal to 1g (9.81 ms^2), i.e., the maximum absolute acceleration that the vehicle is constrained to reach. The input accelerations are also bounded between minimum acceleration and maximum acceleration given in Equation (3.40) for longitudinal acceleration and in Equation (3.41) for lateral acceleration. Also, it will be bounded to never exceed the road borders considering left-width (R_w) and right-width ($-R_w$) from the centreline of the road Equation (3.42). In a point mass model, the lateral velocity, v_y is assumed to as zero as no slip is consider, hence the only acting velocity is v_x is considered as u and it is bounded by a minimum speed u_{min} and

a maximum speed u_{max} in Equation(3.43).

$$\sqrt{{a_x}^2 + {a_y}^2} \leqslant a_{max} \tag{3.39}$$

$$a_{x_{min}} \leqslant a_x \leqslant a_{x_{max}} \tag{3.40}$$

$$a_{y_{min}} \leqslant a_y \leqslant a_{y_{max}} \tag{3.41}$$

$$-R_w \leqslant s_n \leqslant R_w \tag{3.42}$$

$$u_{min} \leqslant u \leqslant u_{max} \tag{3.43}$$

Although, one additional equality constraint is required for the case when only motion sickness minimisation is consider in the subsection 3.6.2. It is given in Equation 3.44:

$$t_f = T_{demand} \tag{3.44}$$

where t_f is the final arrival time must be the same as the T_{demand}, fixed journey time. Boundary conditions have been added, in order to achieve the best possible optimal solution, with minimum speed is set as u_{min}= 5 [m/s]. The summary of boundary conditions required to keep the vehicle within the road boundary, and to start the manoeuvre in a straight line with no lateral velocity are given in Table 3.2 and 3.3.

Table 3.2: Boundary conditions for minimum time case study

$\mathbf{x}$	$\mathbf{x}_0$	$\mathbf{x}_f$
s	0	s_f
v_x	v_0	free
v_y	0	free
s_n	0	free
α	0	free
x	0	free
y	0	free
θ	$\pi/2$	free
t	0	free

3.5.4 Trajectory tracking control

The trajectory tracking control system consists of two controllers responsible for the longitudinal and lateral control of the vehicle. Both controllers are based on PID controls.

Table 3.3: Boundary conditions for motion sickness minimisation case study

$\mathbf{x}$	$\mathbf{x}_0$	$\mathbf{x}_f$
s	0	s_f
v_x	v_0	free
v_y	0	free
s_n	0	free
α	0	free
x	0	free
y	0	free
θ	$\pi/2$	free
t	0	t_f

A look up table will be generated from the optimal solutions from motion planning layer before simulation, containing the state variables such as heading ψ , x and y positions, velocity v of the entire reference path as a functions of the progress s (distance domain).

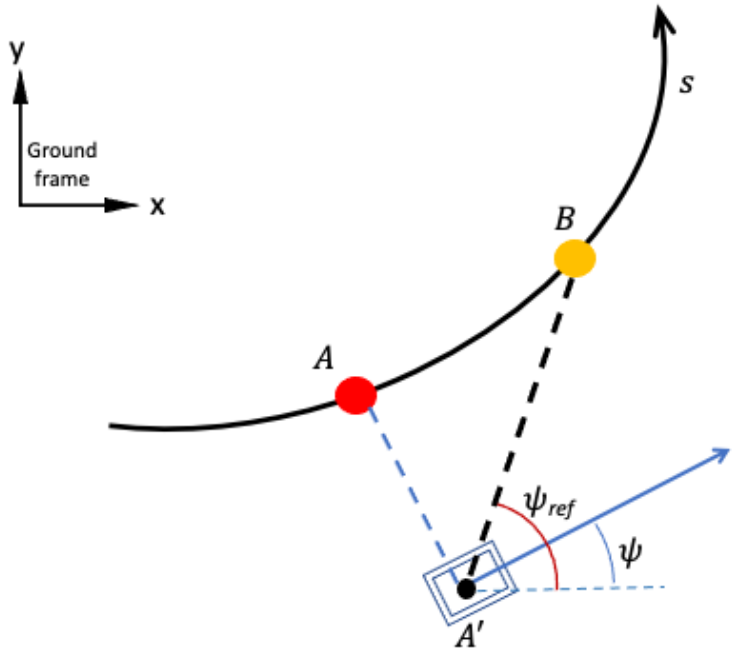

Figure 3.3: Projection point $A^{'}$ and look-ahead point B on the reference path.

For lateral controller, as shown in Figure. 3.3, point A refer to vehicle position, and point $A^{'}$ is the projection point of the vehicle on the reference path. Point B is a look ahead point on the reference path ahead of point $A^{'}$, and the trajectory distance between B and $A^{'}$ refers to look-ahead distance, L_d. The look-ahead is proportional to the velocity

of the vehicle is given in Equation 3.45 as:

$$L_d = v \times t \tag{3.45}$$

where t is a tunable look-ahead time horizon. In this work, a look-ahead time horizon of 0.2 seconds is used which gives good tracking performance. For the lateral control law, using the approach found in [76] for determining the current reference angle, the vehicle tracking the heading angle of line $A^{'}B$ is given as:

$$\psi_{ref} = \tan^{-1}\left(\frac{y_B - y_{A'}}{x_B - x_{A'}}\right) \tag{3.46}$$

The benefit of this approach is that the lateral tracking error and yaw tracking error can be integrated such that the lateral path tracking control can be carried out with one PID controller. The heading error e_ψ of the vehicle is then given as Equation 3.47:

$$e_\psi = \psi_{ref} - \psi \tag{3.47}$$

Therefore, the steering angle can be calculated in Equation 3.48 as:

$$\delta(t) = K_p e_\psi(t) + \int K_i e_\psi(t) + K_d \frac{de_\psi(t)}{dt} \tag{3.48}$$

Although, the selection of the look-ahead distance is crucial, too large or small look-ahead distance would result in overshoot, oscillation and not promptly reducing error in the tracking control.

Similarly for the longitudinal speed controller, the corresponding reference velocity v_{ref} at the progress point A can be obtained from the look-up table. Therefore, the velocity tracking error e_v is given in Equation 3.49 as:

$$e_v = v_{ref} - v \tag{3.49}$$

and the demand longitudinal acceleration input can be calculated using Equation 3.50:

$$a_x(t) = K_p e_v(t) + \int K_i e_v(t) + K_d \frac{de_v(t)}{dt} \tag{3.50}$$

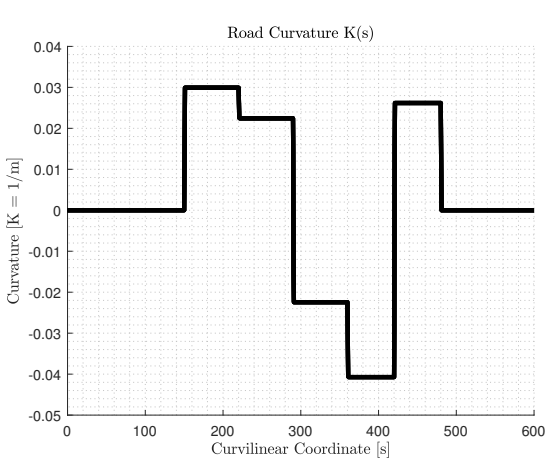

(a)

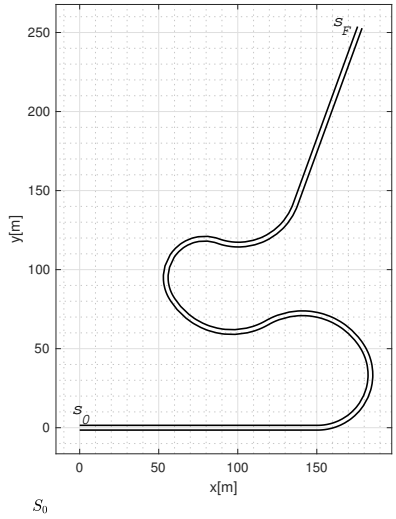

(b)

Figure 3.4: Road track generation (a) Road curvature over the curvilinear coordinate, (b) Trajectory of the road path showing s_0 the starting point and s_f the end point.

3.5.5 Road track generation

The work considers horizontal flat road with normal curvature and under the assumption that gravity is always normal to the road surface. As far as the road path is concerned, it is generated by a series of curvature κ over a distance s, to form a path which consists of straight line and curves. This road track is given in Figure 3.4. In addition, two road path scenarios are proposed, which consider different road widths for the same road track. This is to investigate whether road width would have an effect on the saving the journey time or reducing the sickness. The first scenario (fixed path) doesn't allow any lateral manoeuvrability to the vehicle by setting the road width at zero (i.e. the road boundary of left border and right border measured from the centreline $L_w, R_w = 0m$). In this way, the vehicle travels on the fixed road path. On the other hand, in the second scenario (free path), the road width is increased ($L_w, R_w = 1.5m$), and hence manoeuvrability is offered to the vehicle to move along the lateral axis within the road borders.

3.6 Case studies and results

The objective of this work will be focused on investigating the two cases studies: where the motion planning approach for minimum time problem and motion sickness minimisation problem in automated vehicles. At the same time, mentioned in the subsection 3.5.5, both case studies will use the same road track with two road path scenarios. The two

case studies can be described as below:

1. A minimum time solution without considering motion sickness is first carried out and its result is used as a baseline for comparison.

2. The minimisation of motion sickness is investigated for a set of fixed time (i.e (T_{demand}) with an interval of 5 seconds ranging from 30 seconds to 75 seconds. In addition, a comparison for the optimal solutions obtained from each motion sickness objective is also presented.

The output of the optimal solutions from both cases studies are plotted all together shaping four Pareto frontiers in Figure 3.9. The simulation results for each road scenario (fixed, free) are tabulated in Table B.3 in which the illness rating is compared at four different journey time cases (minimum time, 30 seconds, 45 seconds, and 74 seconds). Then the extensive comparison of four cases is conducted and their accumulated illness rating curve over the journey time are plotted together in Figure 3.10.The optimum motion profiles, G-G diagrams, and trajectories of each scenario for minimum time case study are illustrated in Figures 3.5, 3.7 and 3.8. Similarly, in motion sickness minimisation case, the optimum motion profiles, and G-G diagrams of each road scenario for four different journey time are given in Figures 3.11, 3.12, 3.13 and 3.14.

3.6.1 Minimum time manovering

The motion planning problem in seeking minimum time for the automated vehicles to complete the road journey, the objective function in Equation 3.36 is used for the optimisation to obtain the optimum motion profiles. The journey time for fixed path is 28.13 seconds whereas 25.74 seconds for free path scenario. The saving of the journey time is due to the fact the fact that the vehicles can take the advantage from the road width. This is shown in Figure 3.5, as expected when the path is fixed the vehicle travels along the road centre line whereas the vehicles in free road path can take a different trajectory rather than in a fixed manner. Especially when manovering along the turns, the vehicles travel with a smaller turning radius with overall higher speed compare with fixed path. This is given in Figure 3.6.

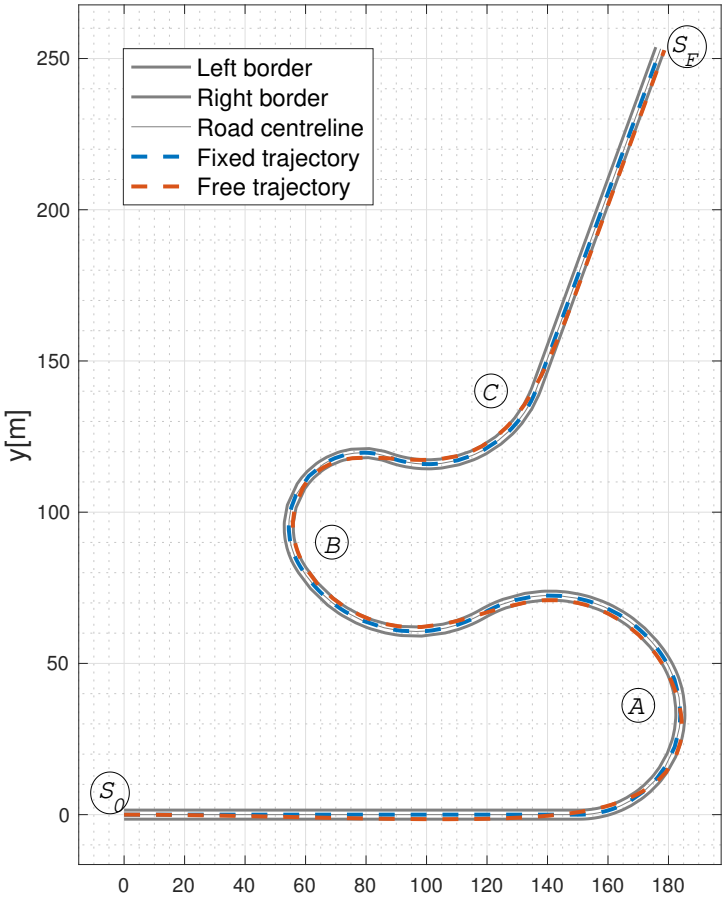

Figure 3.5: Trajectory of the road path comparing two road path scenarios

The motion profiles in Figure 3.7 are consistent in both scenarios, however the velocity and accelerations profile for the whole journey are smoother in free path. As expected, in the minimum time solution the vehicles travel in the velocity potential with rapid change in acceleration during the transition before or after initiating a turn as shown in Fig. 3.12 for both road paths. On the other had, the G-G diagram containing of both lateral and longitudinal accelerations in Figure 3.8 shown that the vehicle is operating within vehicle dynamics limits (i.e., the dynamics feasibility is satisfied). However, the points are mostly scatter around the circumference of the circle indicate that the vehicle dynamics is being push to the maximum limits. This is often for case in lap time simulation problem in race car [73, 74].

Nevertheless, this case study provides a baseline solution for the motion sickness case study. The minimum time solutions mean the fastest journey time achievable within the boundary of dynamics stability limits. At the same, the motion sickness felt by the passengers would be expected to be dreadful due to the rapid changes in the motion

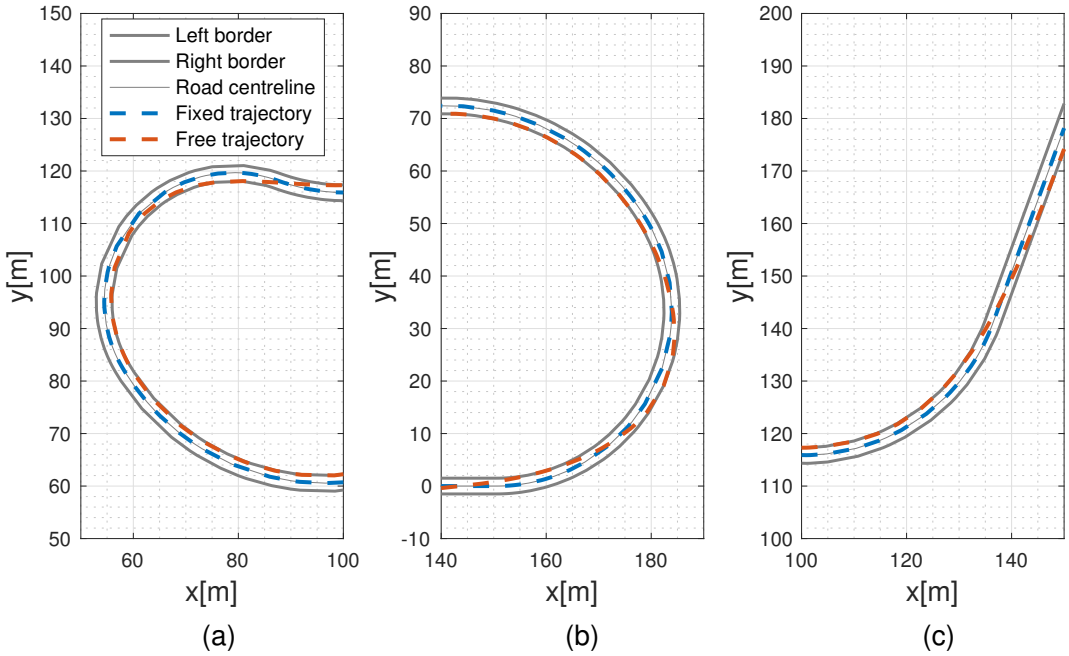

Figure 3.6: Trajectory of the road path comparing two road path scenarios showing section (a) B turn (b) A turn (c) C turn

profiles which ultimately causes low frequency motion. This is discussed in the next case study.

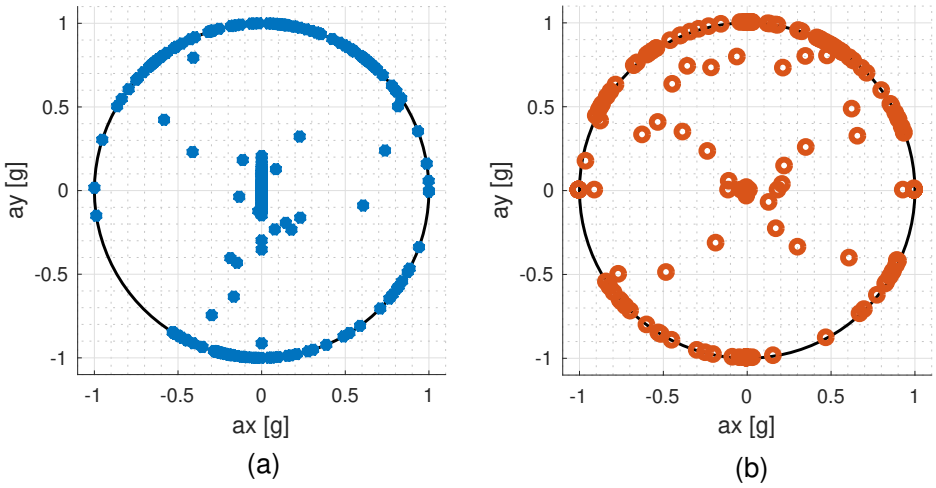

Figure 3.8: G-G diagram showing (a) free road path scenarios (b) fixed road path senarios

.

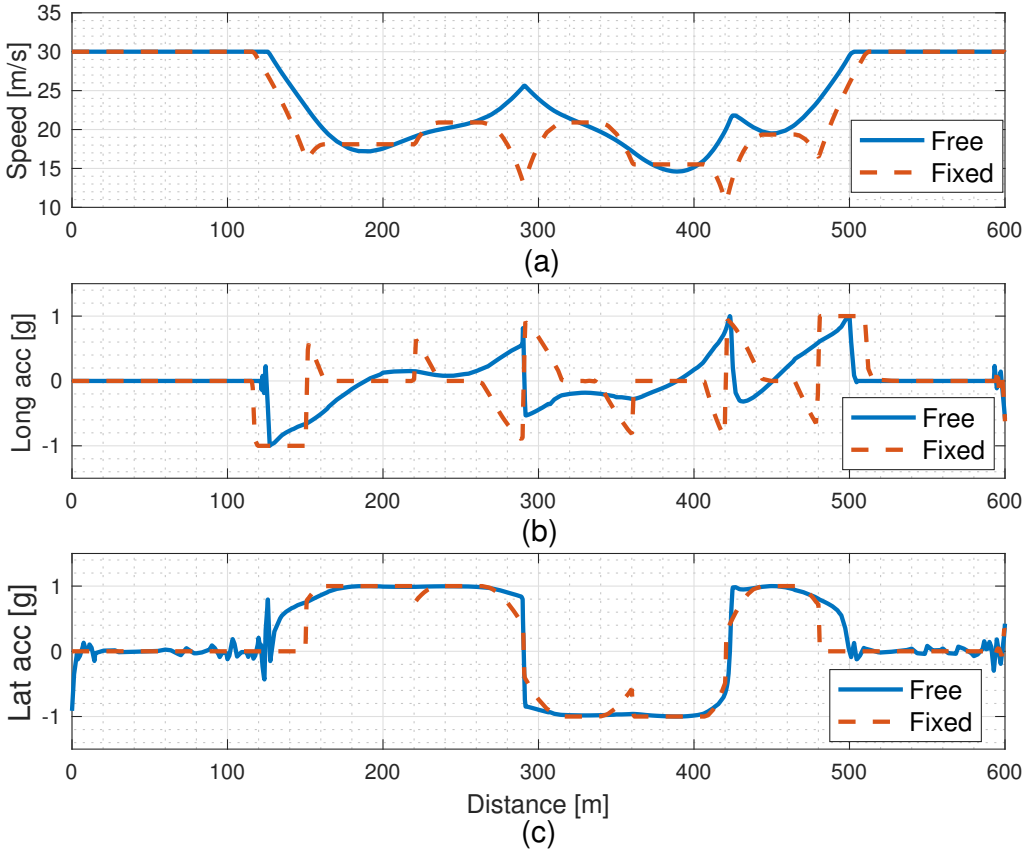

Figure 3.7: Optimum motion profiles for minimum journey time for two road scenarios. (a) Velocity profile (b) longitudinal acceleration, and (c) lateral acceleration

3.6.2 Motion sickness minimisation

The aim of this case study is to minimise motion sickness based on at particular fixed journey time (T_{demand}). In other word, the motion planning problem can be described as:

"What is the optimal velocity (motion) profiles that automated vehicles should follows in order to minimise motion sickness for a particular fixed journey time? "

Therefore, motion sickness objective is selected as the cost function for the OCP formulation. However, since two approaches for motion sickness estimated have been proposed in this work. The OCP will perform the optimisation for each approach (i.e., empirical approach in Equation 4.11) and sensory conflict approach in Equation 3.38). Similarly, two road scenarios on the same road track will be used for comparison.
Four Pareto frontiers are formed when plotting all the optimal solutions obtained from

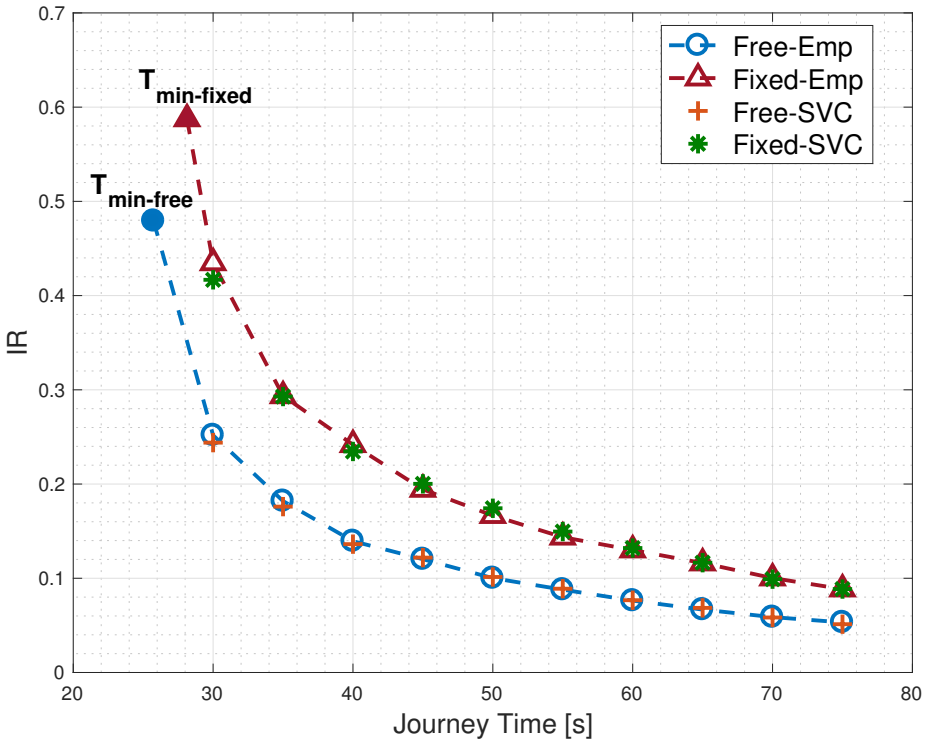

Figure 3.9: Pareto fronts containing two road width cases for each motion sickness modelling. (Emp) stand for empirical approach and (SVC) for subjective vertical conflict approach

different fixed journey times, and also including the result from minimum time case study. In Figure .3.9, It can be seen that there is minimal differences in the optimal solutions obtained from empirical methods and SVC model. This is because in OPC problem, the optimisation focuses on minimising the accelerations which are the control variables found in the cost functions. Therefore, the discussion of the result will be focus on empirical approach for the two road scenarios.

The first data points in each front have been obtained from minimum time solution. The remaining data points in the front are generated by changing the fixed journey time T_{demand}. The illness rating decreases when the journey time taken to complete journey increases. In addition, the shift in Pareto front occurs when the flexibility of the road width is introduced to the road, hence allowing manoeuvrability to the vehicle.
In Figure 3.10, the accumulated illness rating for minimum time solution increases rapidly up to maximum illness rating due to the fact that it is seeking only the fastest journey time. Therefore, harsh accelerating occurs especially when the vehicle is driving through the turn, where contribution of sudden change in both longitudinal and lateral accelera-

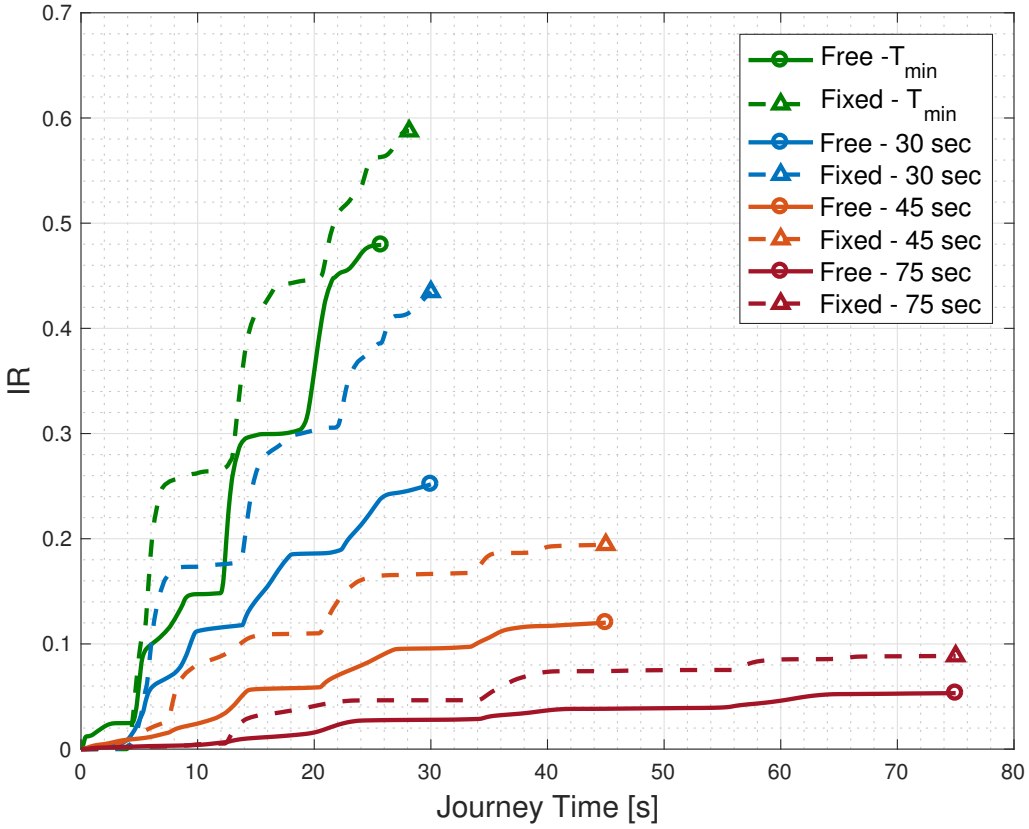

Figure 3.10: Cumulative Illness rating curves containing minimum time and selected fixed journey time.

tion are higher which can be seen in Figure 3.7. On the other hand when journey time is predefined and the objective is shifted to minimise motion sickness, the illness rating for 45 sec has dramatically decreased and further more in the case of 75 sec. Hence, the slower and smoother the vehicles travel, the lesser motion sickness could occur.

Table 3.4: Comparison of illness rating

Journey time	IR_{Fixed}	IR_{Free}
30 sec	0.4348	0.2517
45 sec	0.1943	0.1202
75 sec	0.0885	0.0532

To investigate whether the benefit of road width can contribute for reducing motion sickness. In this respect, the discussion will focus on the three fixed journey time (i.e., 30, 45 and 75 seconds). Since it is more comparable in term the fixed arrival time for the

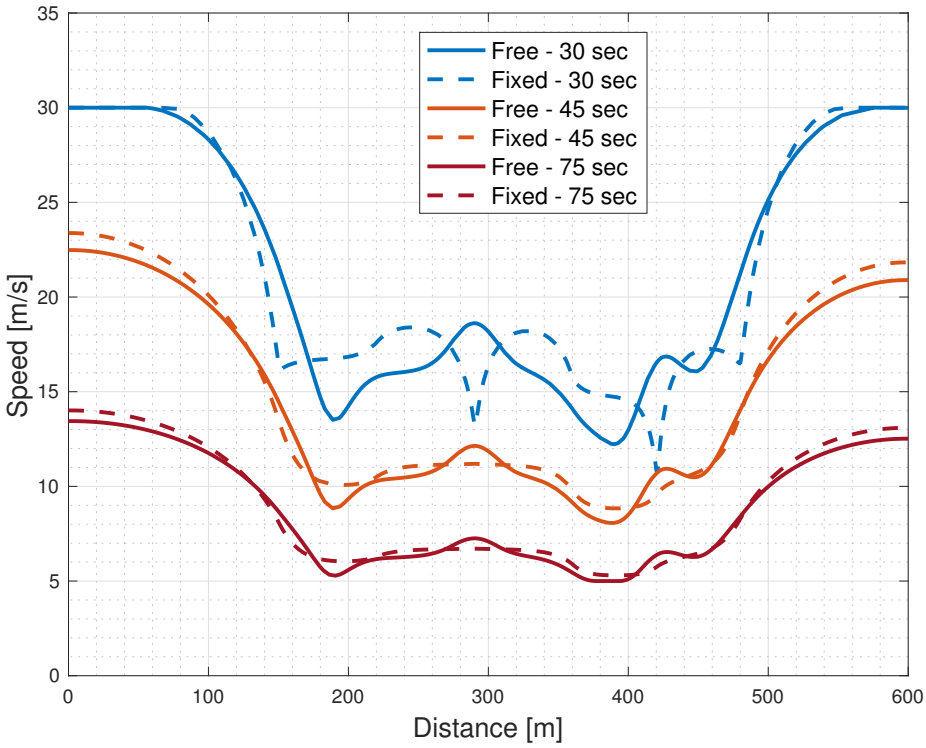

Figure 3.11: Optimum velocity profile over the road distance for all scenarios in three fixed journey time.

road width scenario. The comparison of illness rating for the two road scenarios can be seen in Table 3.4. In the fixed path scenario, it has relatively higher illness rating for the same arrival time compared with free road path due to the limitation on the road width being zero, while trying to minimum sickness at the same time to meet the target arrival time. This has led to a significant reduction of illness rating about 30% from a fixed road path. Comparing different arrival time, it is clear that the illness rating decreases when the journey time is increased.

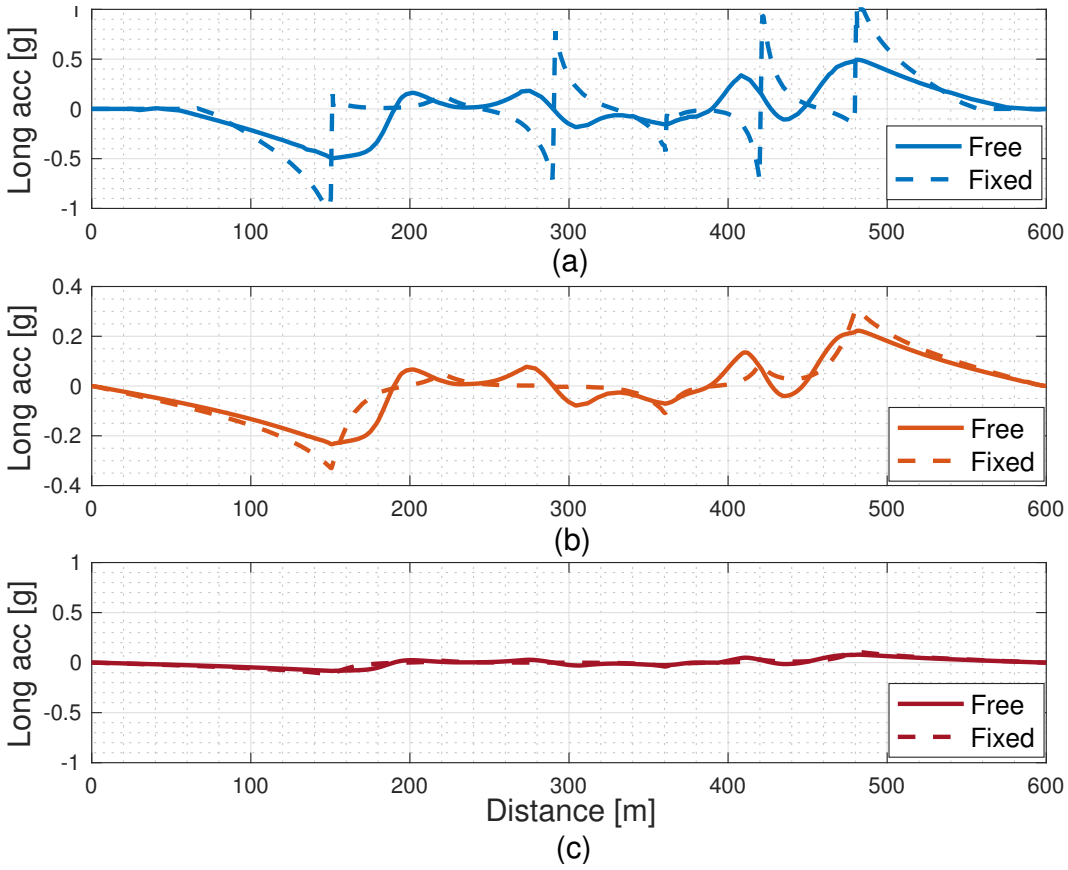

Figure 3.12: Optimum longitudinal acceleration control input over the road distance comparing fixed and free road cases, (a) 30 seconds (b) 45 seconds (c) 75 seconds

The motion profiles such as velocity profile in Figure 3.11, longitudinal acceleration in Figure 3.12, and lateral acceleration in Figure 3.13 are all consistent between fixed and free road path for the three fixed journey time. It can be concluded that free path gives smoother motion profiles and causes less motion sickness since harsh and rapid change in accelerations are significantly less. In addition, vehicle could travel with over all higher speed and maintain lower lateral acceleration by taking a smaller turning radius provided through the road width flexibility. The vehicle will have to travel with higher speed when T_{demand} is smaller which then result in higher sickness compare with larger T_{demand}. In the G-G diagram in Figure 3.14, the boundary is moving away from the circumference and moves toward the centre of the circle when the journey time is increased and also the data points are less scatter in free road path. In this respect, we can conclude that the road width can also benefit in reducing sickness and achieving same arrival time compared with fixed road. Moreover, it improves the vehicle stability.

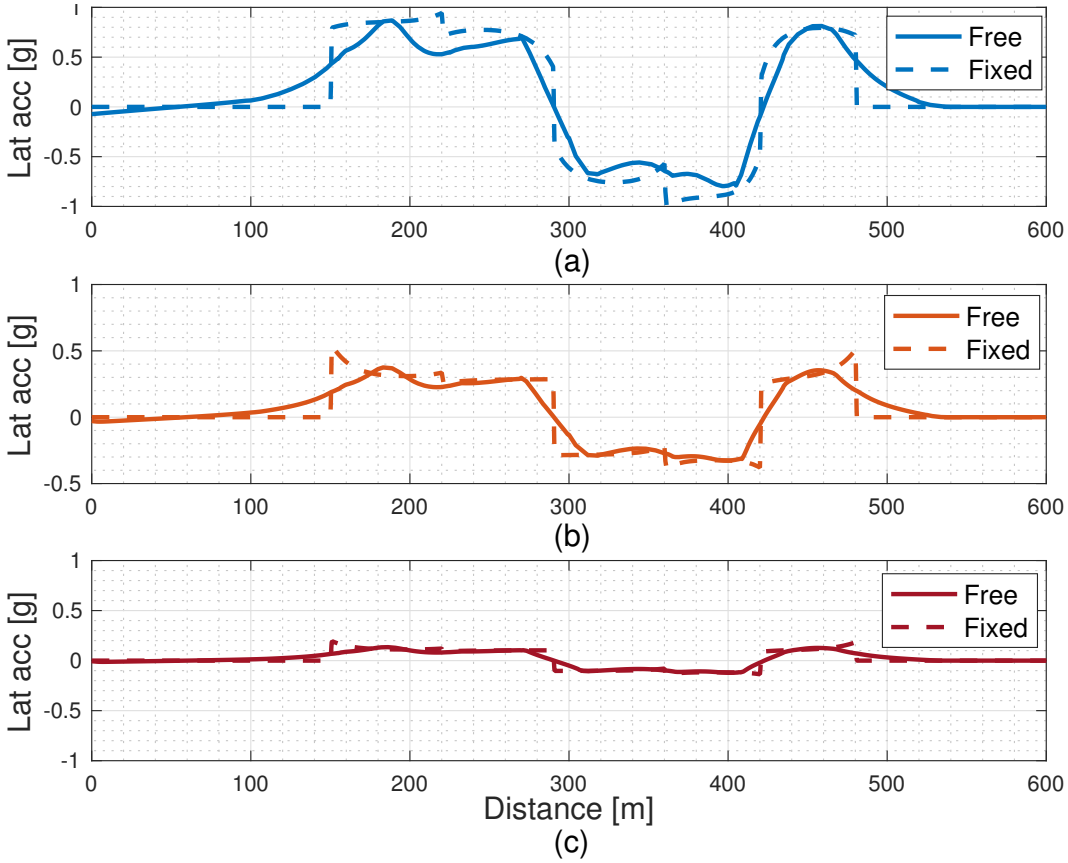

Figure 3.13: Optimum lateral acceleration control input over the road distance comparing fixed and free road cases, (a) 30 seconds (b) 45 seconds (c) 75 seconds

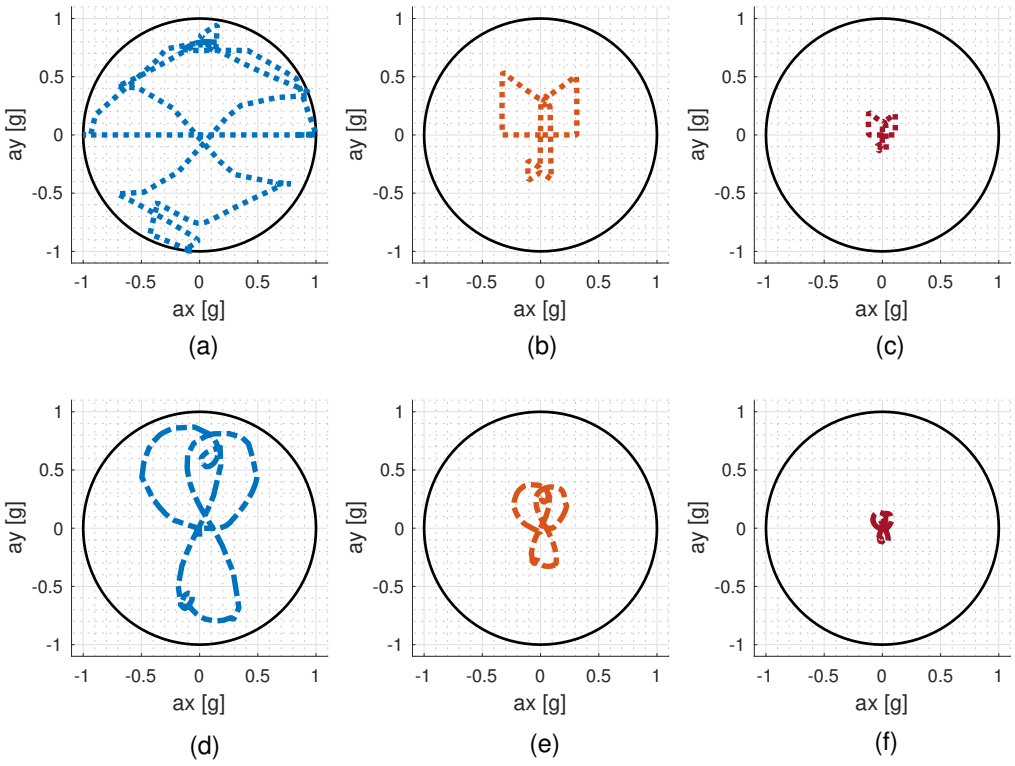

Figure 3.14: G-G diagram showing all three fixed journey time cases in both road with scenarios, (a) 30 seconds (b) 45 seconds (c) 75 seconds are the fixed path scenario, and (d) 30 seconds (e) 45 seconds (f) 75 seconds are the free path scenario.

3.7 Validations

It is critical that the optimal trajectory generated by motion planner is trackable by the low level feedback control, otherwise automated vehicle would not be able to perform such task. Therefore, this section will validate whether the optimal trajectory is dynamically feasible in the context of tracking control. Hence, the trajectory tracking control system described in previous section is used for simulating the optimal trajectory in the 3 DOF single-track vehicle model. In this respect, the optimal solution based on the various fixed journey time (i.e., $t_{demand} = [30, 45,...75]$) will be used for investigating the tracking control.

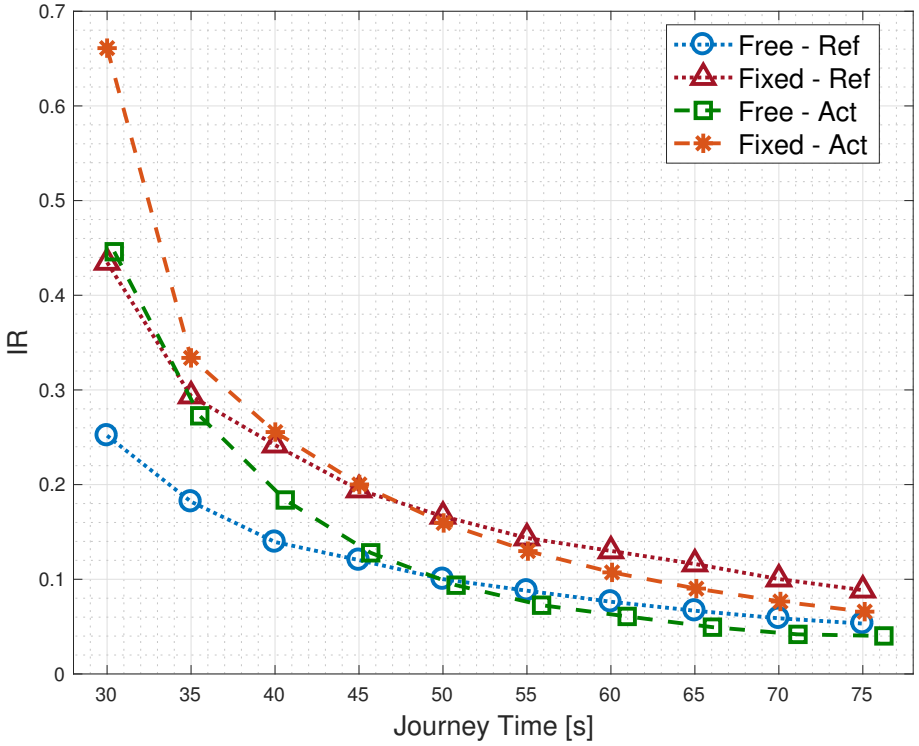

Figure 3.15: Comparison of the Pareto fronts between the reference trajectory and the tracked solutions under empirical approach, where (Ref) stand for reference trajectory and (Act) stand for tracked solution by the feedback controller.

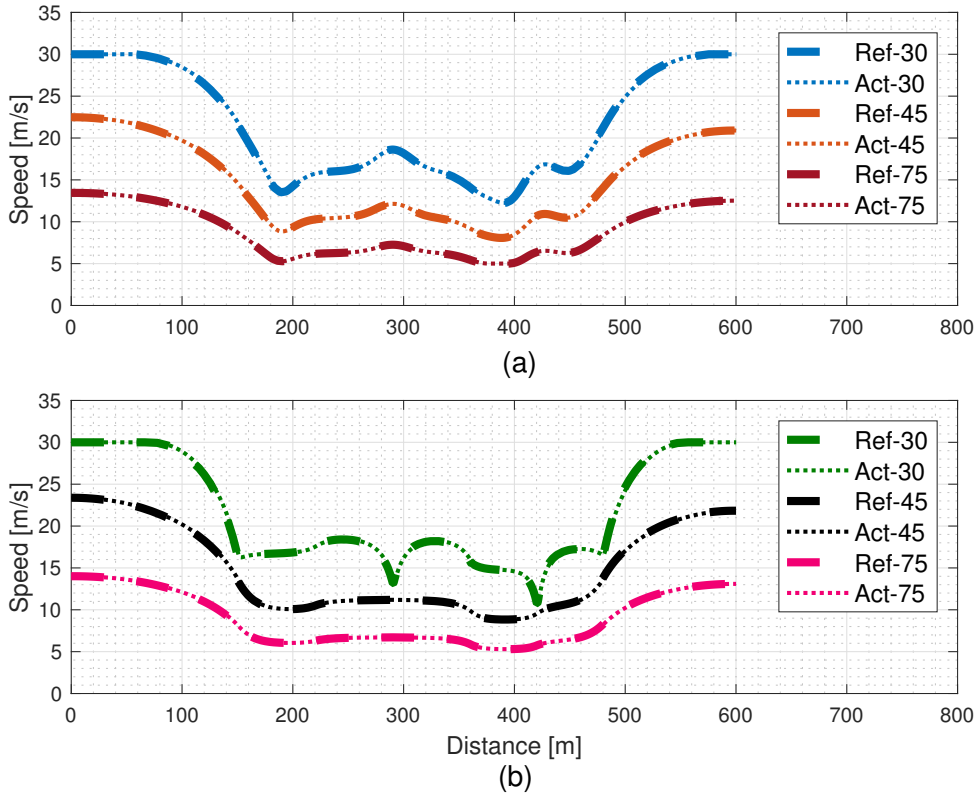

Figure 3.16: Comparison of tracked and references optimum velocity profile over the road distance for three fixed journey time, (a) Free road width (b) Fixed road path

The velocity profile in Figure 3.16 and the path trajectory in Figure 3.17 illustrate that the tracking controllers provide a good tracking performance. The reference velocity profile are smoothly tracked and highly consistent in both road scenarios. This is further seen in accelerations profile in Figure 3.18 and Figure 3.19. However, the Pareto fronts in Figure 3.15 shown that the are some variations in motion sickness between reference motion sickness and the actual tracked sickness around 30s to 40s for both road scenarios. It is particularly at 30s in the fixed road case, its illness rating is an extreme point. This is due to the simplicity of the vehicle model used in the OCP problem compare with the single track vehicle model. Overall, the optimal trajectory solutions from the motion planner are tracked by the controllers. This implies a feasible solution and validate the motion planning algorithm.

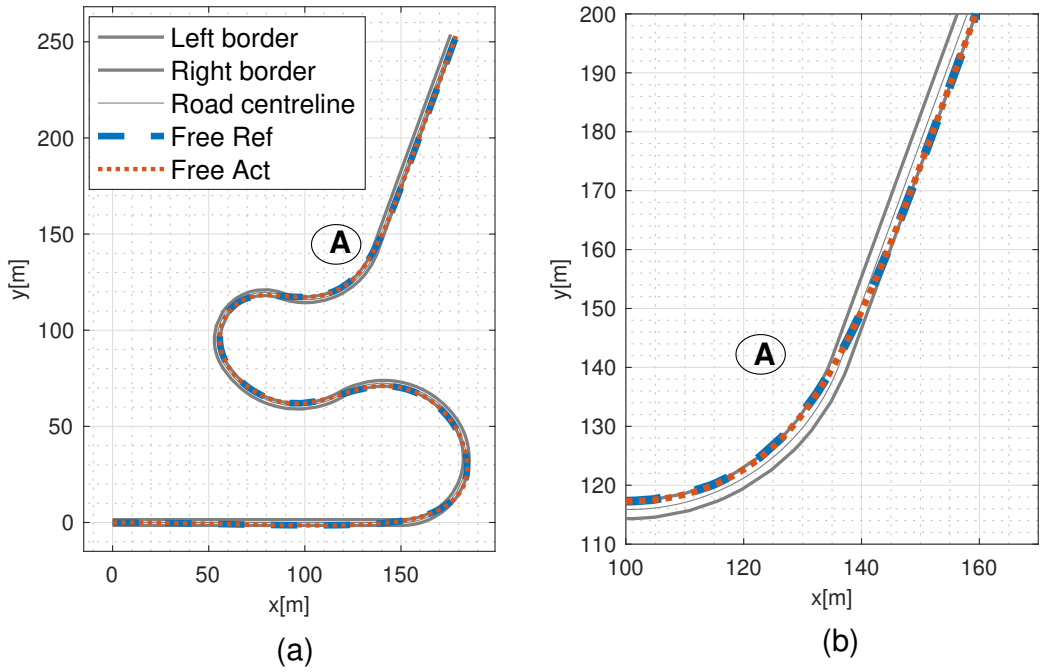

Figure 3.17: Path tracking show good performances as the reference path was tracked nicely by the controller where no deviation can be seen in the road trajectory.

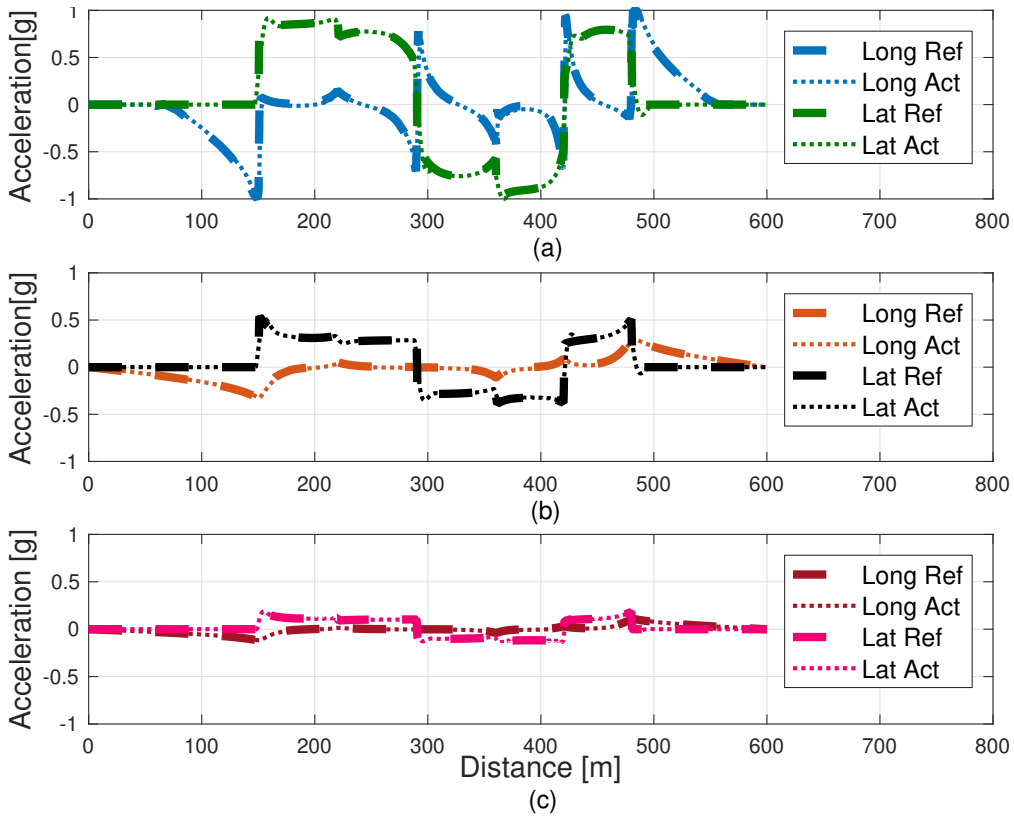

Figure 3.18: Optimum acceleration control input over the road distance in fixed road path comparing Ref and Act, (a) 30 seconds (b) 45 seconds (c) 75 seconds

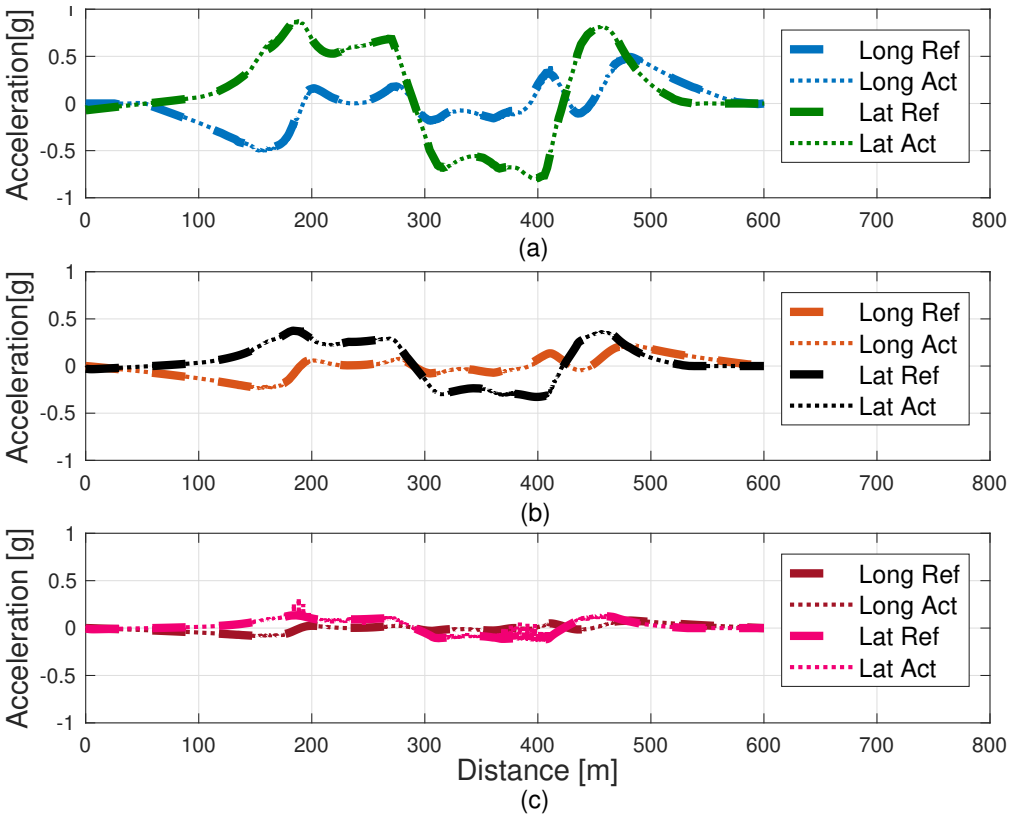

Figure 3.19: Optimum acceleration control input over the road distance in free road path comparing Ref and Act, (a) 30 seconds (b) 45 seconds (c) 75 seconds

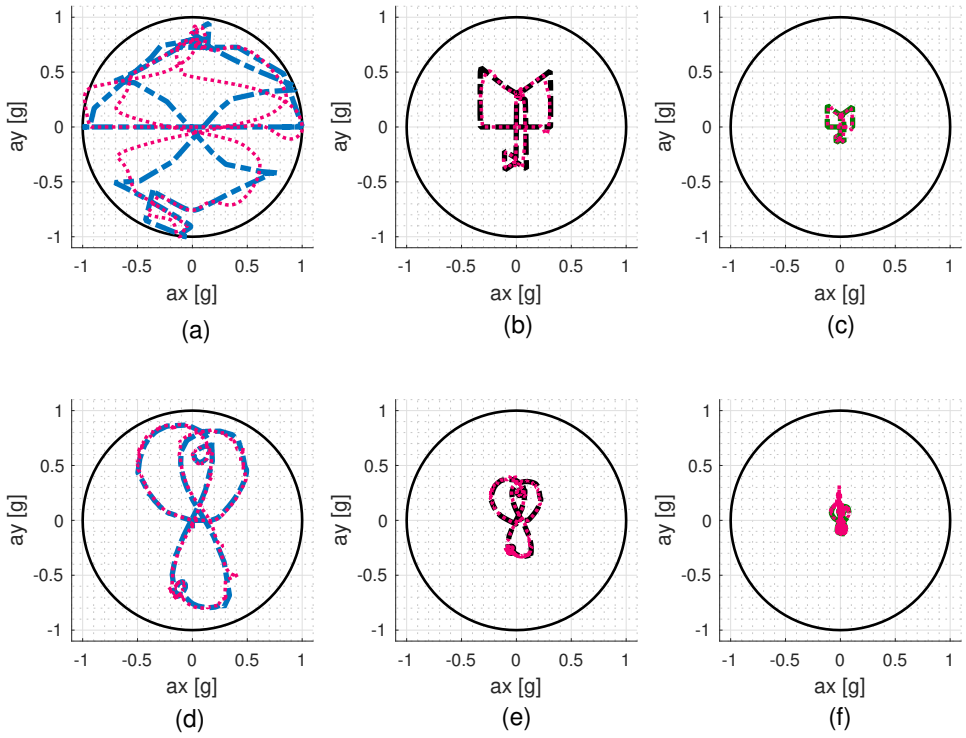

Figure 3.20: G-G diagram showing all three fixed journey time cases in both road with scenarios, where pink line are the solution by the controller, (a) 30 seconds (b) 45 seconds (c) 75 seconds are the fixed path scenario, and (d) 30 seconds (e) 45 seconds (f) 75 seconds are the free path scenario.

3.8 Conclusions

The application motion planning for automated vehicle has been successfully implemented in respect to motion sickness minimisation under a fixed journey time constraint. Motion sickness is minimised by taking the optimum trajectory and velocity profile for any given road path. The road-width flexibility does benefit in term of saving the journey time and reducing motion sickness. However, the illness rating and journey time are relatively small, due to the road track is short. Therefore, a more realistic road length with different road characteristic should be included for the in the future study. The optimal solutions from both motion sickness models are very similar, since the accelerations are the key variables in the cost function. The results also clearly illustrated that motion sickness and journey time are in conflicting with each other. Therefore, in order to achieve optimal solution for both minimum sickness as well as journey time their influences on the Pareto fronts, it is required to investigate the weighting factor between the two and their trade off using multi-objective optimisation. On the other hand, the trajectory tracking controllers based on PID control method were able to track the reference trajectory with

good performances. However, more work on the robustness of such trajectory should be investigate since the OCP problem in this work are under several modelling assumptions and simplification, without considering any disturbance from external agents.

This page is intentionally left blank.

CHAPTER 4

Multiobjective optimisation for motion sickness minimisation in driving dynamics

4.1 Introduction

The previous chapter introduced the application of motion planning for automated vehicles using the OCP approach. However, it considered only for single objective optimisation problem (i.e., minimum time or minimum motion sickness). It has also illustrated that both objectives are in conflict with each other. This is due to the fact that when seeking minimum sickness, the vehicle would move in a slow manner, at constant velocity or come to a stop. Similarly, for minimum journey time, the vehicle would move very fast or at constant acceleration. Hence, question arise as *"how to find the compromise solutions the trade-off between the two such that both motion sickness and journey time ?"* This chapter will apply multi-objective optimisation (MOO) in the fundamentals of motion planning problem to address the above question and to highlight the important role that MOO could play when tackling such problem in automated vehicles.

4.2 Review of Multi-objectives optimisation

In control engineering, MOO has already been applied by the control community as a method to manage many objectives, which often involves conflict situations of many crite-

ria such as control energy, tracking performance, robustness, etc. An excellent summery of MOO applications in control engineering can be found in [77]. In general, most optimisation models with multiple objective are often conflicting and incommensurable, it usually becomes impossible to find an appropriate solution to obtain the optimum values of all the objectives simultaneously. Hence, the notion of Pareto optimality has been introduced to find the best comprise solutions for the decision making process [78]. The Pareto optimality criterion is used to determine the set of Pareto optimal solutions and their corresponding image form a Pareto optimal frontier or trade-off surface.

There are many algorithms for solving MOO problems in-order to obtain the Pareto optimal frontier. These algorithms can be classified in two main groups: Scalarisation methods and Pareto methods. Broad reviews can be found in [79]. The scalarisation methods require transformation of the MOO problems into a single optimisation problem (SOP), normally by using coefficients, exponents, constraint limits, etc. and then methods for single objective optimisation are utilised to search for a single solution. Computationally, these methods and a unique solution efficiently and converge quickly. However, these methods cannot discover the global Pareto solution for non-convex problems [80]. Also, it is not always obvious for the designer to know how to choose the weighting factors for the scalarisation . However, various methodologies have already been applied successfully in many engineering areas for avoid the need to pre-specify arbitrary weighting coefficient. It is also worth mentioning that these weights indicate the relative importance of the corresponding objective function but they do not mean priorities to the objective function. In scalarisation methods, the weighted sum approach is perhaps one of the commonly used methods [81,82]. It is based on adding the weighted objectives to form a single cost function, hence the name weighted sum method.

Only the weighted sum method would be used in this work since the aim is to utilise the application of MOO rather than investigating the differences between methods for solving MOO problems. This is presented in next section.

4.2.1 Multi-objective optimisation

A general multi-objective optimisation problem can be represented as the following vector mathematical programme

$$\text{optimise} \quad \mathbf{F}(x) = [f_1(x), f_2(x), \cdots f_k(x)]^\top \tag{4.1}$$

$$s.t. \quad x \in \mathbf{S} \tag{4.2}$$

$$\mathbf{S} = \left\{ x \middle| \begin{array}{ll} g_i(x) \leq 0, & i = 1, 2, ..., l \\ h_j(x) = 0, & j = 1, 2, ..., m \\ x = [x_1, x_2, \cdots x_n]^\top \end{array} \right\} \tag{4.3}$$

where $\mathbf{F}(x)$ is a vector of objectives functions, f_k is the number of nonlinear objective function, and $g_i(x)$ and $h_i(x)$ are the nonlinear inequality and equality constraint functions respectively. optimise means here either minimise or maximise depending on the application x is a vector of design variables (decision variables), where x_i is a number of independent decision variable. $\mathbf{S}$ is the feasible design space (also called feasible decision space or constraint set) which can be expressed in Equation 4.3. The feasible criterion space $\mathbf{Z}$ (also called feasible cost space or the attainable set) is defined as the set $\{\mathbf{F}(x)|x \in \mathbf{S}\}$ is illustrates in Figure 4.1.

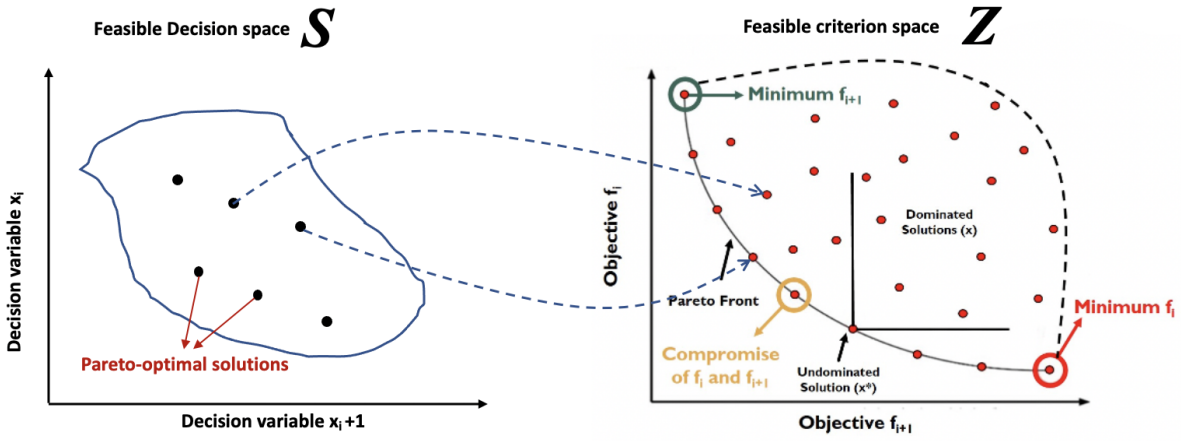

Figure 4.1: Evaluation mapping of the multiobjective problem [77].

The multiple objectives are usually incommensurate and in conflict with one another. This means that, in general, a multiple objective optimisation problem does not have

a single solution that could optimise all objectives simultaneously. Otherwise, there is no need to consider multiple objectives. Because of this, multiple objective optimisation is not to search for optimal solutions but for efficient (non-inferior, non-dominated or Pareto-optimal) solutions that can best attain the prioritised multiple objectives as greatly as possible. Such solutions are referred to as the best compromise solutions. The concept of Pareto optimality is adopted as a criterion to determine the set of Pareto optimal solutions, which is defined as follows:

Definition 4.2.1 *A point* $x^* \in \mathbf{S}$ *is called an Pareto optimal solution if there does not exist any* $x \in \mathbf{S}$ *such that* $\mathbf{F}(x) \leq \mathbf{F}(x^*)$*, and* $f_i(x) < f_i(x^*)$ *are assumed for minimisation.*

i.e., there is no way to improve upon a Pareto optimal point without increasing the value of at least one of the other objective functions. Sometimes, it is useful to have a definition for a suboptimal point that is easier to be reached by the algorithms and simultaneously is sufficient 'good' for practical applications. This is obtained from the Weakly Pareto Optimality and it is defined as follows:

Definition 4.2.2 *A point* $x^* \in \mathbf{S}$ *is called a weakly Pareto optimal solution if there does not exist any* $x \in \mathbf{S}$ *such that* $\mathbf{F}(x) < \mathbf{F}(x^*)$*, and* $f_i(x) < f_i(x^*)$ *are assumed for minimisation.*

A point is weakly Pareto optimal if there is no other point that improves all of the objective functions simultaneously. In contrast, a point is Pareto optimal if there is no other point that improves at least one objective function without detriment to another function. Pareto optimal points are weakly Pareto optimal, but weakly Pareto optimal points are not Pareto optimal.

Definition 4.2.3 *For any given problem, there may be an infinite number of Pareto optimal points, which constitute the Pareto optimal set denoted as* $\mathcal{P}$*. The image of the Pareto optimal set by* $\mathbf{F}$ *is referred to as Pareto optimal frontier or trade-off surface.*

From Figure 4.1, one can find that in a multi-objective optimisation problem there is normally infinite number of Pareto optimal solutions due to the conflicts between objectives. Therefore, multiple objective decision making usually comprises two main steps: generation of Pareto optimal solutions and identification of the best compromise solution which should be a Pareto optimal solution.

4.2.2 Weight Sum Methods

The weighted sum approach is perhaps one of the commonly used methods. It is based on adding the weighted objectives to form a single cost function as follows,

$$\min_{x \in \mathbf{S}} \sum_{i=1}^{n} w_i f_i(x) \tag{4.4}$$

where, $w_i > 0$ for all $i = 1, 2, ..., n$ and $\sum_{i=1}^{n} w_i = 1$. The objective functions are often normalised in the weighted sum when they have different range of values. By consistently varying the weighting w_i an approximation of the Pareto set is obtained.

4.2.3 Multi-objectives Optimal Control

In contrast to classical optimisation , in optimal control, we have to compute an input in such a way that a dynamical system behaves optimally with respect to some specified cost functional. Hence, the system dynamics in Equation 4.6 is added as an additional constraint to the general MOO optimisation formulation. The notations have been changed in order to unify the notation for the control problems.

$$\underset{u \in U}{\text{minimize}} \quad \mathbf{J}(u) = [J_1(u), J_2(u), \cdots J_k(u)]^\top \tag{4.5}$$

$$s.t. \qquad \dot{x} = f(x, u) \tag{4.6}$$

$$g_i(x, u) \leq 0, \quad i = 1, 2, ..., l \tag{4.7}$$

$$h_j(x, u) = 0, \quad j = 1, 2, ..., m \tag{4.8}$$

where $\mathbf{J}$ is the vector of cost function, u is the control variables, x is the state variables, and $g_i(x)$ and $h_i(x)$ are the nonlinear inequality and equality constraint functions respectively.

4.3 Mathematical Formulation

An identical methodology is followed to chapter 4 for optimal control formulation for single objective, however with an additional modifications for multi-objective optimisation . In this respect, the MOCP formulation for motion planning is presented for solving the conflicting nature of motion sickness and journey time in automated vehicle. Although this chapter will adopt illness rating based on empirical approach for motion sickness model on point mass vehicle model. Three case studies are developed to investigate

the effect of driving style, vehicle speed, and road width, which are considered among the main factors affecting the driving dynamics which ultimately leads to motion sickness.

The s distance domain, the state variables $\mathbf{y}$ and control inputs $\mathbf{u}$ can be summarised as:

$$\mathbf{y}(s) = [v_x(s), v_y(s), s_n(s), \alpha(s), x(s), y(s), \theta(s), t(s)]^\top \tag{4.9}$$

$$\mathbf{u}(s) = [a_x(s), a_y(s)]^\top \tag{4.10}$$

As mentioned above, our objective is the minimisation of the motion sickness (J_1) (i.e., illness rating) but also to obtain solution minimum time problem (J_2).

$$J_1 = K \times \left[\left(\int_{s_0}^{s_f} \frac{k_x^2 a_{x,w}^2(s)}{\dot{s}} ds \right)^{\frac{1}{2}} + \left(\int_{s_0}^{s_f} \frac{k_y^2 a_{y,w}^2(s)}{\dot{s}} ds \right)^{\frac{1}{2}} \right] \tag{4.11}$$

$$J_2 = \int_{s_0}^{s_f} \frac{1}{\dot{s}} ds \tag{4.12}$$

In order to achieve minimum motion sickness without compromising the journey time, the problem becomes a multi-objectives optimisation problem. This is solved as using the application MOO such that the objective function includes both illness rating and journey time. The weighted sum methods, where the different targets of the optimisation are separated throughout the optimisation process by assigning with different weighting and are simultaneously minimised , is utilised in this problem. The objective functions are normalised since motion sickness and journey time have different range of values. In this case, feature scaling method (i.e. Min-Max scaling) is used for normalisation so that the range are between o and 1. Thus, the J_1 and J_2 in Equation (4.11) are reformulated into normalised form and given as:

$$j_m = \frac{J_1 - IR_{min}}{IR_{max} - IR_{min}} \tag{4.13}$$

$$j_t = \frac{J_2 - T_{min}}{T_{max} - T_{min}} \tag{4.14}$$

where j_m and j_t are normalised illness rating and journey time. IR_{max} and IR_{min} are maximum and minimum illness rating. Similarly, T_{max} and T_{min} are the maximum and

minimum journey time. Finally, in weighted sum method, the contribution of each cost in the combined cost function is controlled through some weighting factors [w_m, w_t], so that it can be solve as single objective optimisation shown below:

$$J = w_m j_m + w_t j_t \tag{4.15}$$

with $w_m \in [0, 1]$ and $w_t = 1 - w_m$, where w_m and w_t are the weighting for the motion sickness weighting and journey time. In theory, T_{max} would be infinite and IR_{min} would be (infinitely small) zero. Hence, both j_m and j_t would always be zero. In this respect, a minimum speed u_{min} as a boundary is introduced to obtain a baseline value for T_{max} and IR_{min} using only motion sickness cost J_1 in Equation (4.11). On the other hand, T_{min} and IR_{max} are obtained based on when using only minimum time cost function J_2 in Equation (4.12).

In addition, the five inequality constraints in Equations (4.16, 4.17, 4.18, 4.19 and 4.20) will be considered, such that the vehicle will be able to accelerate within the bounds Equation (4.16) set by the friction circle with a_{max} equal to 1g (9.81 ms^2), i.e., the maximum absolute acceleration that the vehicle is constrained to reach. The input accelerations are also bounded between minimum acceleration and maximum acceleration given in Equation (4.17) for longitudinal acceleration and in Equation (4.18) for lateral acceleration. Also, it will be bounded to never exceed the road borders considering left-width (R_w) and right-width ($-R_w$) from the centreline of the road Equation (4.19). The longitvelocity is v_x is considered as u and it is bounded by a minimum speed u_{min} and a maximum speed u_{max} in Equation(4.20).

$$\sqrt{{a_x}^2 + {a_y}^2} \leqslant a_{max} \tag{4.16}$$

$$a_{x_{min}} \leqslant a_x \leqslant a_{x_{max}} \tag{4.17}$$

$$a_{y_{min}} \leqslant a_y \leqslant a_{y_{max}} \tag{4.18}$$

$$-R_w \leqslant s_n \leqslant R_w \tag{4.19}$$

$$u_{min} \leqslant u \leqslant u_{max} \tag{4.20}$$

Boundary conditions have been added, in order to achieve the best possible optimal solution, with minimum speed is set as u_{min}= 5 [m/s]. As far as the road path is concerned, it is generated by a series of curvature κ over a distance s, to form a path which consists

of straight line and curves. The summary of boundary conditions required to keep the vehicle within the road boundary, and to start the manoeuvre in a straight line with no lateral velocity are given in Table 4.1.

Table 4.1: Boundary conditions

y	y_0	y_f
s	0	s_f
v_x	v_0	free
v_y	0	free
s_n	0	free
α	0	free
x	0	free
y	0	free
θ	$\pi/2$	free
t	0	free

4.4 Road Trajectory

In reality, for a specific starting point there would be a number of routes the vehicle could travel to arrive at the final destination. The motion sickness and journey time would also depend on the route taken such as in some cases a short route with many turns might save journey time but would result in higher motion sickness incidence. Similarly, longer route would take longer to arrive with less sickness. The study [10] also found that motion sickness incidence is greater in countryside road due to higher magnitudes of lateral vehicle motion compared to motorway where the road is predominantly straight roadways. This work aims to capture different road characteristic that are included in urban, motorway and countryside road (i.e., a straight road, and turns with high and low curvature). In this respect, a road path, which includes the combination of such characteristics is shown in Figure 4.2. The road is 12.2 km long and it is selected for its duration to be such to extract concrete conclusions for the motion sickness. In addition, the road is assumed to be one way lane with centreline as well as left and right border in which vehicle is able to manoeuvre within the road bound. Also, the road is flat with smooth surface as no suspension dynamics is considered. Finally, no obstacle or disturbance along the road journey as the work presents an offline optimisation solutions.

Figure 4.2: Road path containing different road characteristic where S_0 is the starting point and S_f is the finishing point. The red box A will be used to illustrate the trajectory for differences road width study in section 4.5.3.

4.5 Results

The application of motion planning using optimal control is utilized to mitigate motion sickness in autonomous vehicles. More specifically, for a predefined road path from a specific starting point to a final one, the optimum trajectory is sought within specific and given boundary and constraints in order to minimisethe motion sickness without compromising the journey time. However, both motion sickness and journey time are of conflicting nature in optimisation . Therefore, the weighted sum method in MOO will be apply to solve the trade-off between illness rating and journey time has been extensively studied (4.15) through a set of weighting factors $[w_m, w_t]$. In this respect, the weighting factor for the motion sickness term w_m is varied from 0 to 1 with increment of 0.05. In addition, three case studies are then carried out to investigate the effect of driving styles, maximum driving speed, and road width on the trade-off between illness rating and journey time. More specifically

1. For driving style, combinations of weighting factors are selected to simulated differ-

ent driving styles; ranging from sport, natural, comfort and anti-nausea.

2. For vehicle speed, the maximum allowed speed that the vehicle can drive is varying and its effect on motion sickness is investigated.

3. For road width limit, fixed path and free path scenarios are compared. For fixed path, where the road doesn't allow any lateral manoeuvrability to the vehicle by setting the road width at zero (i.e., the road boundary of left border and right border measured from the centreline $R_w = 0$. On the other hand, in the free path cases, the road width is increased as $R_w > 0$.

The solutions for all the case studies are illustrated and discussed in detail together with figures and tables. In Figure 4.3, the cumulative illness rating curve over the journey time for each set of weighting factor are plotted together forming a Pareto front. From the same Pareto front, the driving style analysis is performed with selected cases [w_1, w_2, w_3, w_4]. In addition, the frequency analysis is carried out using Matlab command: "*fft*" to investigate their frequency weighted acceleration power spectral densities given in Figure 4.4. Also their motion profile in Figure 4.5. Similarly for vehicle driving speed [u_1, u_2, u_3, u_4] and road width [R_{w1}, R_{w2}, R_{w3}] studies, Pareto fronts obtained for different conditions are given in Figure 4.6 and 4.8 as well as the frequency analysis in Figure 4.7 and 4.10. In addition, the optimum trajectories of the road width cases are shown in Figure 4.9. The illness rating and respective journey time for each study are tabulated in Table B.3, B.2 and 4.4.

4.5.1 Driving styles

In this part of the study, the condition for speed limit is set at $u_{max} = 30$ [m/s] with road width limit of $R_w = 1.5$ m. The cumulative illness rating over the journey time for the set of weighting factors is shown in Figure 4.3. The illness rating curve decreases when there is an increase in weighting w_m as the objective function would also prioritize illness rating. However, at the same time it results in longer journey time. When plotting all the cumulative illness rating curves together, a complete Pareto front is obtained in Figure 4.3. This front presents the correlation between the minimum motion sickness with the duration of travel. It is obvious that the faster the vehicle travel, the higher the sickness is. However, the compromise between the two objectives can be identified based on the preference of the user.

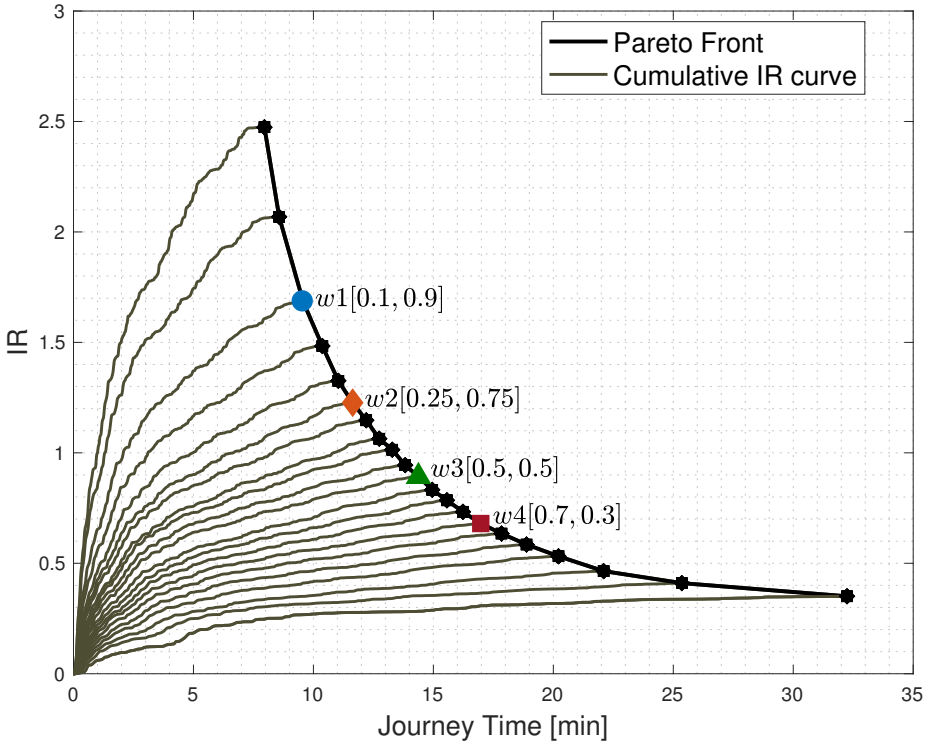

Figure 4.3: Cumulative illness rating curve for each weighting pair forming a Pareto front and showing selected weighting pair for four driving styles.

The optimal solutions from four combination of weighting factors are selected [w_1, w_2, w_3, w_4] and tabulated in Table B.3. In the near future, the automated vehicle will be able to allow the passenger to select a particular driving style based on their preference and taking into consideration the arrival time and the induced motion sickness levels. Thus, the weighting pairs from the optimal Pareto front could be used to represent the different automated driving styles of the same vehicle such that w_1 can be used to represent the sport driving, w_2 for natural, w_3 for comfort, and w_4 for anti-nausea. From Table B.3, it is clear that when $w_m \gg w_t$, the objective would favour the need to reduce motion sickness and compromise the journey time which is w_4, anti-nausea driving. On the other hand for $w_m \ll w_t$, journey time is favoured and in this case w_1, sport driving, as shown in Figure 4.3. In this way the optimal solution is found by varying the weighting factors in order to achieve minimum motion sickness without comprising journey time.

Additionally, frequency analysis is carried out on the resulting accelerations for each driving mode by investigating their power spectral densities shown in Figure 4.4. The trend of the acceleration power spectra is similar for all the driving style while the acceleration spectral in x- and y-axis are in the range below 0.5 Hz. Both spectra have

Table 4.2: Comparison of IR and Journey time between four driving styles.

	$[w_m, w_t]$	IR	$Time[min]$
$sport$	[0.1, 0.9]	1.684	9.6
$natural$	[0.25, 0.75]	1.227	11.6
$comfort$	[0.5, 0.5]	0.8925	14.4
$anti-nausea$	[0.7, 0.3]	0.6799	16.98

a peak at around 0.1 - 0.18 Hz. According to Figure 4.4, lateral acceleration appear to be dominating with higher r.m.s values compared to the longitudinal acceleration due to longer winding road sections. The peak in sport driving is gradually suppressed when switching into other styles especially in anti-nausea driving where the peak is minimum. This is because in sport driving, the acceleration and braking driven by AV would be harsher than any other driving style, especially when initiating the turn, which results in higher lateral acceleration. Similarly in the case of comfort driving, AV drives in a gentle manner considering passenger comfort and avoid motion sickness, but at the same time maintaining the journey time to minimum.

In addition the optimum motion profiles, given in Figure 4.5 also reflect the behaviour of each driving style with highest driving speed in sport driving compared to the other styles The velocity profile in comfort mode is in a smoother transition throughout the journey and prevents vehicle moving too fast or too slow. The velocity profile for all driving style shows similar forms by driving faster at straight road and slow down before initiating the turn and speed up after leaving the turn.

4.5.2 Vehicle speed

In section 4.5.1, it is understood that different driving styles would result in different velocity profiles. However, this case study aims to investigate the influence of the vehicle speed on motion sickness which is based on the maximum allowed speed that the vehicle can drive. So that the vehicle is restricted by u_{max}. In this respect, the maximum speed is varied and set as $u_{max} = [u_1, u_2, u_3, u_4]$ m/s on the same road width at $R_w = 1.5$ m. So, through the variation of u_{max}, the study will focus on motion sickness based on different vehicle speeds. In this respect, we assigned u_1= 20 m/s as V_{max_1}, u_2= 25 m/s as V_{max_2}, u_3= 30 m/s as V_{max_3} and u_4= 40 m/s as V_{max_4}. Similarly based on Equation

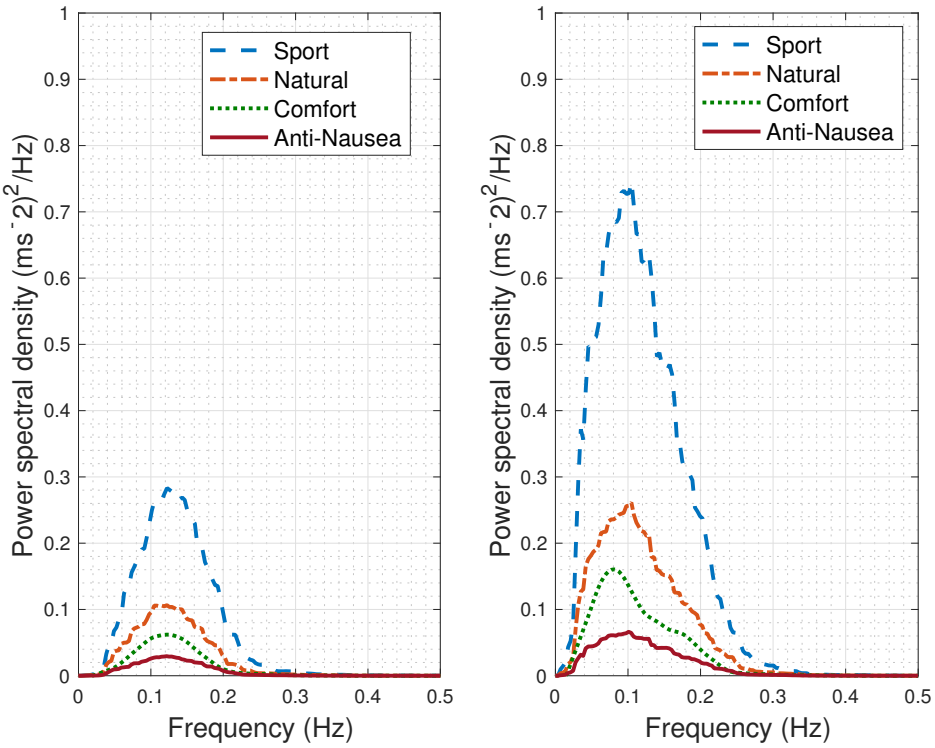

Figure 4.4: Frequency weighted acceleration power spectral densities in the longitudinal (*left*) and the lateral (*right*) axis for four driving styles.

(4.15), a Pareto front is achieved through a set of weighting factors $[w_m,\ w_t]$ for each vehicle.

The Pareto fronts for all four V_{max} are presented in Figure 4.6 containing the relationship between illness rating and journey time based on all the weighting factors. For $w_m \ll w_t$, there is a large variation between the fronts due to the fact the vehicle is able to reach higher driving speed. On the other hand, the variation becomes smaller and all the fronts converge to the same curve, when $w_m \gg w_t$ as the vehicle is now driving as slow as possible to favour motion sickness in the cost function.

In order to investigate in depth, the style of sport driving is selected to be compared for all V_{max}. The respective illness rating and journey are given in Table B.2. It can be seen that V_{max_1} with the lowest vehicle speed results in longest journey time compared to other three vehicles. On the other hand V_{max_4} which can extern highest vehicle speed leads to fastest journey time. Although, there is no significant differences in term of sickness, the journey time could be save up to one and a half minute by adjusting the vehicle speed.

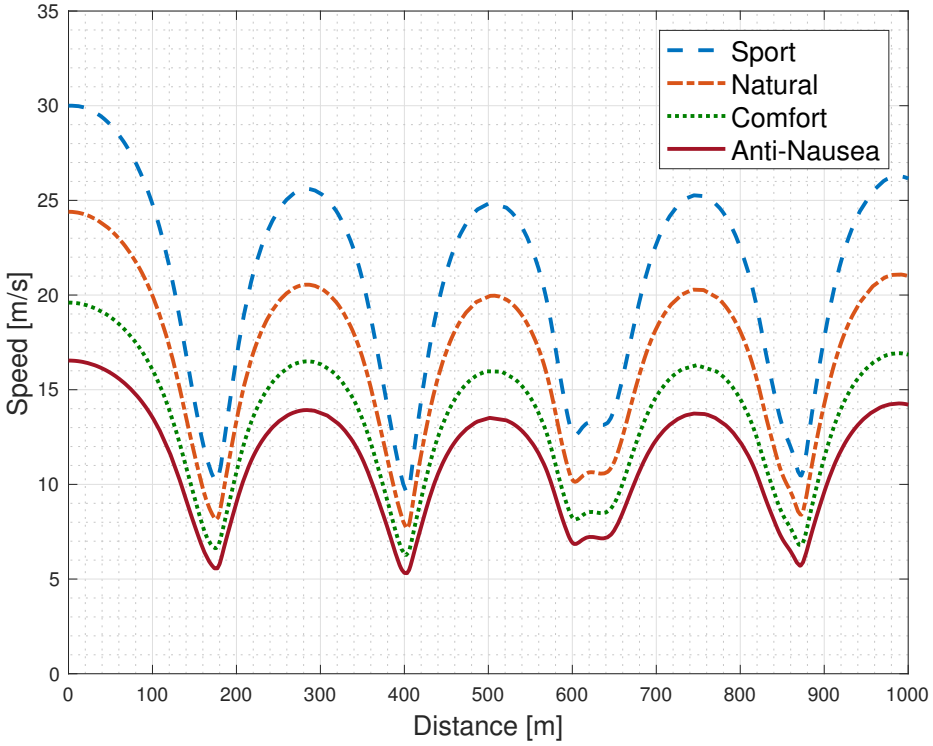

Figure 4.5: The optimum velocity profile along the road journey for four driving styles.

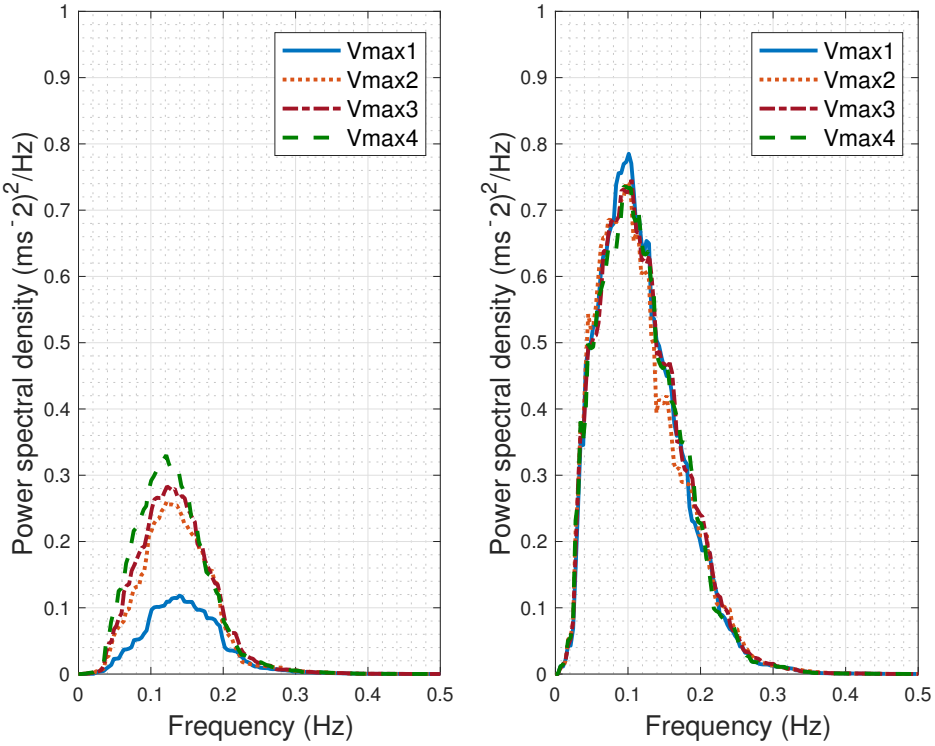

Figure 4.7: Frequency weighted acceleration power spectral densities in the longitudinal (*left*) and the lateral (*right*) axis for four V_{max} in sport driving style.

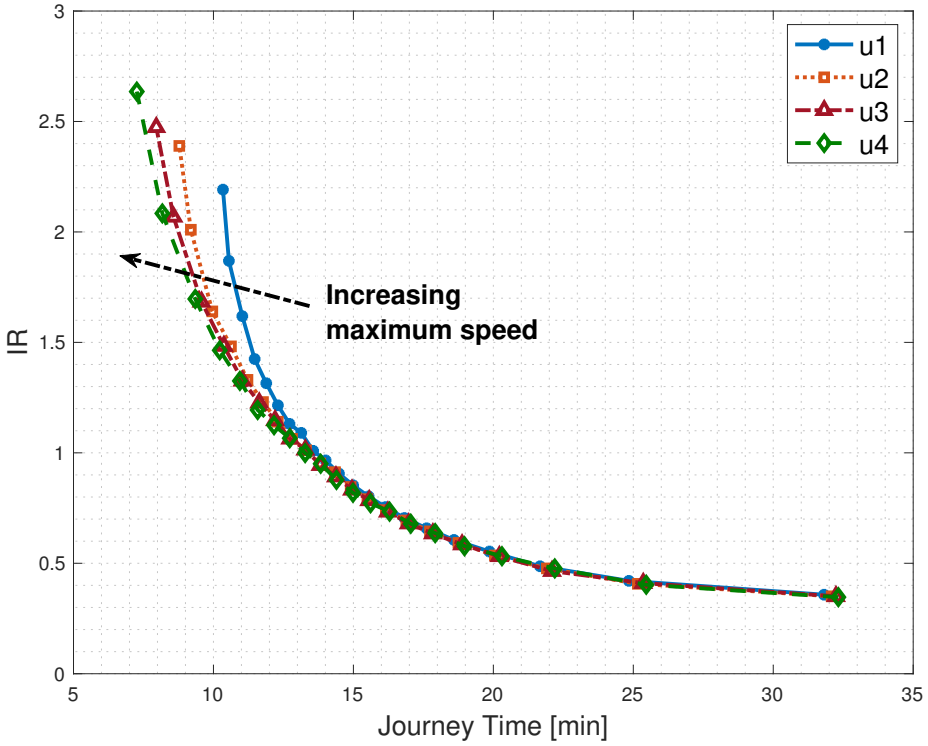

Figure 4.6: Pareto fronts for four driving speed showing large variation when $w_m \ll w_t$.

Table 4.3: Comparison IR and Journey time between four V_{max} in sport driving style.

	IR	$Time[s]$
V_{max_1}	1.61	11
V_{max_2}	1.64	10
V_{max_3}	1.68	9.6
V_{max_4}	1.70	9.4

Similarly, by looking at the power spectral densities for both acceleration shown in Figure 4.7, the variation in low-frequency motion is mainly in fore-and-aft acceleration due to the fact that the differences in accelerating and braking performance affected by the vehicle speed capabilities. The peak in V_{max_3} and V_{max_4} is higher in x-axis, but slightly lower in y-axis compared to the rest. This reflects the nature of the road, as at straight road section, the vehicle with V_{max_3} and V_{max_4} are able to drive at higher speeds to compensate the journey time. Interestingly, it could be assumed that each V_{max} represent a vehicle

from the perspective of the maximum speed capabilities. Since from the literatures [10] and [4], other vehicle dynamics such as chassis, tire or suspension dynamics are known to have less or no significant influence on motion sickness. In this respect, we could present V_{max} such that V_{max_1} is a slower city car, V_{max_2} as a city bus, V_{max_3} as a family car and V_{max_4} as a SUV.

4.5.3 Road width

In [25] and [27], their road width study shown that the vehicle could utilise the available road width to achieve lower sickness while maintaining shorter journey time compared to travelling on a fixed road. However, the effect of different road characteristic described in Section 4.4 on a longer road were not considered. Therefore, the aim of this section is to investigate whether the vehicle could take the advantage of road width when the road is extended to include different road characteristics as well as longer route journey. In this part of the study, the condition for speed limit is set at $u_{max} = 30$ [m/s], but the road width limit of R_w is set to vary. Thus, for the same vehicle driving speed, a fixed road path ($R_w = 0$) and free road paths where ($R_w > 0$) are selected for the analysis such that $R_{w1} = 0$ m, $R_{w2} = 1.5$ m and $R_{w3} = 2.5$ m.

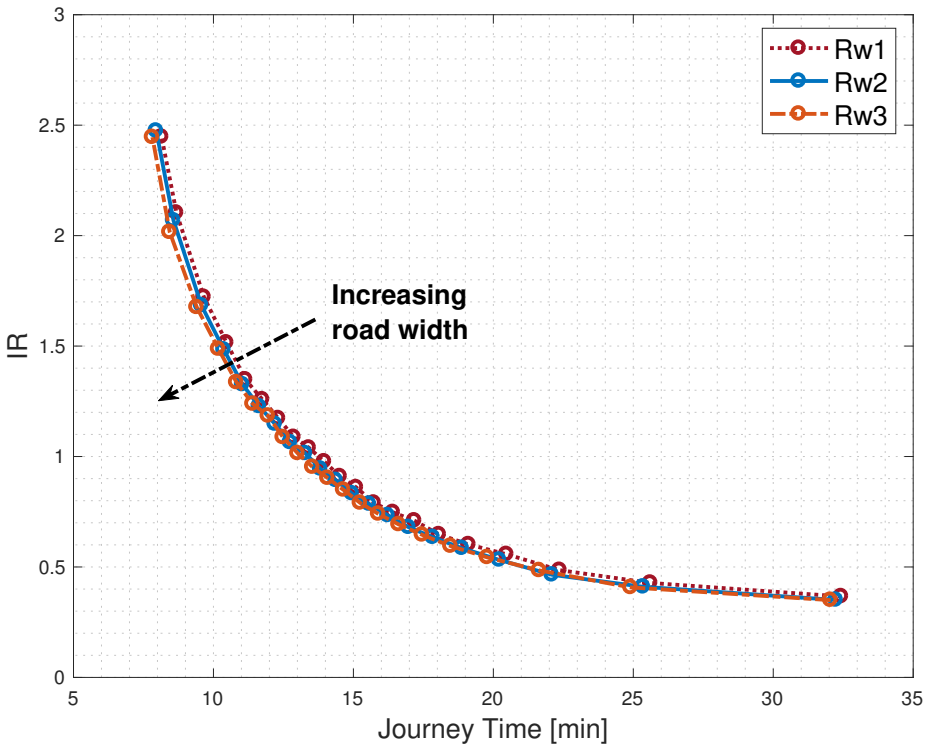

Figure 4.8: Pareto fronts for three road width cases with same speed limit u_3.

Using the same approach as in sections 4.5.1 and 4.5.2, the Pareto front from each road path is shown in Figure 4.8. The variation between the fronts in road width study is significantly small for all driving styles. Nevertheless, it can be seen that the front shift slightly downward when the road width is increased to allow lateral manoeuvrability

however it is notably at $w_m \ll w_t$ region. This is due to the fact that when the road is longer, the advantage of road width become less since any loss in journey time would average out when travelling on different road characteristics when $w_m \gg w_t$.

Table 4.4: Comparison IR and Journey time between three road width cases using comfort driving style.

	IR	$Time[min]$
r_1	1.258	11.8
r_2	1.277	11.6
r_3	1.238	11.4

To put this into a perspective, the style of comfort driving (w_3) is selected to be compared for all the road scenarios. This is presented as r_1, r_2 and r_3 accordingly. The relevant IR and journey time for each road scenario is shown given in Table 4.4. The improvement of the result significantly small and echoed in the low-free frequency spectra shown in Figure 4.10. A section of the road shown in Figure 4.9 illustrated that for fixed scenario, the vehicle travels on the centre-line, whereas for free path scenarios, especially in r_3, the vehicle is able to utilise the road width for a smaller turning radius. However, in this case study, the road width does not contribute to the reduction of sickness and journey time when travelling on a long road journey.

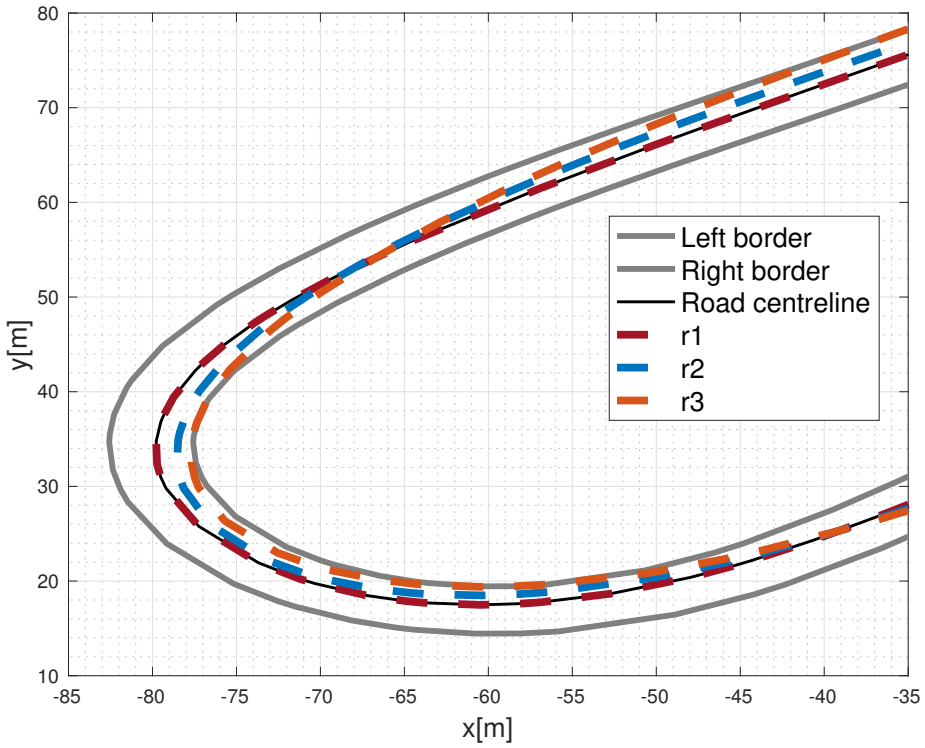

Figure 4.9: The optimum road trajectory in road segment (A) for three road cases.

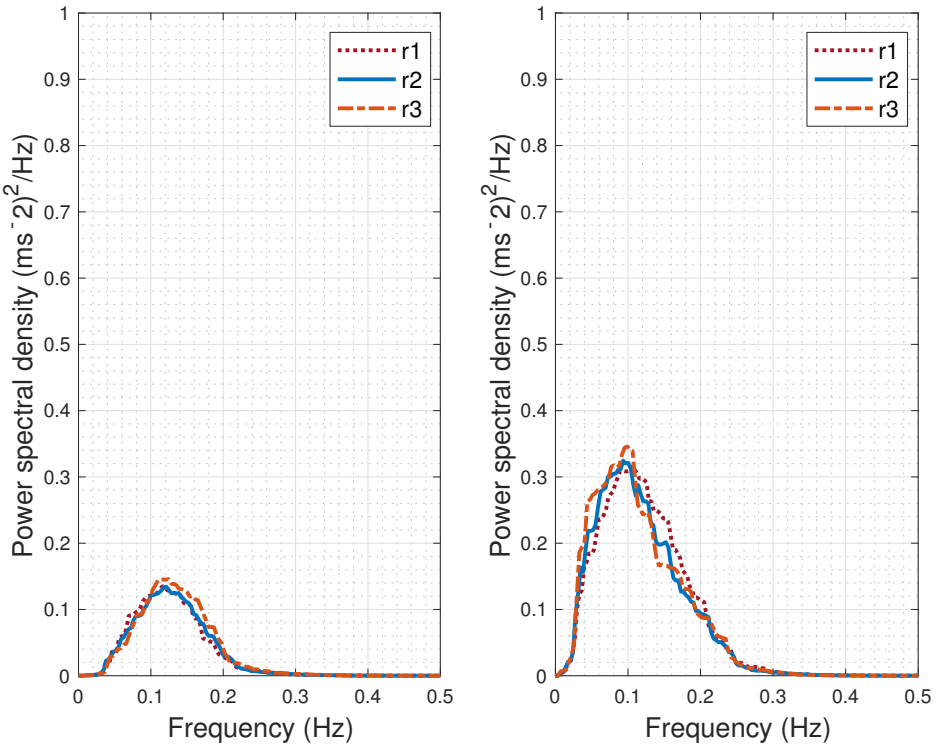

Figure 4.10: Frequency weighted acceleration power spectral densities in the longitudinal (*left*) and the lateral (*right*) axis for road width study using comfort driving.

4.6 Conclusions

The conflicting nature between the motion sickness and journey time is solved using MOO with different weighting. The Pareto front representing the correlation between the two components is obtained and this front also allows user to select their preference driving style. From the three case studies, driving styles have a bigger impact on reducing motion sickness and journey time rather than vehicle speed and the road width. There is a significant impact in vehicle top speed when $w_m \ll w_t$, such that all the vehicles result in similar sickness level, but journey time is shortened for vehicle with higher maximum speed capabilities. However, the effect of road width is negligible when travelling on longer road for the reduction of motion sickness and journey time. This finding is crucial considering the need for automated vehicles to drive on a fixed road path in respect to road safety and also to allow the employment of connected and automated vehicles in the future. This work has mainly focus on addressing the driving dynamics aspect of motion sickness. However, it is also expected that including energy efficiency as one of the main objective functions would result in less motion sickness, however it would require more investigation in the future work

This page is intentionally left blank.

CHAPTER 5

Multi-criteria decision making

5.1 Introduction

Despite the importance of mitigating motions sickness using motion planning by also considering the journey time, the optimum velocity profile with which the vehicle will finally drive should be selected after taking into consideration additional objectives as well. Firstly, the driving style should be smooth enough and not assertive during the ride, as high acceleration values and jerk will make the passenger feel discomfort [83] and the vehicle might be perceived as unstable, while it is not. Few researchers [84, 85] used aggressive driving metrics as the main objective for the motion planning of an AV, while the passengers' confidence of riding or subjective feel (i.e. how the vehicle is perceived to drive) hasn't been used and affects significantly the trust of the passengers towards the driving experience. Additionally, AVs are expected to have a significant impact in the decrease of fuel emissions, therefore the energy efficiency should also be included in the final selection of the optimum velocity profile. As a results, various researchers [86] have used energy efficiency as their main objective in the path planning studies, while Han et al. [87] investigated the fundamentals of energy efficient driving by formulating control problems. Last but not least, apart from constraints that secure the vehicle stability of the vehicle, it is important to consider it as an additional objective as well by using appropriate metrics.

In this direction, the work in this section presents a way to identify the optimum trajectory

profile which the vehicle will finally drive should be selected after taking into consideration multiple objectives. Therefore, as the optimal control is focused on the MS minimisation, a sorting algorithm is applied to seek the optimum solution among the pareto alternatives. The aim is that this solution will correspond to the best velocity profile that ensures the optimum compromise among the motion comfort, the driving behaviour, the energy efficiency, the vehicle stability, the occupants confidence to ride and the journey time.The work in this section share the same method and material in Chapter 3 regarding to OCP formulations. Therefore, a point mass vehicle model is selected with curvilinear coordinates approach is use on same road width scenarios. However, minimum time solution is not of concern in this section.

5.2 Road path and profile

In this work, initially we use the same road path as in Chapter 3(Figure 5.2) to seek the optimum velocity profile and then, a random road profile of Class B [88] (Figure 5.1) is used to study in depth the vehicle dynamic behavior while driving on this road path.

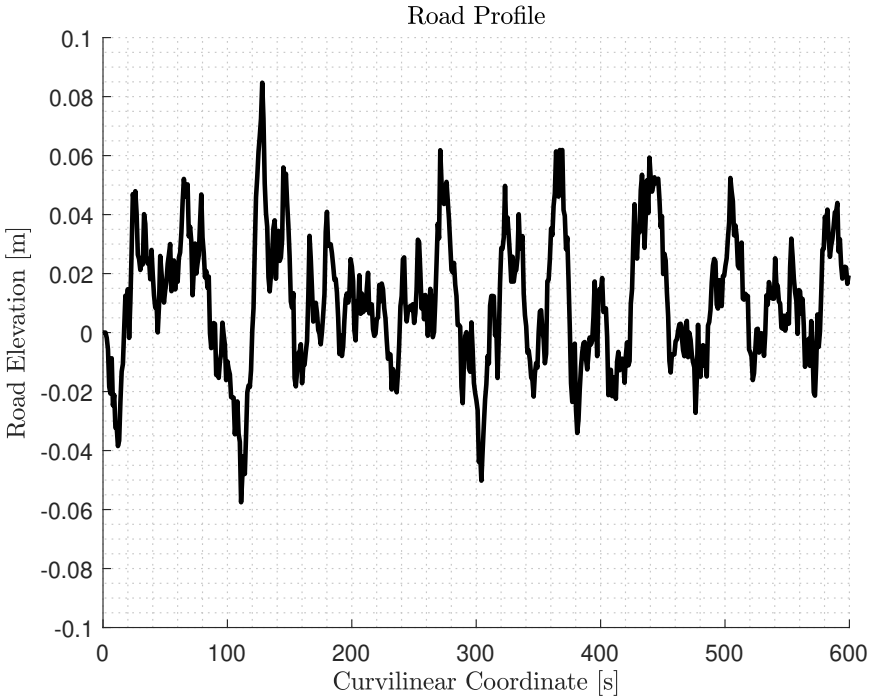

Figure 5.1: Road profile of Class B generated according to ISO-8608 [88].

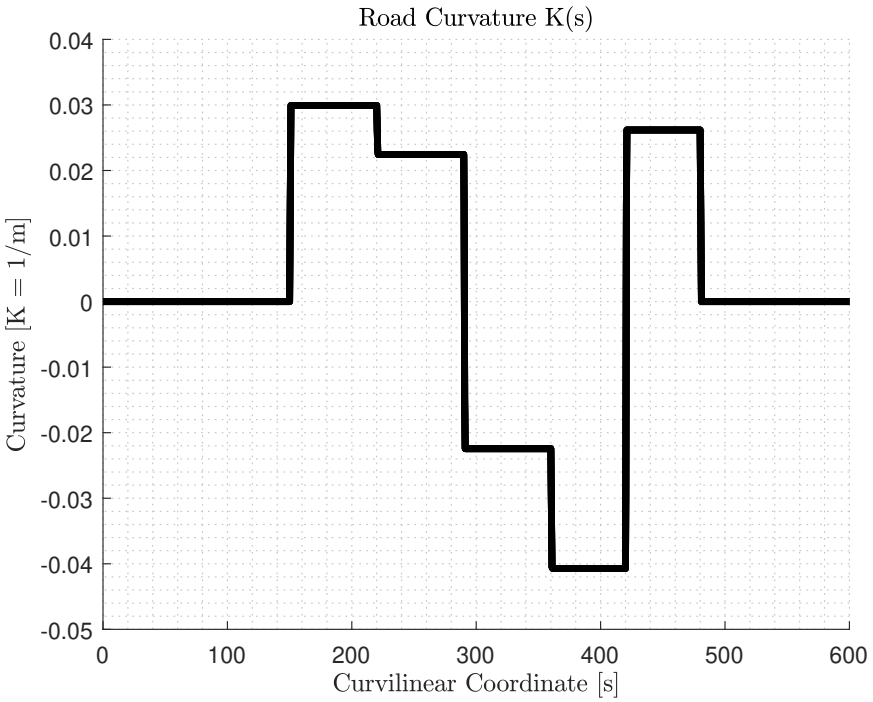

Figure 5.2: Road Path designed road curvature (κ) in distance domain

5.3 Performance Metrics

5.3.1 Motion Comfort-Oriented Metrics

ISO-2631:1998 provides a guideline for measurement and evaluation of human exposure to whole-body mechanical vibration and repeated shock. According to the standard, the ride comfort is assessed by combining the root mean square (RMS) values of the weighted accelerations (RC_{W_i}) measured at the vehicle's centre of gravity. More specifically, for each acceleration, either directional (a_x, a_y and a_z) and rotational ($\ddot{\phi}$, $\ddot{\theta}$ and $\ddot{r}$) the weighted RMS value can be evaluated according to Equation 5.1.

$$RC_{W_i} = \left(\frac{1}{t} \int_0^t a_{i_W}^2 d\tau \right)^{\frac{1}{2}} \tag{5.1}$$

where i refers to the type of the acceleration, either translational (i=x for a_x, y for a_y and z for a_z) or rotational (i= rx for $\ddot{\phi}$, ry for $\ddot{\theta}$ and rz for $\ddot{r}$); a_{W_i} stands for the weighted accelerations in the time domain. In order to obtain the frequency weighted accelerations (a_{W_i}) of the original signal (a_i), it should be transferred in the frequency domain (A_{W_i})

and be weighted based on Equation 5.2:

$$A_{W_i} = WP_{i_1} * WA_{i_2} * A_i \tag{5.2}$$

where WP_{i_1} (Figure 5.3) are the principal frequency weightings depicting the frequency weighting for measurements:

- in the z direction (i_1=k),
- in the vertical recumbent direction except the head (i_1=k),
- in the x-y direction and the horizontal recumbent position (i_1=d)
- to study motion sickness (i_1=f)

while WA_{i_2} (Figure 5.4) are the additional frequency weightings related to:

- measurements in the seat back (i_2=c),
- measurements for rotational vibrations (i_2=e),
- measurement of vibration under the head of recumbent person (i_2=j).

In case there is no need for additional weighting of the measurement, WA is equal to 1.

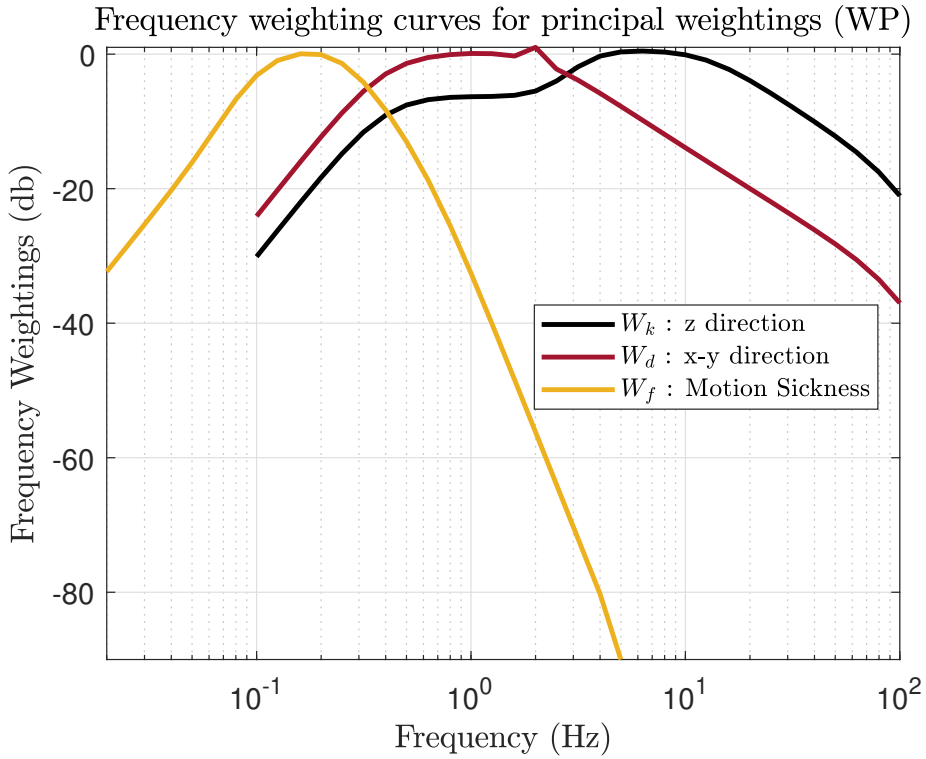

Figure 5.3: Frequency weighting curves for principal weightings (WP)

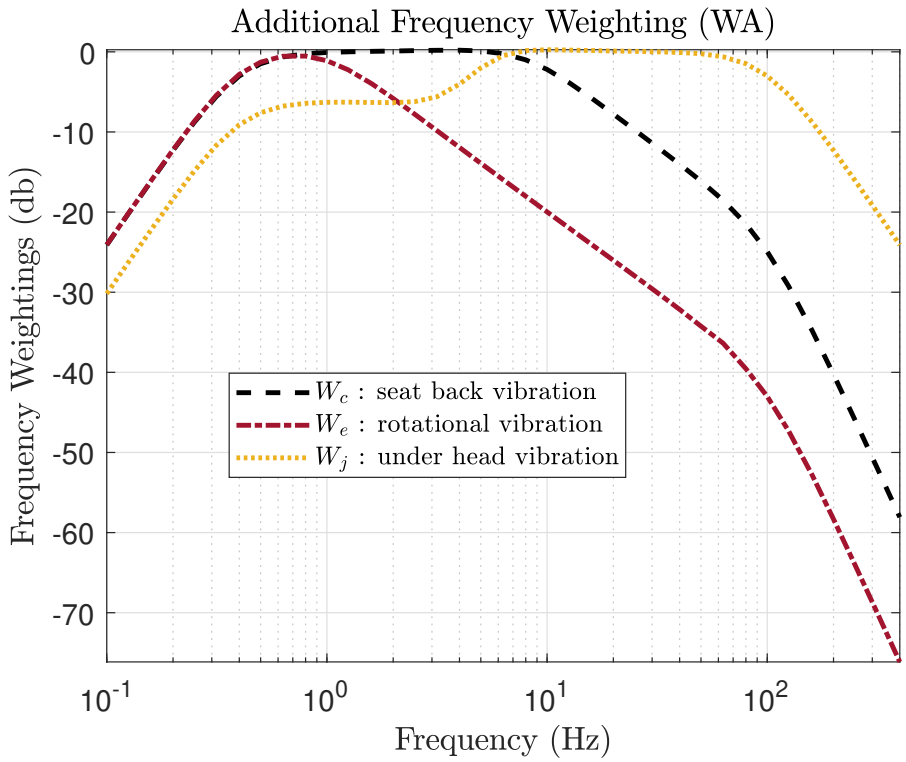

Figure 5.4: Additional Frequency weighting (WA)

The overall ride comfort metric is evaluated by summing all the $RC_{iW_{rms}}$, after multiplying each by appropriate factors (k_i):

$$RC = \left(\sum_{i=1}^{6} k_i^2 RC_{W_i}^2 \right)^{1/2} \tag{5.3}$$

$$RC = \left(k_x^2 RC_{Wx}^2 + k_y^2 RC_{Wy}^2 + k_z^2 RC_{Wz}^2 + k_{rx}^2 RC_{Wrx}^2 + k_{ry}^2 RC_{Wry}^2 + k_{rz}^2 RC_{Wrz}^2 \right)^{\frac{1}{2}} \tag{5.4}$$

where k_i is the multiplying factor for each term (i=x, y, z, rx, ry and rz).

On the other hand, Illness rating (IR) described in Chapter 2 will be used for the assessment of passenger motion sickness.

5.3.2 Aggressive Driving

In principle, driver's aggressiveness should be measured by how fast the drivers accelerates and decelerates and in order to evaluate the levels of aggressive driving (AD) we normally use the jerk of the longitudinal acceleration (a_x). The jerk (J_{a_i}, Equation 5.5) is defined as the rate of change in acceleration and deceleration (a_x), having a significant impact on the safety and comfort of passengers [2]:

$$J_{a_i} = \frac{da_i}{dt} \tag{5.5}$$

where i is x and y for longitudinal (a_x) and lateral acceleration (a_y). An acceleration profile shows how a driver speeds up and slows down, whereas a jerk profile shows how a driver accelerates and decelerates, which is more important in determining driver's aggressiveness. In this work, we will use the sum of J_{a_x} and J_{a_y} RMS values as a metric of aggressive driving, as shown in Equation 5.6:

$$AD = \left(\frac{1}{t}\int_0^t J_{a_x}^2 d\tau\right)^{\frac{1}{2}} + \left(\frac{1}{t}\int_0^t J_{a_y}^2 d\tau\right)^{\frac{1}{2}} \tag{5.6}$$

5.3.3 Energy Efficiency-oriented metrics

One factor which has significant effect on vehicle fuel consumption is the rate at which the vehicle is accelerated, as studies have shown that rapid or frequent accelerations result in increased consumption. The total energy demanded from the vehicle over any cycle is the time integral of the power requirement:

$$E = \int_{T_i}^{T_f} P dt \tag{5.7}$$

where E is the total energy demand, P the instantaneous power requirement, T_i the initial time and T_f the final time. The power required could be expressed as the product of the instantaneous force produced by the propulsion motor (F_m) times the velocity of the vehicle (v):

$$E = \int_{T_i}^{T_f} F_m \mathrm{v}(t) dt = \int_{T_i}^{T_f} \left(m\frac{d\mathrm{v}}{dt} + F_r\right)\mathrm{v}\ dt \tag{5.8}$$

In the above equation, the force produced by the propulsion motor (F_m) consists of two terms, the first ($m\frac{d\mathrm{v}}{dt}$) represents the inertial effect and the second (F_r) denotes the resistive force (i.e. aerodynamic drag and rolling resistance). More specifically, F_r is defined:

$$F_r = \frac{1}{2}\rho_a c_d A_f v(t)^2 + c_r m g \tag{5.9}$$

where ρ_a is the air density; c_d denotes the aerodynamic drag coefficient; A_f the vehicle's frontal area and c_r the rolling resistance coefficient.

In this work, as a metric of energy efficiency (EE) would be the minimisation of the

energy demand (Equation 5.9).

5.3.4 Vehicle Stability-Oriented Metrics

Vehicle Handling

Suspension travel is an important metric that indicates vehicle handling, as it depicts the ability of the system to support the vehicle's static weight. Considering that the vehicle is well supported if the rattle space requirements are kept small. So, the maximum value of the suspension travel is usually selected as index (Equation 5.10) to assess the vehicle handling:

$$ST_i = max(Suspension\ Travel) \tag{5.10}$$

where $i = FR,\ FL,\ RR$ and RL refers to one of the four suspension systems of the vehicle. The detailed equations for the $SuspensionTravel$ for various vehicle models can be found in Papaioannou et al. [89]. In this work, the sum of the maximum suspension travels at the two wheels of the j^{th} axle is used as a metric of vehicle handling, as shown in Equation 5.11.

$$ST[J] = max(ST_{[J]R}) + max(ST_{[J]L}) \tag{5.11}$$

where J is the front (F) and rear (R) axle.

Rollover Stability

The load transfer at each axle (LTR_i, with $i = R, F$) is used in order to evaluate the dynamic roll stability of the vehicle, using Equation 5.13 [90]:

$$LTR[i] = \frac{F_{ztR_i} - F_{ztL_i}}{F_{ztR_i} + F_{ztL_i}} \tag{5.12}$$

LTR is used to assess the rollover propensity of the vehicle by considering the vertical tire forces F_{ztR} and F_{ztL}. This index ranges from -1 to 1 and identifies when either the right or the left wheel has lost contact with the ground. When $LTR[i]$ is close to -1 and 1, then the right or the left wheel of the i^{th} axle is close to lift off, respectively. In this work, the maximum of the absolute values will be used to access the rollover propensity, which will illustrate if either the front or the rear axle has lifted-off.

$$MLTR[i] = max(|LTR[i]|); \tag{5.13}$$

5.3.5 Riding Confidence-Oriented Metrics

Until now vehicles are driven by people and are considered machines to be felt by the driver. For the subjective evaluation of the driver-feel, three main parameters are considered and consist of the confidence drive level, the safe vehicle behavior and the fun to drive [91]. In AVs, two of the three objectives could not be considered any more or could be transformed. More specifically, the confidence drive level could be neglected considering the lack of a driver, and the fun to drive could be transformed to "fun to ride, considering the subjective feel of the passengers and how they perceive the ride in addition to the motion comfort.

A metric able to capture the subjective feel of the occupants is the perceptible roll index (SF_i) have been proposed by Trivedi et al. [92], which combines the most common metric for roll performance, i.e. the roll gradient and the position of the passengers. The SF_i metric is derived by Equation 5.14, and when this value is increased more motion is felt by the occupant:

$$SF_i = \Phi \frac{\pi}{180} r \tag{5.14}$$

where i is equal to D or P, referring to the subjective feel perceived by the occupant in the driver's or the passenger's position ($H-point$) respectively, as shown in Figure 5.5; Φ is the roll gradient (the derivative of the vehicle body roll angle with respect to the lateral acceleration acting at its centre of gravity); r rotational arm of the occupants $H-point$. The $H-point$ is the position of the occupant's hip measured from the front axle ($X-axis$), the centre plane of the vehicle ($Y-axis$) and the road ($Z-axis$). Regarding the rotational arm (r), it is derived from the Equation 5.15:

$$r_i = \sqrt{H_{y_i}^2 + (H_{z_i} - h_i)^2} \tag{5.15}$$

where H_{y_i} and H_{z_i} are the driver's ($i = 1$) and the passenger's ($i = 2$) $H-point$ coordinates in the Y and the Z axis, respectively; h_i is the height of roll axis at H_{x_i} distance from the front axle ($H-point\ plane$).

$$h_i = hrrc + \frac{hfrc - hrrc}{wb} H_{x_i} \tag{5.16}$$

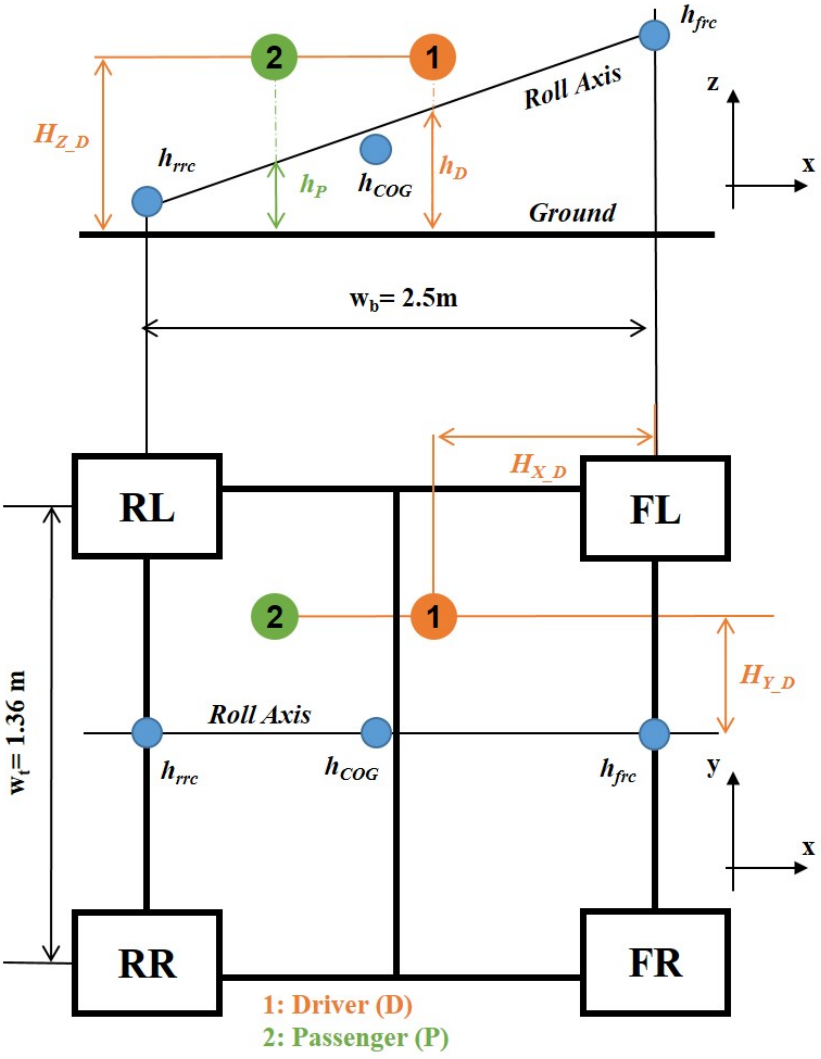

Figure 5.5: Vehicle side (top figure) and top (bottom figure) view

where $hfrc$ and $hrrc$ are the front roll centre height and rear roll centre height. wb is the vehicle wheelbase.

5.4 Optimisation Algorithms

As described, the problem is to find the appropriate vehicle control inputs, that can drive the vehicle along a predefined path from the initial position (s_0) to the final position (s_f), such that the motion sickness (IR) to be minimised for various fixed journey time (JT) cases. This problem could be codified as an optimisation problem with the motion plan of the vehicle to be its solution. More specifically, it will be solved as an optimal control problem (OCP), while afterwards, a sorting algorithm ($k-\varepsilon$) will be used to seek the optimum solution among the alternatives by considering additional objectives. The OCP formulation will not be discussed in this section as it is found in Chapter 3. This approach of selecting a main objective for the main optimisation procedure (i.e. the OCP) and adding additional objectives in the sorting algorithms have been used successfully by Papaioannou et al. [39] in the optimisation of passive and semi-active vehicle suspensions.

5.5 Multi-Criteria Decision Making

5.5.1 Pareto Front

The optimisation is described as a problem of minimisation of objective functions. In single objective optimisation problems, the focus is turned on a scalar number, while in multiobjective optimisation (MOO) the objective function is a vector and there isn't a single solution that optimizes the problem. When the objective functions are in conflict in MOO problems, an infinite number of solutions exists shaping the Pareto front, which finally presents the trade-offs in compromising the different objectives. In this work, in order to generate a Pareto set of optimal solutions, the formulated single objective optimal control problem for minimizing MS will be solved for different fixed time solutions (T_{demand_i}).

5.5.2 Sorting Algorithm k-ε

The solutions of the Pareto set are equally good and satisfy different subjective preferences, while the number increases as the complexity of the problem formulation is increased. In this work, we will apply the $k-\varepsilon$ sorting algorithm [93], which is able

not only to vet solutions taking into consideration if an objective is or not better by another, but also to quantify the entity of this variation. Through the $k-\varepsilon$ optimality method, solutions which "have something more" than the others are identified and proposed to the designer. More specifically, according to this method, all the Pareto solutions are $k-$optimal. Thus, if $k=0$ for a solution then it is just Pareto optimal, whereas if $k=n-1$, where n is the objectives number, then the so called "utopia point" is identified and is the global optimum. The k levels are evaluated according to Equation 5.17.

$$\mathrm{k}{=}min_Z\left(\sum_{i=1}^{n}\Gamma(\Delta f_i)\right)-1 \tag{5.17}$$

where Δf_i is the difference between the i^{th} objective of the considered solution compared to a different Pareto optimal solution; $\Gamma(x)$ is a merit function evaluated based on Equation 5.18. In order $k-\varepsilon$ to seek the "something more" than the other, an indifference threshold ε is included in the merit function. So, if the difference Δf_i is lower than ε, selected by the designer, the solution is not sorted out as in other methods. The use of this threshold offers a continuous degree of optimality in the solutions.

$$\Gamma(\Delta f_i)=\begin{cases}0\ , & \Delta f_i\geq\varepsilon\\ 1-\frac{\Delta f_i}{\varepsilon}\ , & 0<\Delta f_i<\varepsilon\\ 1\ , & \Delta f_i\leq 0\end{cases} \tag{5.18}$$

5.6 Result

In this work, two optimisation algorithms are combined to seek the optimum velocity profile among the alternatives that have shaped a Pareto front and consist of optimal solutions of OCP problems with different fixed time for the minimisation of motion sickness. More specifically, the procedure is described by Figure 5.6 and is divided in three steps.

- Firstly, an optimal control problem is formulated for multiple fixed journey time (JT) solutions and is solved using GPOPS II solver with MATLAB suite [63]. After obtaining all the optimal solutions, a Pareto Front (Figure 5.7a) is generated.
- Secondly, after having obtained the velocity profiles (Figure 5.7b) for various fixed

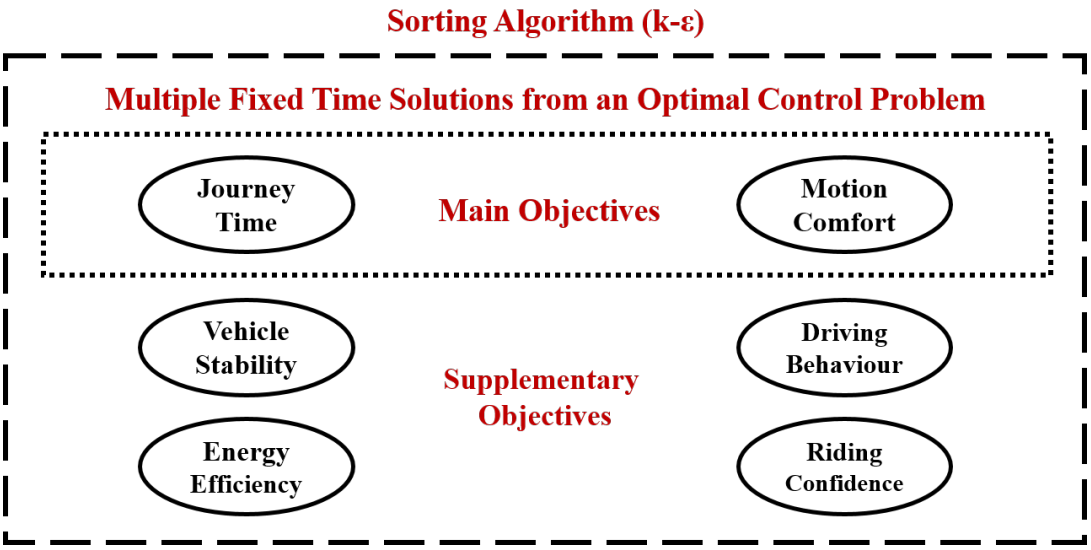

Figure 5.6: The procedure which combined the OCP and a sorting algorithm for identifying the optimum velocity profile to assign to the predefined path.

solutions, a commercial software (CARMAKER) is used to follow the predefined path with the assigned velocity in order to evaluate more performance aspects of the vehicle behaviour and the passengers condition (Figure 5.8). In order to achieve it, the lateral control for path-following is realised taking advantage of IPG Driver, which is a closed-loop control algorithm provided by IPG CARMAKER. Also, a PID controller is utilised for the longitudinal control and the velocity tracking.

- Finally, the k-ε algorithm, a sorting algorithm for multi-decision criteria making, is applied to seek the optimum solution among the Pareto alternatives considering the additional objectives. Prior to this, in order to generate more alternatives of JT, the Pareto Fronts of all the objectives with regards $JT = T_{demand_i}$ are interpolated for T'_{demand_i}.

5.7 Optimal Control Problem

Regarding the first part of this work, the minimisation of motion sickness is investigated for a set of fixed journey time cases (i.e $JT = T_{demand_i}$), as shown in Equation 5.19.

$$JT = T_{demand_i} \in [35, 75] \tag{5.19}$$

with an interval of 5 seconds. The road path selected is fixed without allowing any lateral manoeuvrability to the vehicle by setting the road width at zero (i.e. the road

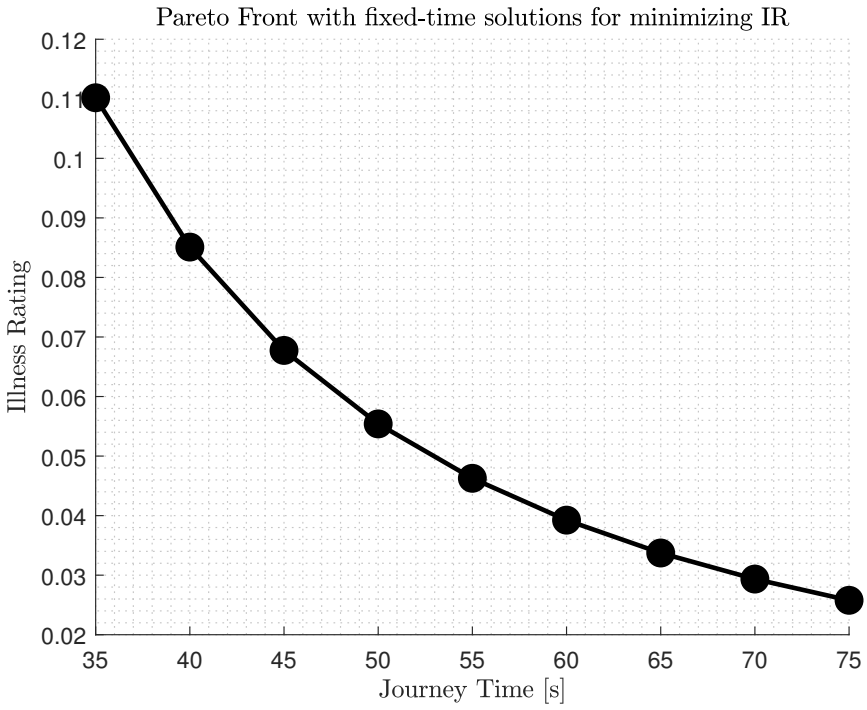

(a)

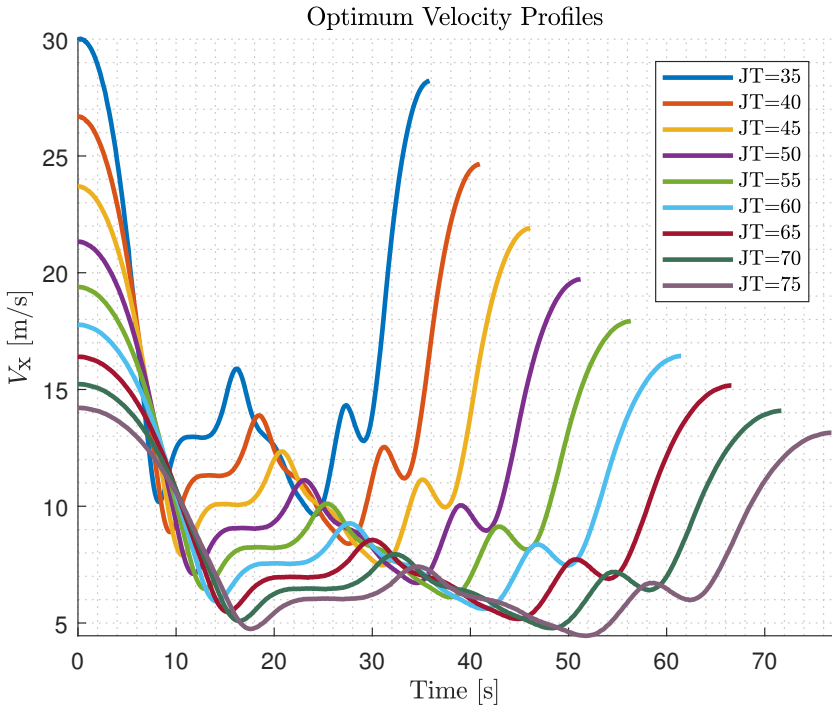

(b)

Figure 5.7: (a) The Pareto front with the optimal solutions obtained from the OCP for different fixed time cases (T_{demand_i}) for the minimisation of IR and (b) their corresponding optimal velocity profiles.

boundary of left border and right border measured from the centreline $L_w, R_w = 0m$). The output of these solutions is plotted shaping the Pareto front (Figure 5.7a) and illustrating the conflicting relation of our objectives. According to Figure 5.7a, the IR metric is decreasing with higher rate at the first three cases (around 22% per 5 *sec* increase until 50 *sec*), while afterwards the decrease is less (around 16%). The above remark is also depicted in the optimal velocity profiles assigned in the path (Figure 5.7b) for each JT case. According to Figure 5.7b, all the optimal velocity profiles follow the same patern, as they are assigned to the same path, but with harsher and more aggressive accelerations when the JT is smaller.

5.8 Additional Objectives

As described previously, CARMAKER is used to assign the optimal velocity profile to the predefined path with higher accuracy and assess more performance aspects, which have been described in Section 5.3. The fraction of change of each metric with regards to the corresponding value of the fastest case ($JT = 35s$) is plotted versus journey time (JT) in Figure 5.8. The additional metrics are divided into four groups of metrics, where the one referring to (A) motion comfort (RC and IR) and driving behaviour (AD) is illustrated in Figure 5.8a, (B) to energy efficiency (EE) is illustrated at Figure 5.8b (C) to vehicle stability (STF, STR, $LTRF$ and $LTRR$) is illustrated at Figure 5.9a), and (D) to riding confidence (SF_D and ST_P) is illustrated at Figure 5.9b). The pattern illustrated in these figures presents the relation of each metric with JT, when assigning different velocity profiles to a predefined path, and this would be the shape of their Pareto Front with regards to JT, if their value was plotted instead the fraction of decrease.

First of all, regarding the comfort-oriented metrics (Figure 5.8a) a conflicting relation with the journey time is illustrated, as expected. The increase of the journey time leads to smoother accelerations and decelerations and hence, the comfort perceived by the occupants is increased. Based on the comparison of the various metrics (RC, IR and AD), we can extract conclusions about the efficiency of our cost function (IR). According to this Figure 5.8a, the decrease occurred in AD is greater than IR, which served as our cost function in the OCP formulation. This illustrates that IR metric could accommodates the improvement of the driving behaviour and that it seems to be more efficient for improving motion comfort compared to AD, which is used extensively in the literature.

On the other hand, RC metric illustrates smaller decrease compared to the cost function for the various JT cases, as it considers additional terms such as the vertical accelerations, as shown in Equation 5.3. Although all three objectives show a similarly trends in reduction, but more work will be required to investigate whether IR alone could provide a better approximation compare with other objectives in the assessment of comfort.'

Secondly, as far as the energy efficient metric (Figure 5.8b) is concerned, it illustrates a conflicting relation with JT as well. The increase of the JT from 35 s to 40 s offers a significant decrease of 65% in the vehicle's energy consumption, while afterwards the decrease is much less for the larger JT cases, i.e. after 60 s we identify 2% for each interval. Thirdly, as far as the riding confidence-oriented metrics 5.9b are concerned, they have a non-conflicting relation with the JT, so SF_D and SF_P evaluated at the occupant in the driver and passenger position is increasing as the JT is increased. This can be translated in an increase of the motions felt as the JT is increased, hence riding confidence deteriorates.

Last but not least, the vehicle stability-oriented metrics (Figure 5.9a) have a more complicated relation with JT. More specifically, $MLTRR$ and $MLTRF$ illustrate a conflicting relation with JT, with the $MLTRF$ to be constantly decreasing and offering a more stable front axle without the risk of lift-off as the JT is increasing.On the other hand, $MLTRR$ doesn't improve in the first JT cases ($JT \leq 45$ s), which means that the rear axle of the vehicle continues to experience lift-off in one of its wheels during the journey in these cases. However, when JT becomes more than 45 s the rear axle of the vehicle is becoming more stable. Similar complicated relation with JT exists in STF and STR, which illustrate different and irregular variations but small (10%) while the JT is increased.

5.9 Sorting Algorithm k-ε

Having evaluated the additional objectives for the all the JT cases, the Pareto Fronts of all the additional objectives are interpolated for T'_{demand_i}, where $T'_{demand_i} = [35 : 0.1 : 75]$, in order to generate more alternatives. Afterwards, the k-ε algorithm is applied to seek the optimum solution among the Pareto alternatives considering the additional objectives described in Section 5.8. All the additional objectives are normalised for the sorting

algorithm. More specifically, the objective function of k-ε is defined as follow :

$$f = [RC,\ JT,\ AD,\ EE,\ STF,\ STR, ... \\ ST_D,\ SF_P,\ LTRF,\ LTRR] \quad (5.20)$$

while the threshold (ε) is selected to be :

$$\varepsilon = P_i[max(f_1), ..., max(f_n)] \quad (5.21)$$

where valude of P_i= 0.6 is selected so that k-ε algorithm to deliver only single optimum solution from the Pareto Front. According to Figure 5.11, the optimum solution, which has managed to compromise all the objectives including in Equation 5.20, is located at $JT = 58.2\ s$ the $k-$value of this solution is 7.3, which means it is dominating the rest objectives by 7.3 out of 9 (the value that the utopia point should have).

5.10 Conclusions

To sum up, an OCP problem was formulated to seek the optimal velocity profile for minimizing motion sickness at multiple fixed time solutions. The impact of increasing the journey time, i.e. assigning a smoother velocity profile to the road path, to multiple performance aspects was quantified and their conflicting or not relation with journey time was illustrated. The quantification of the impact that journey time increase had to the multiple performance aspects outlined the importance of considering them as well in the motion planning process. Finally, an approach combining two optimisation algorithms, i.e. the OCP and the $k-\varepsilon$ method, is applied successfully to seek the best velocity profile that ensures the optimum compromise between motion comfort and driving behaviour, energy efficiency, vehicle stability, occupants confidence to ride and journey time.

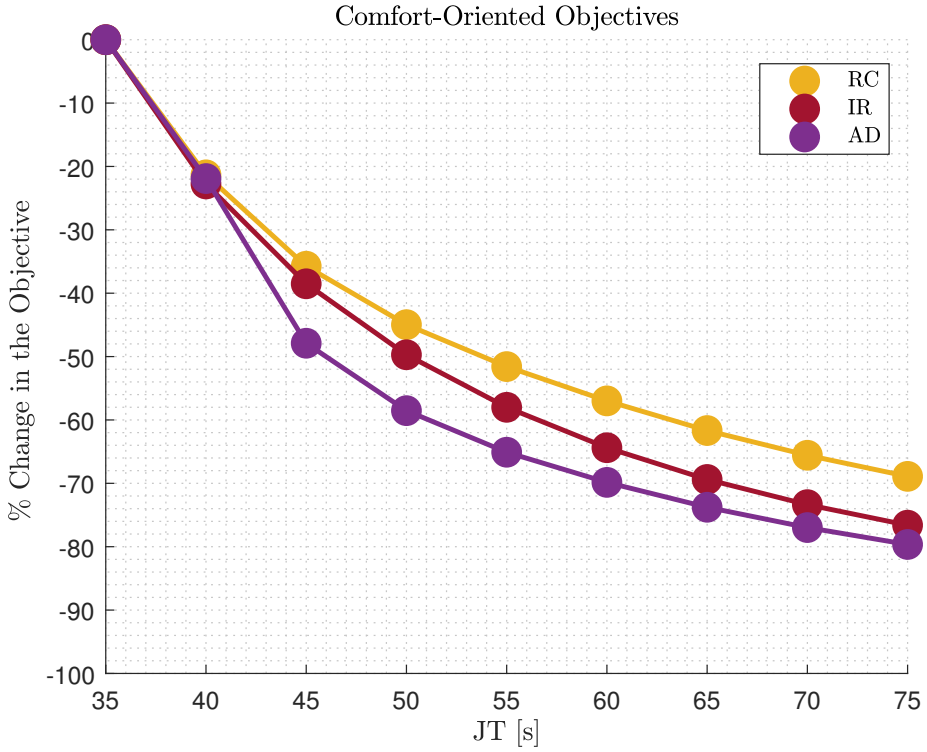

(a)

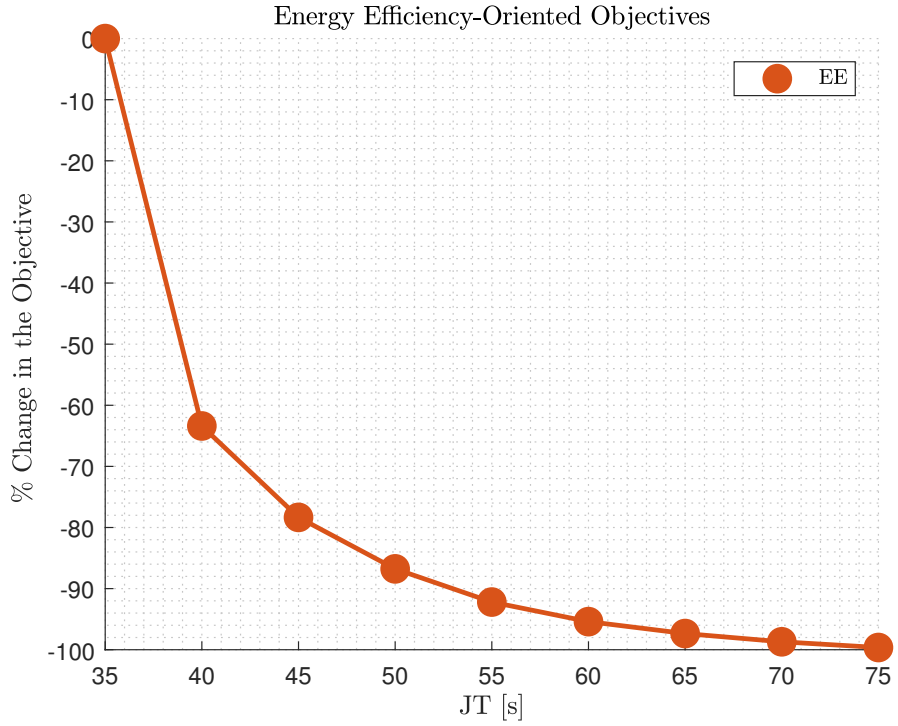

(b)

Figure 5.8: Additional performance metrics evaluated by the outputs of a CARMAKER vehicle model following the predefined path with the assigned velocity obtained by the OCP (Figure 5.7b) for different fixed time cases (a) comfort-oriented objectives, (b) energy efficiency-oriented objectives

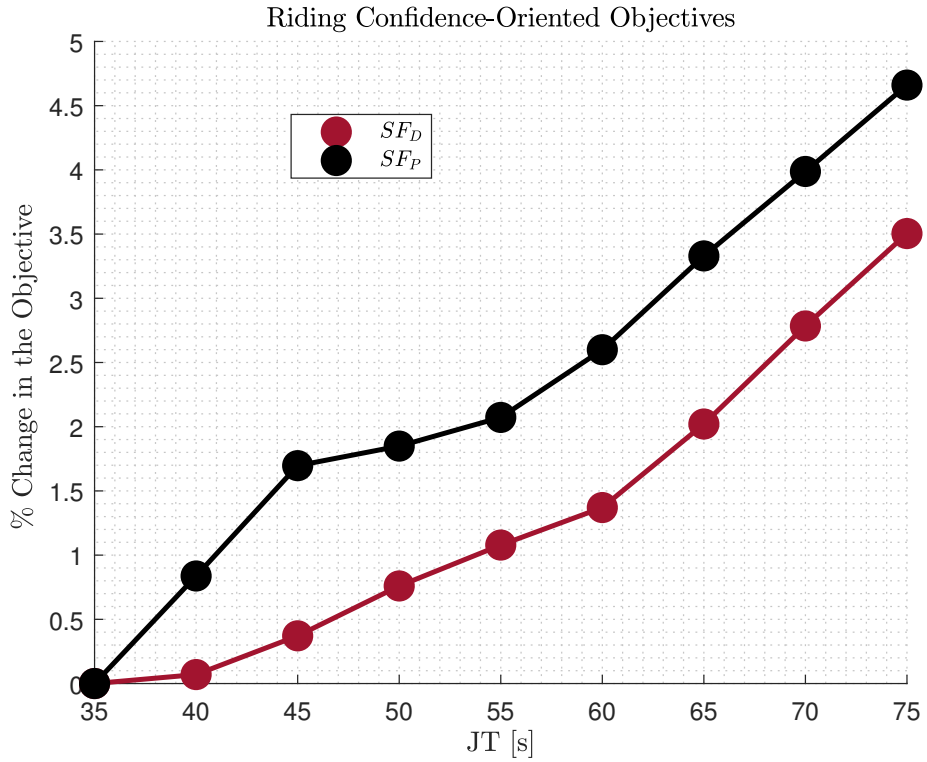

(a)

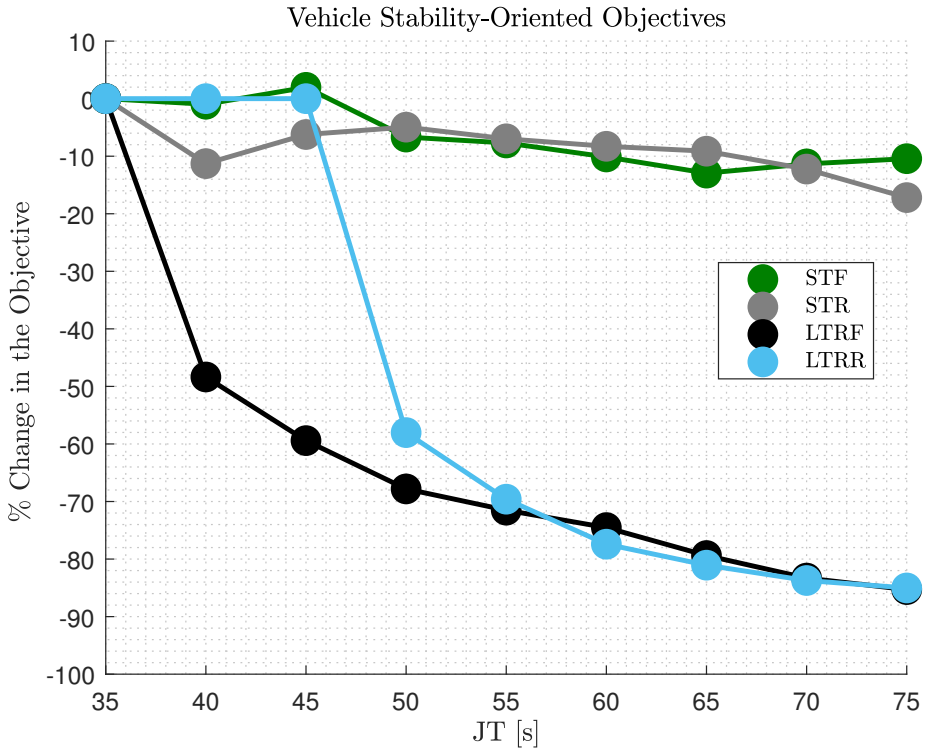

(b)

Figure 5.9: Additional performance metrics evaluated by the outputs of a CARMAKER vehicle model following the predefined path with the assigned velocity obtained by the OCP (Figure 5.7b) for different fixed time cases (a) riding confidence-oriented objectives, (b) vehicle stability-oriented objectives

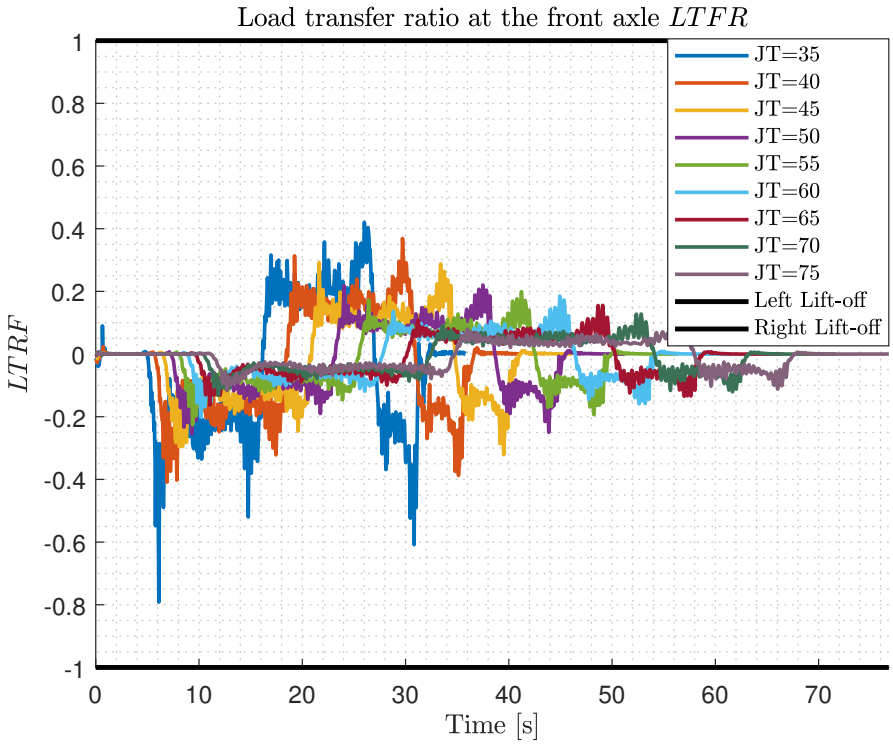

(a)

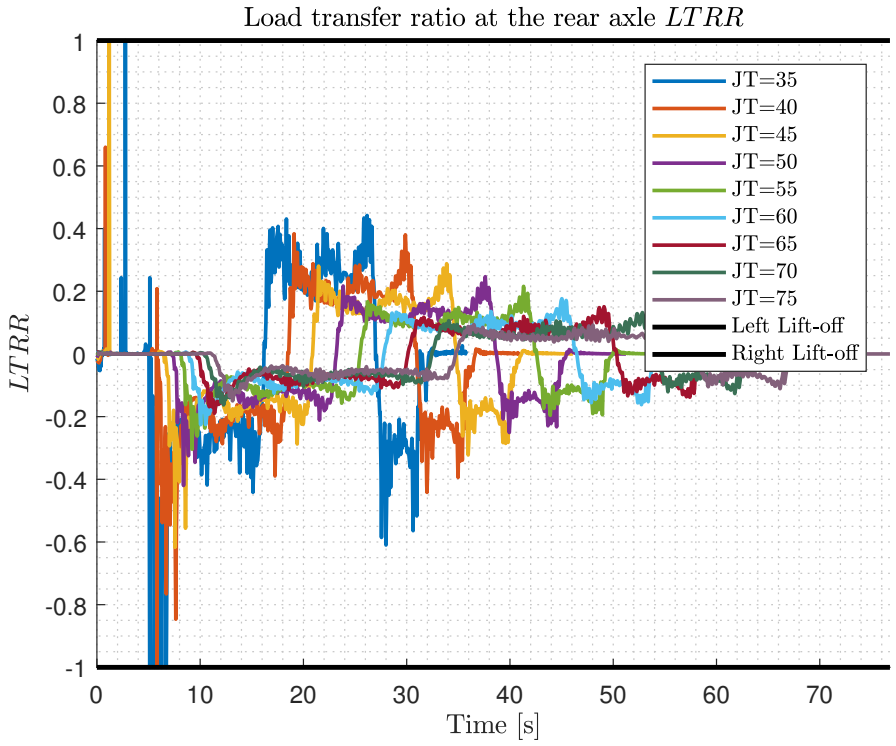

(b)

Figure 5.10: Load transfer ratio (LTR) at the (a) front ($LTRF$) and (b) rear ($LTRR$) axles for all the optimal solution for different JT.

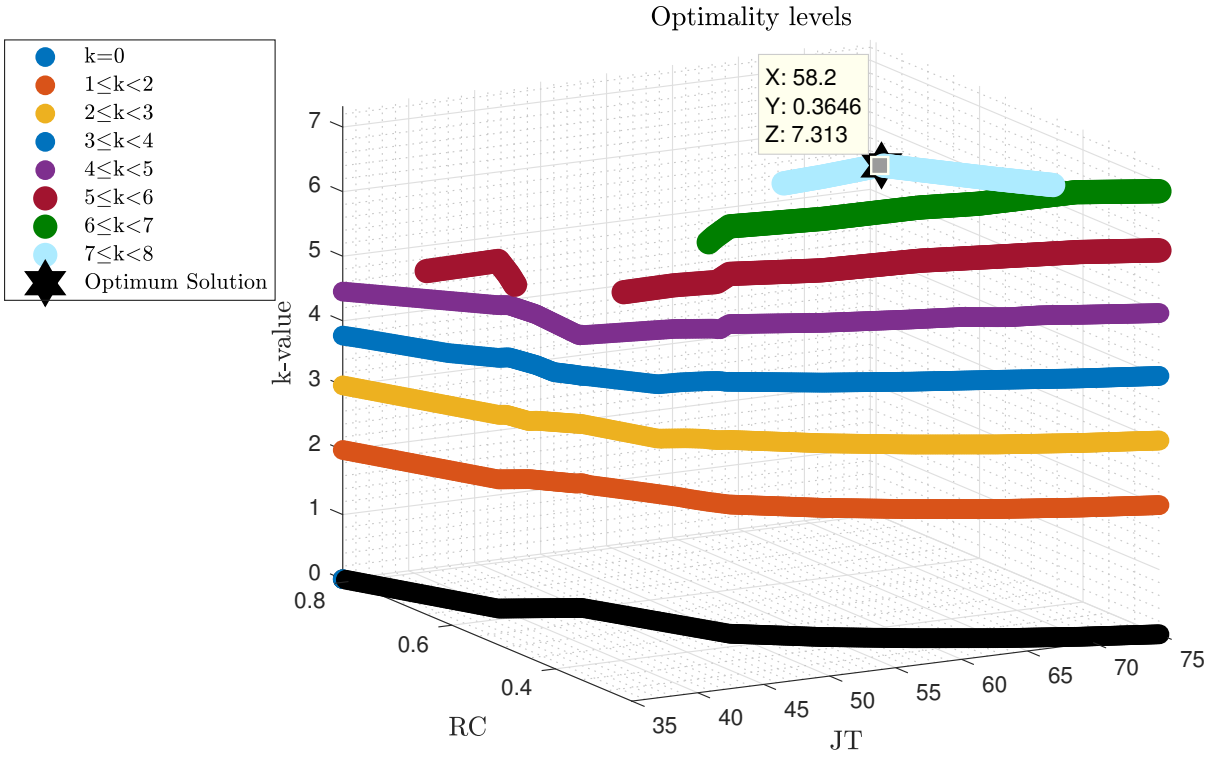

Figure 5.11: Optimum solution obtained by the sorting algorithm considering multiple design criteria (RC, AD, EE, STF, STR, LTF, LTR, SF_D and SF_P)

CHAPTER 6

Conclusions

6.1 Summary

6.1.1 Motion sickness modelling

This thesis discussed an overall review of the theory behind motion sickness and motion sickness modelling. The theory of sensory conflict has been discussed in great detail. Motion sickness is caused by low frequency motion typically below 0.5 Hz as this motion causes conflict in the sensory system. In the automated vehicles, the driving dynamics has been found to be the root cause due to driving behaviour, vehicle driving speed and road route. In addition, ergonomics and seating arrangements are also found to be the key factors in causing motion sickness. The severity of motion sickness is determined by the direction, magnitude, and duration of the oscillation of the motion. From the comparison of the two methods for motion sickness modelling, it can be concluded that both approach applying weighting or filtered to the actual acceleration before they are evaluated in different manner. Therefore, in some sense they are similar, though only SVC model could provide habituation. The next chapters of the work are to investigate on how to implement the models in the motion planning problem for motion sickness minimisation.

6.1.2 Optimal trajectory generation for motion sickness minimisation and tracking control

The application motion planning for automated vehicle has been successfully implemented in respect to motion sickness minimisation under a fixed journey time constraint. Motion sickness is minimised by taking the optimum trajectory and velocity profile for any given road path. The road-width flexibility does benefit in term of saving the journey time and reducing motion sickness. However, the illness rating and journey time are relatively small, due to the road track is short. Therefore, a more realistic road length with different road characteristic should be included for the in the future study. The optimal solutions from both motion sickness models are the similar since the accelerations are the key variables in the cost function. The results also clearly illustrated that motion sickness and journey time are in conflict with each other. This is due to the fact that when seeking minimum sickness, the vehicle would move in a slow manner, at constant velocity or come to a stop. Similarly, for minimum journey time, the vehicle would move very fast or at constant acceleration. Therefore, in order to achieve optimal solution for both minimum sickness as well as journey time their influences on the Pareto fronts, multi-objective optimisation (MOO) was applied for solving the trade-off for a comprise solution. On the other hand, the trajectory tracking controllers based on PID control method were able to track the reference trajectory with good performances. However, more work on the robustness of such trajectory should be investigate since the OCP problem in this work are under several modelling assumptions and simplification, without considering any disturbance from external agents.

6.1.3 Multi-objective optimisation for minimisation of motion sickness and journey time

The weighted sum method in MOO had been applied to solve the trade-off through a set of weighting factors [w_m, w_t]. The Pareto front representing the correlation between the two components is obtained and this front also allows user to select their preference driving style. From the three case studies, driving styles have a bigger impact on reducing motion sickness and journey time rather than vehicle speed and the road width. There is a significant impact in vehicle speed in the region where time weighting are higher than motion sickness weighting, as all the vehicles result in similar sickness level, but journey

time is shortened for vehicle with higher maximum speed capabilities. However, the effect of road width is negligible when travelling on longer road for the reduction of motion sickness and journey time. This is due to the fact that the road used in this study has a relatively longer straight road section and the advantage of road-width which is mainly for turns become less effective in reducing the lateral acceleration in this type of road journey. This finding is crucial considering the need for automated vehicles to drive on a fixed road path in respect to road safety and also to allow the employment of connected and automated vehicles in the future.

6.1.4 Multi-criteria decision making

Despite the importance of mitigating motions sickness using motion planning by also considering the journey time, the optimum velocity profile with which the vehicle will finally drive should be selected after taking into consideration additional objectives as well. Therefore, a sorting algorithm is applied to seek the optimum solution among the pareto alternatives. Finally, an approach combining two optimisation algorithms, i.e. the OCP and the $k - \varepsilon$ method, is applied successfully to seek the best velocity profile that ensures the optimum compromise between motion comfort and driving behaviour, energy efficiency, vehicle stability, occupants confidence to ride and journey time.

6.1.5 Computational performance

In this work, based on the model assumptions and the used of solver, the computational time to performance a single task (i.e. for a given fixed journey time) in the OCP problem ranges from 15 seconds to a few minutes. This is similar for MOO problem with different weighting to compute a weighting pair. On the other hand, the computation time could take up to 10 minutes to perform sorting algorithm for multi-criteria decision making. The OCP formulation approach and the models used on this work are readily transferable to more advance planning algorithms. The optimal trajectory for each task is generated within short computational time. Thus with some improvements, this approach could either provide as a reference or implement to the advance motion planning in autonomous vehicle industry.

6.2 Contribution

A novel approach has been proposed that minimise motion sickness through motion planning by generating optimal trajectories for the entire journey that guarantee reduce motion sickness and improve comfort, safety and dynamically feasible. The application of multi-objective optimisation for solving the trade-off between minimising motion sickness and journey time has been demonstrated in the motion planning problems. Furthermore, a multi-criteria decision making has been incorporated to find the final optimal solution with additional objectives. The impacts that this thesis provides are as follows:

- Motion sickness can be minimised by tackling the driving dynamics by implementing motion sickness modelling in the motion planning problems, which is an ideal in the development of automated vehicle algorithm.
- The trade-off between motion sickness and journey time provides future development of the automated vehicle technology to let users choose their preferences. This can be choosing a driving style in term of their preference on arriving at a reasonable journey time with less motion sickness.
- The road-width study also provide an additional contribution such that a fixed road would be an ideal for the planning of infrastructural development to accommodate autonomous vehicles.
- Finally, the work in the thesis pave a path for the development of vehicular technologies to implement in real world driving.

6.3 Future work

The thesis has demonstrated the application motion planning in minimising motion sickness in automated vehicles. The following are the proposed developments for the future work:

- The optimal control problems calculation in this thesis are under several modelling assumptions and simplification, without considering any disturbance from external agents. Thus, the optimal trajectories returned by the motion planner under such condition represent open-loop references which is unlikely to be exactly reproduce by real-world vehicles. Therefore, a robust open-loop trajectory is desired in order

to enhance the correlation between numerical-control and real-world driving. The robustness of such trajectory can be achieved by tightening a selection of inequality constraints involved in the context of motion sickness would allow some margin of error when uncertainties or disturbances were to appear.

- In this work, the tracking controllers were based on PID control methods to follow the trajectory generated by the motion panner. Ideally, the feedback controllers should be designed to work in real-time and to provide good tracking performance. This can be done by implementing model-predictive control (MPC).

- The extension of the current work could include higher-fidelity models with different simulation scenarios for motion sickness minimisation such as lane-changing, static obstacle avoiding, road traffic with stateflow. This way, various optimal trajectories can be obtained by simulating all scenarios, and neural network could also be used together for the development for real time application.

- For a real comparison to determine the effectiveness of the generated trajectory in term of reducing motion sickness. This would require to carry out experimental studies such that by driving the real vehicle to follow the trajectory and the individual passenger give a motion sickness rating based on their experiences. This way, the motion planning solutions can be validated with the real-world solution. Although the discrepancy might be varied due to the experimental work involves human aspect which tends be subjective. Hence, a large scale of population would be ideal.

This page is intentionally left blank.

APPENDIX A

Motion sickness model

A.1 6 -DOF Subjective vertical conflict model

Kamiji [35] developed mathematical model of motion sickness in 6 DOF in three-dimensional space based on the SVC model by Bels to predict motion sickness incidence for various motion stimuli including translation and rotation of the head. It has been verified that the model could predict distribution characteristics of Griffin's 'mild nausea' [48] very well.

The 6 DOF-SVC conflict model in three dimensional space shown in Figure **??** is divided into two part, where the upper part of the block diagram estimates the sensed vertical which would be discussed in this paper to highlight the important principal. However, the detail discussion of the lower part of the block diagram (internal model) which estimates the expected vertical and all the parameters used in the model can be found in [35], [29] and [32]. The validity of this model had been examined and compared with existing experimental result [8] and [48]

As mentioned in section 2.2.1, the vestibular system contains two types of sensory organs: the semicircular canals and the otolith organs. SCC organs act as angular accelerometers

measuring head angular velocity ω, and the transfer function for SCC here is given as:

$$\omega_{s_i} = \frac{\tau_a \tau_d s^2}{(1+\tau_a s)(1+\tau_d s)} \omega_i \tag{A.1}$$

Where ω_s is the sensed angular velocity and $i = (x, y, z)$, τ_a is the adaptation time constant and τ_d is the dominant decay time constant of the SCC.

Generally, the three dimensional angular velocity will constantly effect change the orientation of the gravitational force, this physical effect must be taken into account and this is performed using a simple nonlinear differential equation, assuming that gravity is constant is given as:

$$\frac{dg}{dt} = -\omega \times g \tag{A.2}$$

However, it is thought that the sensed angular velocity information from SCC plays a key role and the sensed vertical v_s is estimated from the otolith-canal interaction given as:

$$\frac{dv_s}{dt} = \frac{1}{\tau}(f_s - v_s) - \omega_s \times v_s \tag{A.3}$$

Where v_s is the sensed vertical and τ is time constant.

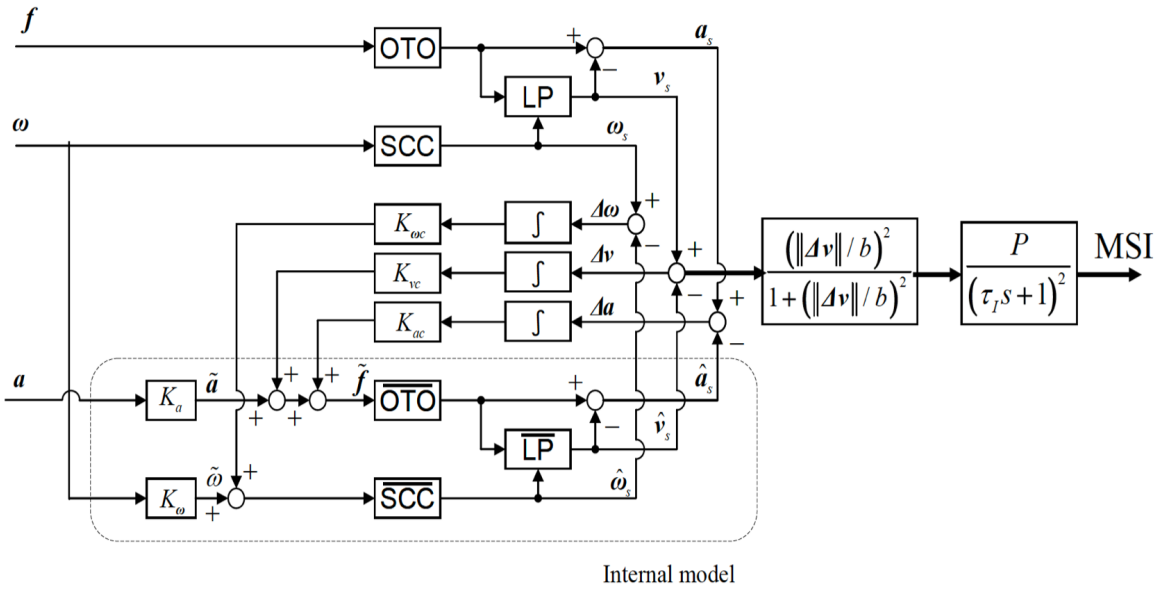

Figure A.1: 6DOF- SVC model [**?**]

APPENDIX B

Initial works on motion sickness minimisation

B.1 Road width study

In this section, the motion planning of self-driving vehicles is applied in order to minimise motion sickness and journey time. More specifically, for a predefined road path from a specific starting point to a final one, the optimum velocity profile is sought within specific and given boundary and constrains. Therefore, three cases have been set up to investigate the compromise of motion sickness with minimum journey time in motion planning.

- Case 1 : $J = F_1 \quad , w_{f_1} = 1 \; and \; w_{f_2} = 0$
- Case 2 : $J = F_2 \quad , w_{f_1} = 0 \; and \; w_{f_2} = 1$
- Case 3 : $J = F_1 + F_2 \quad , w_{f_1} = 1 \; and \; w_{f_2} = 1$

All the above cases are tested for two scenarios, which consider different road widths in the same road path. The first scenario (Scenario 1) doesn't allow any lateral manoeuvrability to the vehicle by setting the road width at zero (i.e. the road boundary of left border and right border measured from the centreline $L_w, R_w = 0m$). In this way, the vehicle travels on the fixed road path. On the other hand, in the second scenario (Scenario 2), the road width is increased ($L_w, R_w = 4m$), and hence manoeuvrability is offered to the vehicle to move along the lateral axis within the road borders.
The simulation results for each scenarios are tabulated in Table B.3 and B.2 respectively. In both tables, the journey time and illness rating for each case are presented. Similarly,

the optimum velocity profile and trajectory followed for each case is illustrated in Fig. B.1 and B.6.

B.1.1 Scenario 1: Fixed Path

First of all, as expected, the vehicle traveled along the reference path in all cases shown in Fig. B.1. According to Table. B.3, Case 1 yield the highest illness rating with shortest journey time as its objective is to achieved minimum time only. On the other hand, Case 2 achieved lowest illness rating but with highest journey time, as its cost function represented motion sickness. In addition, Case 3 where both time and illness rating were considered as not only the minimum motion sickness was achieved but also shorter journey time compared to Case 2. Taking minimum time solution i.e. Case 1 to be the baseline, it can be seen that the time taken for the vehicle to complete the journey increases significantly by 60.5% while it is 50.2% for Case 3. However, when comparing their illness rating, IR significantly reduces to 44.3% for Case 2, and 43% for Case 3. It can be concluded that when both journey time and motion sickness are taken into consideration, better result could be obtained. Regarding Fig. B.1, the velocity profile of

Table B.1: Journey time and illness rating for Scenario 1

	T [s]	**IR**
Case 1	18.53	0.079
Case 2	29.73	0.044
Case 3	27.84	0.045

the vehicle in Case 1 decelerates and accelerates rapidly along the path whenever possible to decrease journey time in which increases case 1 illness rating. On the other hand for Case 2, the vehicle travels at constant speed of 10 [m/s] which is in agreement with the result in Table B.3 which imply that the the journey time is longer but lower illness rating. Finally, when both illness rating and time are considered in case 3, velocity profile accelerate as fast as it can to compensate the time while maintaining the minimum illness rating.

B.1.2 Scenario 2: Non-zero Lateral Manoeuvrability

For this scenarios, the optimal trajectory is within the road bounds and it is able to track the reference road path which is shown in Fig. B.6. Similarly the trend here are in

agreement with fixed path where case 1 has the highest illness rating with short journey time where Case 2 has the lowest illness rating but longest duration of travel. Similarly, comparing the results with Case 1, it can be seen that the time taken for the vehicle to complete the journey increases significantly by 82.9% while it is 71.9% for Case 3. However, when comparing illness rating, IR significantly reduces to 54.1% for Case 2, and 52.7% for Case 3. This is also consistent with the result from fixed path scenario. However, comparing each case with fixed path scenarios, it is clear that all the result have significant improvement as both journey time and illness rating are relatively lower as shown in Table B.2. This is because of lateral manoeuvrability allowed the vehicle to take different trajectory within the road bound, which minimises journey time and reduces sickness.

Table B.2: Journey time and illness rating for Scenario 2

	T [s]	**IR**
Case 1	15.28	0.074
Case 2	27.94	0.034
Case 3	26.27	0.035

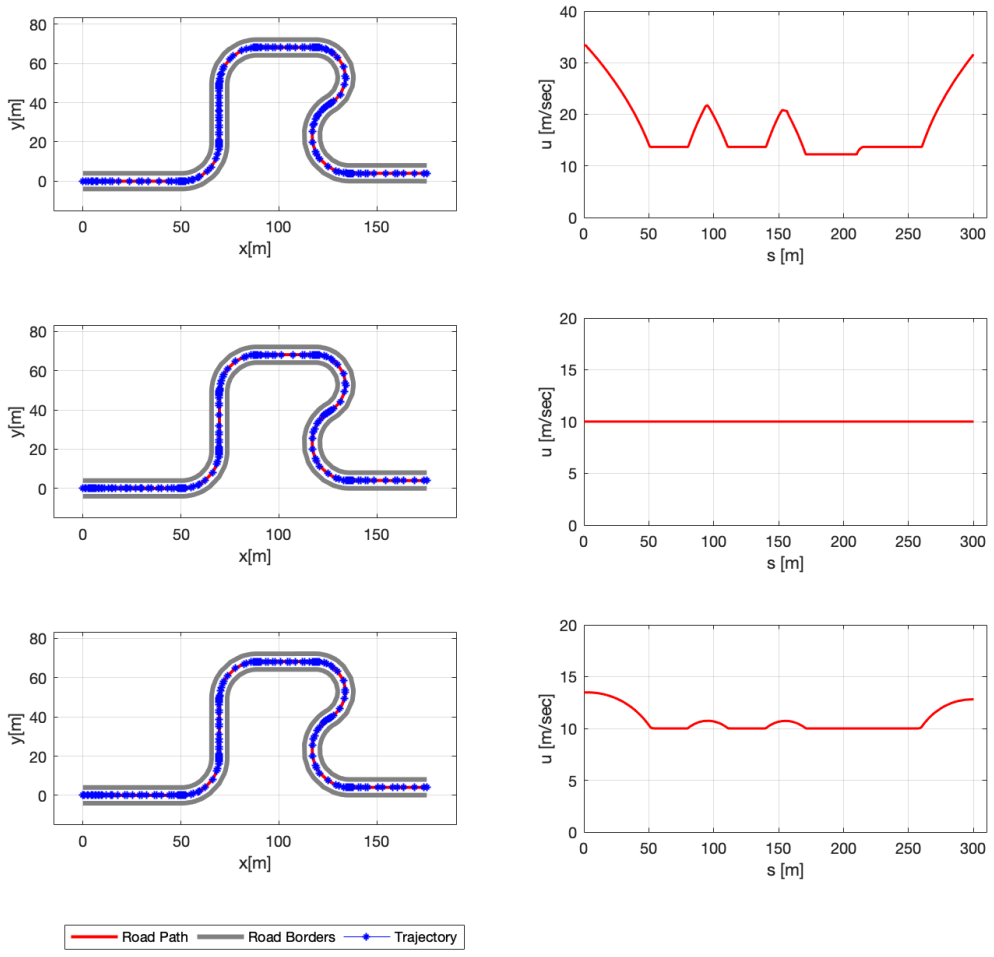

Figure B.1: Optimum Trajectory (Left) and Velocity profile (Right), Case 1(Top), Case 2 (Middle), Case 3 (Bottom)

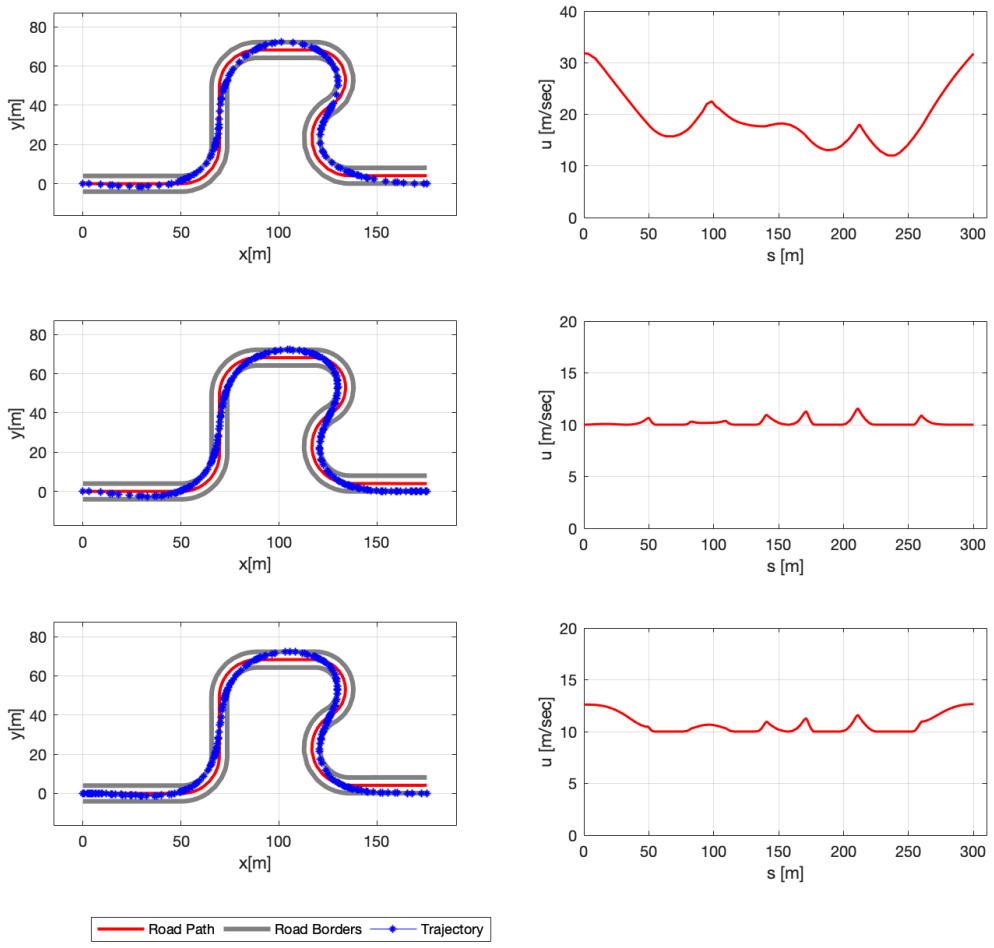

Figure B.2: Optimum Trajectory (Left) and Velocity profile (Right), Case 1(Top), Case 2 (Middle), Case 3 (Bottom)

B.2 Road curvature study

In this work, the optimal control technique is applied to vehicle dynamics in order to minimise motion sickness and journey time. Therefore, three cases have been set up to investigate the compromise of motion sickness with minimum journey time in various route scenarios.

- Case 1 : $J = F_1$, for minimum time
- Case 2 : $J = w_1 F_1 + w_2 F_2$, for combined objectives
- Case 3 : $J = F_2$, for minimum motion sickness

where w_1 and w_2 are the weighting factor. Three different road routes are presented to investigate the effect of road paths on motion sickness. The selected routes have the same length for all the straight and curvature sections (i.e. A, B, C, D and E), however the road curvature $\kappa(s)$ at B and D sections are gradually decrease from K1, K2 to K3 shown in Fig **??**a and the road trajectory can be seen in Fig. **??**b. All the above cases are tested with the condition where the road doesn't allow any lateral manoeuvrability to the vehicle by setting the road width at zero (i.e. $L_w, R_w = 0m$). In this way, the vehicle travels on the fixed road path. The simulation results for each case with three road route are tabulated in Table. B.3, where the journey time and illness rating for each case are presented. Similarly, the optimum velocity profile for each case is illustrated in Fig. B.6.

Table B.3: Optimal solution for journey time and illness rating

	K1		K2		K3	
	Time [s]	**IR**	**Time [s]**	**IR**	**Time [s]**	**IR**
Case 1	5.80	0.641	15.07	0.591	14.22	0.535
Case 2	7.31	0.437	16.56	0.394	15.66	0.348
Case 3	25.23	0.163	24.13	0.147	22.85	0.130

According to Table. B.3 for all the road routes. Case 1 yield the highest illness rating with shortest journey time as its objective is to achieved minimum time only. On the other hand, Case 3 achieved lowest illness rating but with highest journey time, as its cost function represented motion sickness. In addition, Case 2 where both time and illness rating were considered as not only the minimum motion sickness was achieved compared to Case 1 but also shorter journey time compared to Case 3. Taking minimum time

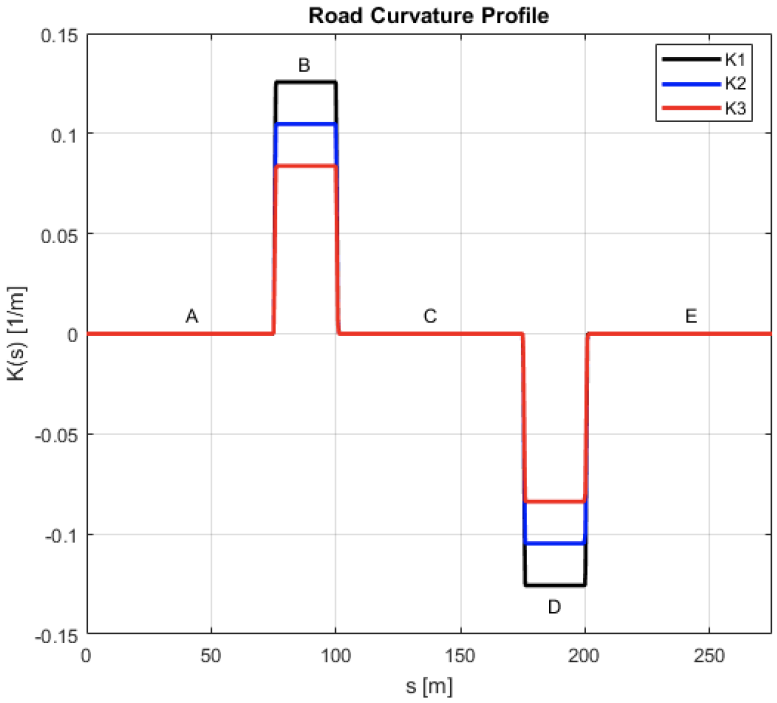

Figure B.3: Road curvature profile

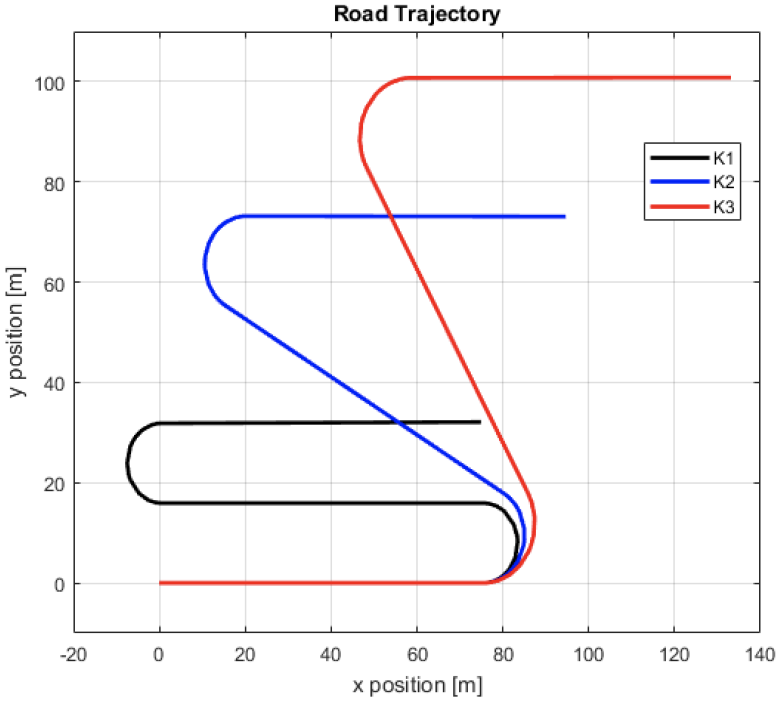

Figure B.4: Road Trajectory

Figure B.5: Trajectory of the three roads

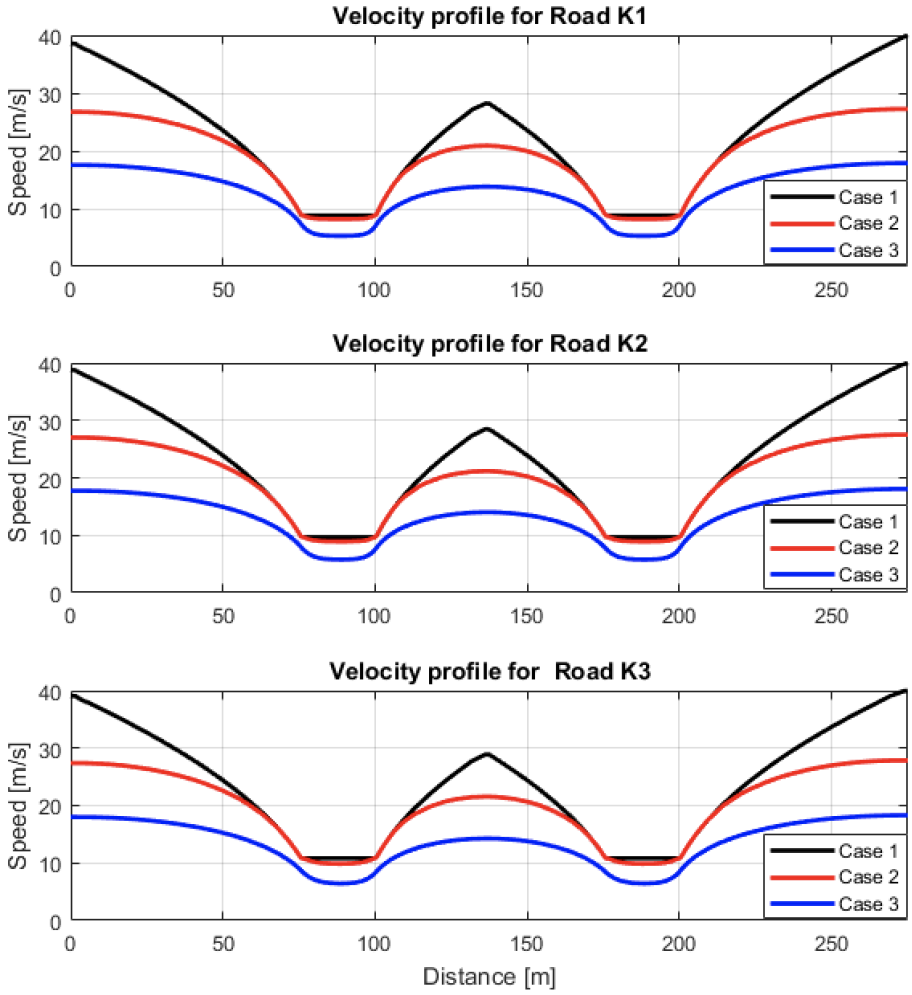

Figure B.6: Comparison of the velocity profile

solution i.e. Case 1 to be the baseline, it can be seen that the time taken for the vehicle to complete the journey increases significantly by about 10% for Case 2 while it is 60% for Case 3. However, when comparing their illness rating, IR significantly reduces to more than 30% for Case 2, and 75% for Case 3. It can be concluded that when both journey time and motion sickness are taken into consideration, better result could be obtained. Regarding Fig. B.6, again for all road routes, the velocity profile of the vehicle in Case 1 decelerates and accelerates rapidly along the path whenever possible to decrease journey time in which increases illness rating. On the other hand for Case 2, where both illness rating and time are considered, the vehicle travels as fast as it can but in a smooth manner to avoid rapid change and to compensate the time while maintaining the minimum illness rating. Finally in Case 3, the vehicle accelerates very slowly and smoothly a long the road as rapid change in the acceleration would result in higher illness rating and hence the journey time is longer. Similarly, the journey time and illness rating decreases as

the road curvature decreases, as higher κ in road K1 would first result in higher lateral acceleration and hence required to further slow down compares with lower κ in road K2.

This page is intentionally left blank.

References

[1] Moavenzadeh, J. and Lang, N.S., 2018. "*Reshaping Urban Mobility with Autonomous Vehicles: Lessons from the City of Boston*". In World Economic Forum.

[2] Le Vine, Scott, Alireza Zolfaghari, and John Polak. "*The tension between autonomous cars' impacts on intersection level-of-service and their occupants' use of travel time for leisurely or economically-productive activities.*" Proceedings of the 94th Annual Meeting of the Transportation Research Board, January 2015.

[3] Sivak, Michael, and Brandon Schoettle. "*Motion sickness in self-driving vehicles.*" 2015.

[4] Griffin, M.J. and Newman, M.M., "*An experimental study of low-frequency motion in cars*". Proceedings of the Institution of Mechanical Engineers, Part D: Journal of Automobile Engineering, 2004. 218(11), pp.1231-1238.

[5] Diels, Cyriel, et al. "*Motion sickness in automated vehicles: the elephant in the room.* Road Vehicle Automation 3. Springer International Publishing, 2016. 121-129.

[6] Diels, C. and Bos, J.E., 2015. "*Design guidelines to minimise self-driving carsickness*". In Automated Vehicles Symposium.

[7] Khalid, H., Turan, O. and Bos, J.E., 2011. "*Theory of a subjective vertical?horizontal conflict physiological motion sickness model for contemporary ships.* Journal of marine science and technology, 16(2), pp.214-225.

[8] Griffin, Michael J. "*Handbook of human vibration*". Academic press, 2012.

[9] Cheung, B., and Nakashima, A. "*A review on the effects of frequency of oscillation on motion sickness*". No. DRDC-TR-2006-229. Defence research and development Toronto (Canada),2006.

[10] Turner, Mark, and Michael J. Griffin. "*Motion sickness in public road transport: the effect of driver, route and vehicle.*"Ergonomics 42.12 (1999): 1646-1664.

[11] Turner, M., 1999. "*Motion sickness in public road transport: passenger behaviour and susceptibility.*" Ergonomics, 42(3), pp.444-461.

[12] Salter S, Thake D, Kanarachos S, Diels C. "*Motion Sickness Prediction Device for Automated Vehicles.* "International Journal of Mechanical and Production Engineering. 2019 May 21;7(2):68-74.

[13] Salter S, Diels C, Herriotts P, Kanarachos S, Thake D. "*Motion sickness in automated vehicles with forward and rearward facing seating orientations.*" Applied ergonomics. 2019 Jul 1;78:54-61.

[14] Schmidt, E.A., Kuiper, O.X., Wolter, S., Diels, C. and Bos, J.E., "*An international survey on the incidence and modulating factors of carsickness.* Transportation Research Part F: Traffic Psychology and Behaviour, 71, pp.76-87, 2020.

[15] Paddeu, D., Parkhurst, G. and Shergold, I. "*Passenger comfort and trust on first-time use of a shared autonomous shuttle vehicle*". Transportation Research Part C: Emerging Technologies, 2020. 115, p.102604.

[16] Elbanhawi, Mohamed, Milan Simic, and Reza Jazar. "*The effect of receding horizon pure pursuit control on passenger comfort in autonomous vehicles.*" Intelligent Interactive Multimedia Systems and Services 2016. Springer International Publishing, 2016. 335-345.

[17] Elbanhawi, Mohamed, Milan Simic, and Reza Jazar. "*In the passenger seat: investigating ride comfort measures in autonomous cars.*" IEEE Intelligent Transportation Systems Magazine 7.3 (2015): 4-17.

[18] Diels, Cyriel. "*Will autonomous vehicles make us sick.*" Contemporary Ergonomics and Human Factors (2014): 301-307.

[19] Diels, Cyriel, and Jelte E. Bos. "*Self-driving carsickness.*" Applied ergonomics 53 (2016): 374-382.

[20] Mansfield, N.J., 2004. "*Human response to vibration.*" CRC press.

[21] Frstberg J. "*Ride comfort and motion sickness in tilting trains*", Doctoral dissertation, KTH Royal Institute of Technology, 2000.

[22] Qazizadeh A. "*On Active Suspension in Rail Vehicles*", Doctoral dissertation, KTH Royal Institute of Technology, 2017.

[23] H. Dong, L. Zhang, Y. Chen, et al. "*Multi-objective train trajectory design based on dynamic programming.*" Proceedings of the Chinese Control Conference. Nanjing: IEEE, 2014.

[24] He, D., Zhou, L. & Sun, Z. "*Energy-efficient receding horizon trajectory planning of high-speed trains using real-time traffic information.*" Control Theory Technol. 18, 204?216 (2020).

[25] Htike Z, Papaioannou G, Velenis E, Longo S. "*Motion Planning of Self-driving Vehicles for Motion Sickness Minimisation.*" In2020 European Control Conference (ECC) 2020 May 12 (pp. 1719-1724). IEEE.

[26] Htike Z, Papaioannou G, Siampis E, Velenis E, Longo S. "*Motion Sickness Minimisation in Autonomous Vehicles Using Optimal Control.*" In International Conference on Robotics in Alpe-Adria Danube Region 2020 Jun 19 (pp. 275-282). Springer, Cham.

[27] Htike, Z., Papaioannou, G., Siampis, E., Velenis, E. and Longo, S., "*Minimisation of Motion Sickness in Autonomous Vehicles.* In 2020 IEEE Intelligent Vehicles Symposium (IV) (pp. 1135-1140). IEEE.

[28] Wada, T. and Kamij, N. "*A mathematical model of motion sickness in 6DOF motion and its application to vehicle passengers*". arXiv preprint arXiv:1504.05261. 2015.

[29] Wada, Takahiro, et al. "*Effect of driver's head tilt strategy on motion sickness incidence.*" IFAC Proceedings Volumes 43.13 (2010): 192-197.

[30] Wada, Takahiro. "*Motion Sickness in Automated Vehicles.*" Advanced Vehicle Control: Proceedings of the 13th International Symposium on Advanced Vehicle Control (AVEC'16), September 13-16, 2016, Munich, Germany. CRC Press, 2016.

[31] Wada, Takahiro, and Norimasa Kamij. "*A Mathematical Model of Motion Sickness in 6DOF Motion and Its Application to Vehicle Passengers.*" arXiv preprint arXiv:1504.05261 (2015).

[32] Wada, Takahiro, Satoru Fujisawa, and Shunichi Doi. "*Analysis of driver's head tilt using a mathematical model of motion sickness.*"International Journal of Industrial Ergonomics (2016).

[33] Wada T, Konno H, Fujisawa S, Doi SI. "*Can passengers? active head tilt decrease the severity of carsickness? Effect of head tilt on severity of motion sickness in a lateral acceleration environment.* Human factors. 2012 Apr;54(2):226-34.

[34] Konno, Hiroyuki, Satoru Fujisawa, and Takahiro Wada."*Analysis of motion sensation of car drivers and its application to posture control device.*" SICE Annual Conference (SICE), 2011 Proceedings of. IEEE, 2011.

[35] Kamiji, Norimasa, et al. "*Modeling and validation of carsickness mechanism.*" SICE, 2007 Annual Conference. IEEE, 2007.

[36] Uefune, Tomoya, Takahiro Wada, and Kohei Sonoda. "*Computation of the Vestibulo-Ocular Reflex for eye closure based on the 6DOF-SVC model.*" Systems, Man, and Cybernetics (SMC), 2016 IEEE International Conference on. IEEE, 2016.

[37] Papaioannou G, Voutsinas A, Koulocheris D. "*Optimal design of passenger vehicle seat with the use of negative stiffness elements.*" Proceedings of the Institution of Mechanical Engineers, Part D: Journal of automobile engineering. 2020 Feb;234(2-3):610-29.

[38] Wu, Z., Liu, Y. and Pan, G., " *A smart car control model for brake comfort based on car following*". IEEE transactions on intelligent transportation systems, 2009. 10(1), pp.42-46.

[39] Papaioannou, G. and Koulocheris, D. , "*An approach for minimizing the number of objective functions in the optimization of vehicle suspension systems*". Journal of Sound and Vibration, 2018. 435, pp.149-169.

[40] Hiraoka T, Kunimatsu T, Nishihara O, Kumamoto H. "*Modeling of driver following behavior based on minimum-jerk theory*". InProc. 12th World Congress ITS 2005 Nov.

[41] British Standards Institution 1987, "*British standard guide to measurement and evaluation of human exposure to whole-body mechanical vibration and repeated shock,*" British Standards Institution, London.

[42] International Organization for Standardization, 1997. "*Mechanical vibration and shock-Evaluation of human exposure to whole-body vibration-Part 1: General requirements.*" The Organization.

[43] ISO 8041, " *Human response to vibration - Measuring instrumentation*". 2005

[44] Bles, W., Bos, J.E., De Graaf, B., Groen, E. and Wertheim, A.H. "*Motion sickness: only one provocative conflict?*". Brain research bulletin, 1998, 47(5), pp.481-487.

[45] Lawther, A. and Griffin, M.J., 1986. "*The motion of a ship at sea and the consequent motion sickness amongst passengers.*" Ergonomics, 29(4), pp.535-552.

[46] Lawther, A. and Griffin, M.J., 1988. "*Motion sickness and motion characteristics of vessels at sea.*" Ergonomics, 31(10), pp.1373-1394.

[47] Lawther, A. and Griffin, M.J., 1987. "*Prediction of the incidence of motion sickness from the magnitude, frequency, and duration of vertical oscillation.*" The Journal of the Acoustical Society of America, 82(3), pp.957-966.

[48] Donohew, Barnaby E., and Michael J. Griffin."*Motion sickness: effect of the frequency of lateral oscillation.*" Aviation, Space, and Environmental Medicine 75.8 (2004): 649-656.

[49] O'Hanlon, James F., and Michael E. McCauley. "*Motion sickness incidence as a function of the frequency and acceleration of vertical sinusoidal motion.*" No. 1733-1. CANYON RESEARCH GROUP INC GOLETA CA HUMAN FACTORS RESEARCH DIV, 1973.

[50] Oman, Charles M. "*Sensory conflict in motion sickness: an observer theory approach.*"1989.

[51] Oman, Charles M. "*Motion sickness: a synthesis and evaluation of the sensory conflict theory.*" Canadian journal of physiology and pharmacology 68.2 (1990): 294-303.

[52] Reason, James T. "*Motion sickness: Some theoretical and practical considerations.*" Applied ergonomics 9.3 (1978): 163-167.

[53] Golding JF. " *Motion sickness susceptibility.* " Autonomic Neuroscience. 2006 Oct 30;129(1-2):67-76.

[54] Golding JF, Bles W, Bos JE, Haynes T, Gresty MA. " *Motion sickness and tilts of the inertial force environment: active suspension systems vs. active passengers.*" Aviation, space, and environmental medicine. 2003 Mar 1;74(3):220-7.

[55] Bast, H., Delling, D., Goldberg, A., Mller-Hannemann, M., Pajor, T., Sanders, P., Wagner, D. and Werneck, R.F. "*Route planning in transportation networks*". In Algorithm engineering (pp. 19-80). 2016. Springer, Cham.

[56] Brechtel S., Gindele T., and Dillmann R., "*Probabilistic MDP-behavior planning for cars,*" in 14th International Conference on Intelligent Transportation Systems, pp. 1537?1542, IEEE, 2011.

[57] Paden B, Čáp M, Yong SZ, Yershov D, Frazzoli E. "*A survey of motion planning and control techniques for self-driving urban vehicles.* "IEEE Transactions on intelligent vehicles. 2016 Jun 13;1(1):33-55.

[58] González D, Pérez J, Milanés V, Nashashibi F. "*A review of motion planning techniques for automated vehicles.* " IEEE Transactions on Intelligent Transportation Systems. 2015 Nov 26;17(4):1135-45.

[59] Kelly M. " *An introduction to trajectory optimization: How to do your own direct collocation.* " SIAM Review. 2017;59(4):849-904.

[60] Kelly MP. " *Transcription methods for trajectory optimization: a beginners tutorial.* " arXiv preprint arXiv:1707.00284. 2017 Jul 2.

[61] Huang G, Lu Y, Nan Y. " *A survey of numerical algorithms for trajectory optimization of flight vehicles.* "Science China Technological Sciences. 2012 Sep;55(9):2538-60.

[62] Rao AV. " *A survey of numerical methods for optimal control.* "Advances in the Astronautical Sciences. 2009 Aug 10;135(1):497-528.

[63] Patterson MA, Rao AV. " *GPOPS-II: A MATLAB software for solving multiple-phase optimal control problems using hp-adaptive Gaussian quadrature collocation methods and sparse nonlinear programming.* "ACM Transactions on Mathematical Software (TOMS). 2014 Oct 27;41(1):1.

[64] Perantoni G, Limebeer DJ. "*Optimal control for a formula one car with variable parameters.*" Vehicle System Dynamics. 2014 May 4;52(5):653-78.

[65] Smith EN, Velenis E, Tavernini D, Cao D. "*Effect of handling characteristics on minimum time cornering with torque vectoring.*" Vehicle system dynamics. 2018 Feb 1;56(2):221-48.

[66] R. S. Sharp & Huei Peng (2011)"*Vehicle dynamics applications of optimal control theory,*" Vehicle System Dynamics, 49:7, 1073-1111, DOI: 10.1080/00423114.2011.586707

[67] Gill PE, Murray W, Saunders MA. "*SNOPT: An SQP algorithm for large-scale constrained optimization.* " SIAM review. 2005;47(1):99-131.

[68] Wachter A, Biegler LT. "*On the implementation of an interior-point filter line-search algorithm for large-scale nonlinear programming.*" snMathematical programming. 2006 Mar;106(1):25-57.

[69] Dal Bianco, N., Bertolazzi, E., Biral, F. and Massaro, M.. " *Comparison of direct and indirect methods for minimum lap time optimal control problems*". Vehicle System Dynamics, 2019. 57(5), pp.665-696.

[70] Febbo H, Jayakumar P, Stein JL, Ersal T. " *NLOptControl: A modeling language for solving optimal control problems*" arXiv preprint arXiv:2003.00142. 2020 Feb 29.

[71] Althoff M, Koschi M, Manzinger S. "*CommonRoad: Composable benchmarks for motion planning on roads.*" In2017 IEEE Intelligent Vehicles Symposium (IV) 2017 Jun 11 (pp. 719-726). IEEE.

[72] Hult R, Tabar RS. "*Path planning for highly automated vehicles*" . Mathesis, Gothenburg. 2013.

[73] Lot R, Biral F. "*A curvilinear abscissa approach for the lap time optimization of racing vehicles.*" IFAC Proceedings Volumes. 2014 Jan 1;47(3):7559-65.

[74] Lot R, Dal Bianco N. "*Lap time optimisation of a racing go-kart.* " Vehicle System Dynamics. 2016 Feb 1;54(2):210-30.

[75] Tavernini D, Massaro M, Velenis E, Katzourakis DI, Lot R. "*Minimum time cornering: the effect of road surface and car transmission layout.*" Vehicle System Dynamics. 2013 Oct 1;51(10):1533-47.

[76] Miková, Ľ., Gmiterko, A., Kelemen, M., Virgala, I., Prada, E., Hroncov, D. and Varga, M.,"*Motion control of nonholonomic robots at low speed.*" International Journal of Advanced Robotic Systems, 2020

[77] Yang JB, Whidborne JF. "*Multiobjective optimisation and control.*" Research Studies Press; 2003.

[78] Marler RT, Arora JS. "*Survey of multi-objective optimization methods for engineering. Structural and multidisciplinary optimization.*" 2004 Apr 1;26(6):369-95.

[79] Andersson J. "*A survey of multiobjective optimization in engineering design. Department of Mechanical Engineering, Linktjping University.*" Sweden. 2000.

[80] Logist F, Houska B, Diehl M, Van Impe J. "*Fast Pareto set generation for nonlinear optimal control problems with multiple objectives. Structural and Multidisciplinary Optimization.* " 2010 Oct 1;42(4):591-603.

[81] Gambier A, Badreddin E. "*Multi-objective optimal control: An overview.* " In2007 IEEE International Conference on Control Applications 2007 Oct 1 (pp. 170-175). IEEE.

[82] Grodzevich O, Romanko O. "*Normalization and other topics in multi-objective optimization.*" 2006

[83] Bellem H, Schnenberg T, Krems JF, Schrauf M. "*Objective metrics of comfort: developing a driving style for highly automated vehicles.* "Transportation research part F: traffic psychology and behaviour. 2016 Aug 1;41:45-54.

[84] Ziegler J, Bender P, Dang T, Stiller C. "*Trajectory planning for bertha?a local, continuous method.*" In2014 IEEE intelligent vehicles symposium proceedings 2014 Jun 8 (pp. 450-457). IEEE.

[85] Hegeds F, Bcsi T, Aradi S, Gpr P. "*Model based trajectory planning for highly automated road vehicles.*" IFAC-PapersOnLine. 2017 Jul 1;50(1):6958-64.

[86] Herrmann T, Christ F, Betz J, Lienkamp M. "*Energy management strategy for an autonomous electric racecar using optimal control.*" In2019 IEEE Intelligent Transportation Systems Conference (ITSC) 2019 Oct 27 (pp. 720-725). IEEE.

[87] Han J, Vahidi A, Sciarretta A. "*Fundamentals of energy efficient driving for combustion engine and electric vehicles: An optimal control perspective.*" Automatica. 2019 May 1;103:558-72.

[88] ISO8608, "*Mechanical vibration-Road surface profiles-Reporting of measured data,*" Tech. Rep., 1995. [Online]. Available: https://www.iso.org/standard/71202.html

[89] Papaioannou G, Dineff AM, Koulocheris D. "*Comparative study of different vehicle models with respect to their dynamic behavior.*" International Journal of Automotive and Mechanical Engineering. 2019 Oct 4;16(3):7061-92.

[90] Papaioannou G, Gauci C, Velenis E, Koulocheris D. "*Sensitivity Analysis of Vehicle Handling and Ride Comfort with Respect to Roll Centers Height.*" InThe IAVSD International Symposium on Dynamics of Vehicles on Roads and Tracks 2019 Aug 12 (pp. 1730-1739). Springer, Cham.

[91] . Nuti AC. "*Objective metric x subjetive evaluation.* " SAE Technical Paper; 2003 Nov 18.

[92] Trivedi Z, Lakhera V. "*Perceptible Roll.* " SAE International Journal of Commercial Vehicles. 2015 Apr 14;8(2015-01-1585):147-51.

[93] Gobbi M. "*A k, k-ϵ optimality selection based multi objective genetic algorithm with applications to vehicle engineering.* " Optimization and Engineering. 2013 Jun;14(2):345-60.